ANL-7548

ANL-7548

RETURN TO ANL (IDAHO) LIBRARY.

# Argonne National Laboratory

## REACTOR DEVELOPMENT PROGRAM PROGRESS REPORT

January 1969

The facilities of Argonne National Laboratory are owned by the United States Government. Under the terms of a contract (W-31-109-Eng-38) between the U. S. Atomic Energy Commission, Argonne Universities Association and The University of Chicago, the University employs the staff and operates the Laboratory in accordance with policies and programs formulated, approved and reviewed by the Association.

MEMBERS OF ARGONNE UNIVERSITIES ASSOCIATION

The University of Arizona
Carnegie-Mellon University
Case Western Reserve University
The University of Chicago
University of Cincinnati
Illinois Institute of Technology
University of Illinois
Indiana University
Iowa State University
The University of Iowa
Kansas State University
The University of Kansas
Loyola University
Marquette University
Michigan State University
The University of Michigan
University of Minnesota
University of Missouri
Northwestern University
University of Notre Dame
The Ohio State University
Ohio University
The Pennsylvania State University
Purdue University
Saint Louis University
Southern Illinois University
University of Texas
Washington University
Wayne State University
The University of Wisconsin

## LEGAL NOTICE

This report was prepared as an account of Government sponsored work. Neither the United States, nor the Commission, nor any person acting on behalf of the Commission:

A. Makes any warranty or representation, expressed or implied, with respect to the accuracy, completeness, or usefulness of the information contained in this report, or that the use of any information, apparatus, method, or process disclosed in this report may not infringe privately owned rights; or

B. Assumes any liabilities with respect to the use of, or for damages resulting from the use of any information, apparatus, method, or process disclosed in this report.

As used in the above, "person acting on behalf of the Commission" includes any employee or contractor of the Commission, or employee of such contractor, to the extent that such employee or contractor of the Commission, or employee of such contractor prepares, disseminates, or provides access to, any information pursuant to his employment or contract with the Commission, or his employment with such contractor.

Printed in the United States of America
Available from
Clearinghouse for Federal Scientific and Technical Information
National Bureau of Standards, U. S. Department of Commerce
Springfield, Virginia 22151
Price: Printed Copy $3.00; Microfiche $0.65

ANL-7548
Reactor Technology

ARGONNE NATIONAL LABORATORY
9700 South Cass Avenue
Argonne, Illinois 60439

# REACTOR DEVELOPMENT PROGRAM PROGRESS REPORT

January 1969

Robert B. Duffield, Laboratory Director
Stephen Lawroski, Associate Laboratory Director

| Division | Director |
|---|---|
| Chemical Engineering | R. C. Vogel |
| EBR-II Project | M. Levenson |
| Metallurgy | M. V. Nevitt |
| Reactor Engineering | L. J. Koch |
| Reactor Physics | R. Avery |

Report coordinated by
L. B. Fosdick and A. Glassner

Issued February 28, 1969

## FOREWORD

The Reactor Development Program Progress Report, issued monthly, is intended to be a means of reporting those items of significant technical progress which have occurred in both the specific reactor projects and the general engineering research and development programs. The report is organized in accordance with budget activities in a way which, it is hoped, gives the clearest, most logical overall view of progress. Since the intent is to report only items of significant progress, not all activities are reported each month. In order to issue this report as soon as possible after the end of the month editorial work must necessarily be limited. Also, since this is an informal progress report, the results and data presented should be understood to be preliminary and subject to change unless otherwise stated.

The issuance of these reports is not intended to constitute publication in any sense of the word. Final results either will be submitted for publication in regular professional journals or will be published in the form of ANL topical reports.

The last six reports issued
in this series are:

| | |
|---|---|
| July 1968 | ANL-7478 |
| August 1968 | ANL-7487 |
| September 1968 | ANL-7500 |
| October 1968 | ANL-7513 |
| November 1968 | ANL-7518 |
| December 1968 | ANL-7527 |

## REACTOR DEVELOPMENT PROGRAM

### Highlights of Project Activities for January 1969

#### EBR-II

A scheduled extended shutdown of the reactor for maintenance and installation of plant modifications began after Run 32 had been completed on January 2. Maintenance and modifications are proceeding on schedule. At the time of the shutdown, the reactor had accumulated a total of 22,765 MWd of operation.

Initial steps were taken to phase out remote processing and fabrication of fuel in the FCF hot line. All fuel for EBR-II will be made in the FCF cold line and by a commercial vendor. FCF activities will emphasize postirradiation examination, experimental support, and reactor support. The acceptance rate for vendor-produced fuel continued to improve; it reached 100% for some batches. A total of 5551 elements had been received from the vendor as of January 15.

The first tagging of unencapsulated mixed-oxide fuel elements with a mixture of xenon isotopes was accomplished by General Electric Co. with ANL consultation.

#### ZPPR

ZPPR continues to be in operational readiness awaiting approval for operation. The past month has been spent in training personnel and getting them familiar with systems operation.

Nonoperational efforts on Doppler equipment, the data-collection system, and the counting-room computer are continuing.

#### ZPR-3

Assembly 56A of ZPR-3 was loaded with the inner radial reflector, axial reflector, and core having the composition of the FTR Resumed Phase-B Critical Program, Assembly I. Critical mass and control-rod worths were determined. The assembly is being modified by the substitution of a combination of nickel and sodium for the present iron outer reflector. Minor additional changes are being made to the core in order to produce greater geometrical regularity, and to the present safety rods and adjacent columns in order to obtain more uniform local core composition.

#### ZPR-6 and -9

Although the work of the electrical contractor in the conversion of the ZPR-6 and -9 facilities to plutonium operation is nearing completion, some weeks remain before the reactors will be able to operate. The reactor cooling-system installation is about to begin, and tests of the confinement cell leakage and the efficiency of the sand filters will be made in the intervening period.

TABLE OF CONTENTS


| | Page |
|---|---|
| I. LIQUID METAL FAST BREEDER REACTORS--CIVILIAN | 1 |
| A. Fuel Development--LMFBR | 1 |
| 1. Oxide | 1 |
| 2. Carbide | 3 |
| B. Physics Development--LMFBR | 4 |
| 1. Theoretical Reactor Physics | 4 |
| 2. Experimental Reactor Physics | 12 |
| 3. ZPR-3 Operations and Analysis | 16 |
| 4. ZPR-6 and -9 Operations and Analysis | 18 |
| 5. ZPPR Operations and Analysis | 26 |
| C. Component Development--LMFBR | 28 |
| 1. Reactor Mechanism and Instrumentation | 28 |
| 2. Fuel Handling, Vessels, and Internals--Core Component Test Loop | 32 |
| D. Systems and Plant--LMFBR | 33 |
| 1. 1000-MWe Plant | 33 |
| E. EBR-II | 34 |
| 1. Research and Development | 34 |
| a. Reactor Experimental Support--Reactor Analysis and Testing | 34 |
| b. Nuclear Analysis Methods Development | 44 |
| c. Equipment--Fuel Related | 45 |
| d. New Subassemblies Design and Experimental Support | 47 |
| e. Instrumented Subassembly | 47 |
| f. Packaged Loop | 48 |
| g. Process Chemistry | 48 |
| h. Experimental Irradiation and Testing | 50 |
| i. FCF Equipment Improvement | 51 |
| j. Superheater and EM Pump Study and Test | 51 |
| k. Feasibility Study of Fuel Failure Detection--Chemical and Mechanical Methods | 53 |
| l. Materials-Coolant Compatibility | 54 |
| m. Driver Fuel Transient Performance Studies--TREAT Experiments | 55 |
| n. Leak Detection and Location--Xenon Method | 55 |
| o. Oxide Driver | 57 |

TABLE OF CONTENTS


| | Page |
|---|---|
| 2. Operations | 58 |
| a. Reactor Plant | 58 |
| b. Fuel Cycle Facility Operations | 62 |
| PUBLICATIONS | 77 |
| II. OTHER FAST REACTORS--CIVILIAN--OTHER FAST BREEDER REACTORS | 78 |
| A. Fuel Development | 78 |
| 1. Other Fuel Jacket Alloy Studies | 78 |
| III. GENERAL REACTOR TECHNOLOGY | 82 |
| A. Applied and Reactor Physics Development | 82 |
| 1. Theoretical Reactor Physics--Research and Development | 82 |
| 2. Nuclear Data--Research and Development | 83 |
| B. Reactor Fuels and Materials Development | 88 |
| 1. Fuels and Cladding | 88 |
| 2. Radiation Damage on Structural Materials--Research and Development--In-Reactor Creep Studies | 92 |
| 3. Techniques of Fabrication and Testing--Research and Development | 95 |
| C. Engineering Development | 98 |
| 1. Research and Development | 98 |
| D. Chemistry and Chemical Separations | 105 |
| 1. Aqueous and Volatility Processes--Research and Development--Fluoride Volatility Process | 105 |
| 2. Closed Cycle Processes--Research and Development--Compact Pyrochemical Processes | 107 |
| 3. General Chemistry and Chemical Engineering--Research and Development | 111 |
| PUBLICATIONS | 113 |

TABLE OF CONTENTS


| | Page |
|---|---|
| IV. NUCLEAR SAFETY | 115 |
| A. Reactor Kinetics--Other Reactor Kinetics--Research and Development | 115 |
| 1. Accident Analysis and Safety Evaluation | 115 |
| 2. Reactor Control and Stability | 116 |
| 3. Coolant Dynamics | 117 |
| 4. Core Structural Safety | 119 |
| 5. Fuel Meltdown Studies with TREAT | 122 |
| 6. Materials Behavior and Energy Transfer | 128 |
| 7. Fast Reactor Safety Test Facility Study | 130 |
| B. TREAT Operations | 130 |
| 1. Reactor Operations | 130 |
| 2. Development of Automatic Power Level Control System | 131 |
| PUBLICATIONS | 132 |

# I. LIQUID METAL FAST BREEDER REACTORS--CIVILIAN

## A. Fuel Development--LMFBR

### 1. Oxide

#### a. Fuel Studies

##### (i) Fuel Element Performance (L. A. Neimark, F. L. Brown, R. Natesh, and W. F. Murphy)

Last Reported: ANL-7527, pp. 1-2 (Dec 1968).

Relating calculated fuel temperatures to observed microstructures in Elements HOV-15, SOV-3, SOV-7, and TVOV-1 has proved to be difficult because of the irradiation history of these elements. Initial operation at the EBR-II power level of 45 MW apparently caused fuel melting in the center regions of these elements. Subsequent restructuring and the improvement of both the effective thermal conductivity of the fuel and the fuel-cladding interface conductance (at the power level of 45 MW) would change the temperature profile from that at the initial conditions; the extent of fuel melting would decrease, and further restructuring would occur in the form of columnar-grain growth toward the center of the element. Also, axial convective mixing in the molten fuel would tend to reduce the axial temperature gradients in the molten fuel and thus yield a more uniform axial boundary of melting. A more or less uniform boundary is indicated by the microstructures of these elements. Clear delineation of this boundary is tenuous, however, because further restructuring occurred during the last few days these elements were under irradiation, while the reactor was operated at 30 MW or less. In HOV-15, this later-stage restructuring was most prominent at the midplane of the element and decreased at the ends. Efforts will continue to establish the temperature profiles in these elements at various stages during irradiation.

Further examination of the fuel-cladding interface of Element SOV-3 by means of a shielded microprobe revealed the presence of cesium in the stainless steel cladding to a depth of at least 60 $\mu$. The area examined in SOV-3 was from the midplane of the fuel column, and the calculated temperature at the fuel-cladding interface at this location was 600°C. Cesium-rich regions, 6 to 12 $\mu$ thick, were found at the fuel-cladding interface. Within the cladding, cesium was present in the grain boundaries, predominantly at grain-boundary triple points. The microprobe examination is continuing.

Fabrication of 15 of the 19 $(U_{0.8}Pu_{0.2})O_2$ fuel elements for the Group 0-3 irradiation experiment in EBR-II has been completed. The

Group 0-3 experiment was designed to study fuel-swelling accommodation by various means of void deployment, including distributed porosity in solid pellets, distributed porosity around packed spherical and angular powders, and the fuel-cladding gap. The effect of restraint on swelling accommodation by Types 304, 316, and 318 stainless steels also is being investigated. Table I.A.1 lists the nominal design parameters of the fuel elements in Group 0-3. The elements will be irradiated at a nominal peak linear power rating of 14 kW/ft to maximum burnups of 80,000 MWd/MT, with interim dimensional inspections at approximately 35,000 and 60,000 MWd/MT. Some elements will also be destructively examined at these burnups.

TABLE I.A.1. Nominal Design Parameters of Group 0-3 Fuel Elements

| No. of Elements | Fuel Form | Fuel Material | Type of Stainless Steel Cladding | Cladding Thickness (in.) | Fuel-cladding Gap (in.) | Smear Density (%) |
|---|---|---|---|---|---|---|
| 4 | Vipac | Dynapak | 304 | 0.020 | - | 80 |
| 2 | Vipac | Sol-gel | 304 | 0.015 | - | 80 |
| 2 | Vipac | Sol-gel | 316 | 0.015 | - | 80 |
| 1 | Vipac | Sol-gel | 318 | 0.015 | - | 80 |
| 2 | Pellet | Coprecipitated | 304 | 0.015 | 0.0025 | 80 |
| 2 | Pellet | Coprecipitated | 304 | 0.015 | 0.0025 | 84 |
| 2 | Pellet | Coprecipitated | 304 | 0.015 | 0.0075 | 77 |
| 2 | Pellet | Coprecipitated | 316 | 0.015 | 0.0025 | 84 |
| 2 | Pellet | Coprecipitated | 318 | 0.015 | 0.0025 | 84 |

The completed elements include five that contain vibratorily compacted Sol-gel spheres and ten that contain solid pellets. Four elements are being loaded with vibratorily compacted angular particles of Dynapak fuel. Preirradiation measurements (weight, volume, diameter, length, bow, and balance point) are now being made of the fabricated elements, and work is progressing on the EBR-II Safety Evaluation Report.

(ii) Compatibility between Uranium-Plutonium Oxide and Cladding Alloys (T. W. Latimer)

Last Reported: ANL-7518, p. 4 (Nov 1968).

Heat treatments of three compatibility couples have been completed, and the specimens are being prepared for metallographic examination and microhardness measurements. One couple consists of unalloyed vanadium (containing 520 ppm oxygen) in contact with $(U_{0.8}Pu_{0.2})O_{1.97}$ for 1000 hr at 800°C. The other two couples consist of V-15 w/o Cr-5 w/o Ti and V-10 w/o Cr in contact with $(U_{0.8}Pu_{0.2})O_{1.97}$ for 1000 hr at 700°C. These measurements and the results of six previous compatibility tests (see Progress Report for October 1968, ANL-7513, Fig. I.A.2, p. 3) are expected to elucidate the effects of alloying elements and temperature on the diffusion of oxygen from the fuel to the cladding.

## 2. Carbide

### a. Fabrication and Evaluation

#### (i) Fuel Element Performance (L. A. Neimark and T. W. Latimer)

Last Reported: ANL-7527, pp. 2-4 (Dec 1968).

Mass-spectrometric analysis of the fission gases recovered from the plenum of Element HMV-5 indicates a release of 18.1% of the calculated amount of gas generated. This amount agrees well with a release of 16.6% found for Element SMV-2. (This value for SMV-2 is slightly higher than the amount reported in ANL-7527, owing to a correction in the calculated amount of gas generated.) The fuel in both elements was a vibratorily compacted physical mixture of UC and PuC particles. The elements achieved an estimated burnup of 7.2 a/o.

The gas in the plenum of Element NMV-11 was sampled in an attempt to locate more fission gas than the small amount released to the plenum of the irradiation capsule through the large cracks in the fuel cladding. Initially we believed that no fission gas could be obtained from an element plenum which contained numerous longitudinal cracks in the cladding over the fuel section. However, an insufficient amount of helium cover gas had been recovered from the capsule plenum to account for the helium that was originally in both the capsule and element plenums. If a passage existed between the two plenums at the time the capsule was sampled, a larger quantity of gas should have been found. The sampling of the element plenum was undertaken even though metallographic sections had already been removed from the element; only 1 in. of fuel remained attached to the plenum section. The open end of the fuel was sealed with epoxy before sampling.

Surprisingly, the pressure in the element plenum, when sampled, was 1.35 atm; the gas consisted primarily of helium (the cover gas in the element), xenon, and krypton. The fission gas amounted to an additional 1.0% of the amount generated; previously 1.5% was found in the capsule plenum. The helium and a small quantity of argon (from welding) accounted for virtually all of the cover gas originally in the element plenum. These results might indicate that at the time of failure of the element, no gas passage existed between the plenum and fuel regions. However, the calculated pressure in the capsule plenum of 1.30 atm was virtually the same as that in the element plenum, which indicates that the two plenums might have been at pressure equilibrium. In that event, blockage of the gas passage between the element plenum and the fuel section would have occurred after the element failed. A metallographic examination of the plenum-fuel interface will be made to determine the nature of the apparent obstruction in this area.

## B. Physics Development--LMFBR

### 1. Theoretical Reactor Physics

#### a. General Fast Reactor Physics (H. H. Hummel)

##### (i) Correlation, Evaluation, and Interpretation of Integral Data

Last Reported: ANL-7500, p. 5 (Sept 1968).

(a) Changes to ENDF/B Cross Sections in the Energy Range from 26 keV to 3.5 MeV. Further calculations have been made to determine the influence of changing ENDF/B cross sections to the values of various "consistent" sets for $^{235}U$ $\sigma_f$, $^{238}U$ $\sigma_c$, and $^{239}Pu$ $\sigma_f$.

(1) Cross-section Sets Used. These consistent cross-sections sets, which are discussed in ANL-7500 and by Kallfelz and Poenitz,* can be described briefly as follows:

Sets 1-3: These sets are based on series of measurements using three different experimental methods and standards. Set 1, which has the highest values, generally agrees most closely with the ENDF/B values.

Set 4: This is a weighted average of Sets 1-3.

In Figs. I.B.1 and I.B.2 the values of these sets along with those of ENDF/B are shown for $^{235}U$ $\sigma_f$ and $^{238}U$ $\sigma_c$. The percents shown at the bottom of the figures are the "uncorrelated errors" described in ANL-7500.

Two further sets have been defined as follows:

Set 4 Adjusted: All values as in Set 4, except that the $\sigma_f$ and $\sigma_c$ values for $^{239}Pu$ are raised to the upper uncorrelated error limit, and the $^{238}U$ $\sigma_c$ is reduced to the lower uncorrelated error limit.

Set 4 Adjusted B: Same as Set 4 Adjusted, except that $\sigma_f$ and $\sigma_c$ for $^{235}U$ and $^{238}U$ $\sigma_f$ values are raised to the upper uncorrelated error limit. After the adjustments, the $^{238}U$ $\sigma_\gamma$ are close to those for Set 3, whereas the $^{239}Pu$ and $^{235}U$ $\sigma_f$ values are about midway between those for Set 1 and Set 4.

---

*Kallfelz, J. M., and Poenitz, W., in Reactor Physics Division Annual Report, 1967-1968, ANL-7410.

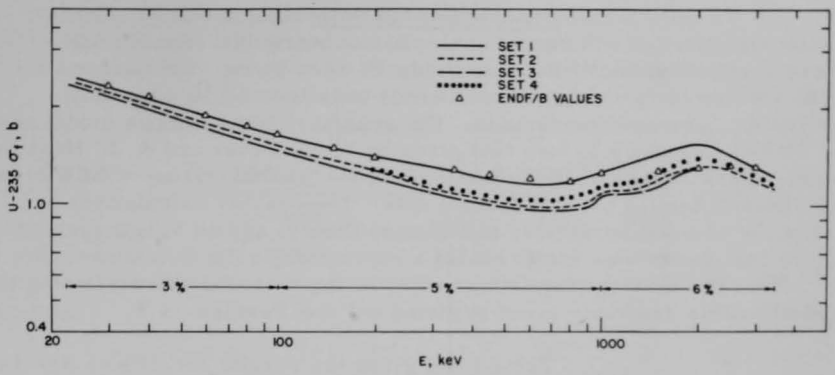


Fig. I.B.1. Fission Cross Section of $^{235}U$ for Various Sets. Below 200 keV, Set 4 coincides with Set 2. The percentages at the bottom of the figure are the estimated uncorrelated uncertainties for Set 4.

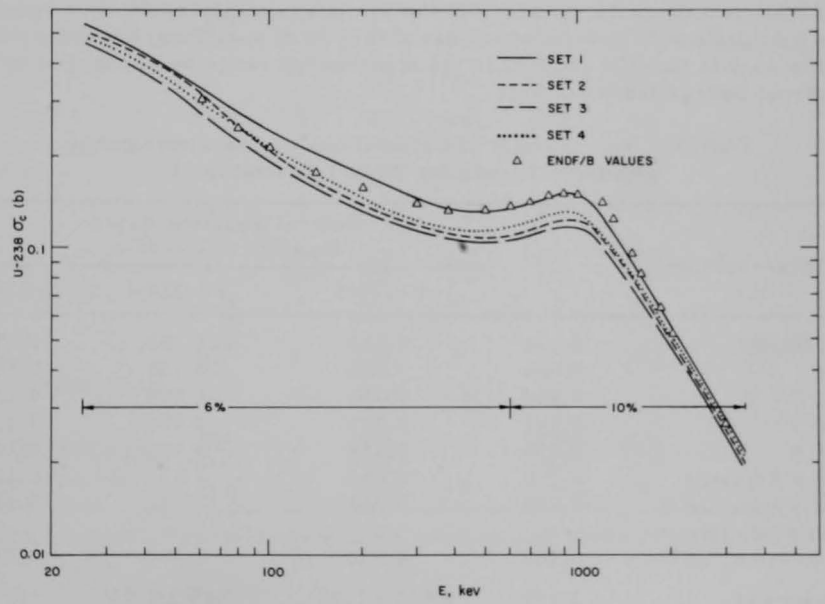


Fig. I.B.2. Capture Cross Section of $^{238}U$ for Various Sets. The percentages at the bottom of the figure are the estimated uncorrelated uncertainties for Set 4.

(2) Reactor Calculations. The methods of cross-section preparation and reactor calculations were described in ANL-7500, where results for the ZPR-3 Assembly 48 were given. Calculations for ZPR-3 Assembly 11 and the Los Alamos unreflected $^{235}U$ assembly "GODIVA" have been performed. The spherical homogeneous model used for ZPR-3 Assembly 11 was that given by W. G. Davey and A. L. Hess to the members of the Cross Section Evaluation Working Group (CSEWG) for the Phase-II testing of the ENDF/B data. The reactor calculations for Assembly 11 were performed in diffusion theory, and an $S_4$ transport-theory calculation was run to obtain a correction to the diffusion-theory k of +1.7%. The Godiva calculations were in $S_{16}$ transport theory, using the model for this assembly given by Hemment and Pendlebury.*

Table I.B.1 gives the results for ZPR-3 Assembly 11. Table I.B.2 compares all results, including those already reported in ANL-7500, with experiment. The terms good, fair, and poor used in Table I.B.2 to describe the agreement "grade" are, of course, somewhat subjective. The approximate limits on the percent difference, (calc-exp) for each of the "grades," was chosen differently for different columns of the table to reflect the accuracy of the various parameters.** For some of the calculations of Godiva, which has a very hard spectrum, the somewhat outdated data for $^{235}U$ and $^{238}U$ in the high-energy range were changed to those of Davey† above 2.2 MeV.

TABLE I.B.1. Results of Calculations in One-dimensional Diffusion Theory for ZPR-3 Assembly 11

| Cross-section Set | k | Central Reaction Rates Relative to U-235-f | | |
|---|---|---|---|---|
| | | U-238-f | Pu-239-f | U-238-c |
| ENDF/B | 0.974 | 0.033 | 1.103 | 0.121 |
| Set 1 | 0.966 | 0.036 | 1.130 | 0.127 |
| Set 2 | 0.938 | 0.033 | 1.109 | 0.125 |
| Set 3 | 0.941 | 0.033 | 1.103 | 0.121 |
| Set 4 | 0.953 | 0.034 | 1.111 | 0.123 |
| Set 4 Adjusted | 0.966 | 0.034 | 1.177 | 0.166 |
| Set 4 Adjusted B | 0.989 | 0.034 | 1.132 | 0.111 |
| ENDF/B, except U-238 $\sigma_c$ of Set 4 | 0.992 | 0.032 | 1.101 | 0.112 |
| Measured | 1.000 | 0.038 ± 0.001 | 1.19 ± 0.02 | - |

*Hemment, P. C. E., and Pendlebury, E. D., Proceedings of International Conference on Fast Critical Experiments and Their Analyses, October 11-13, 1966, ANL-7320, p. 88.

**For example, for Assembly 48, a plutonium assembly, the lower limits for each "grade" for the calculated $k_{eff}$ were higher than for the other assemblies, to reflect the fact that the ENDF/B plutonium-α may be too low in the low-keV range (ANL-7500). An increased plutonium-α would decrease $k_{eff}$.

†Davey, W. G., Nucl. Sci. Eng. 32, 33 (1961).

TABLE I.B.2. Summary of Agreement between Calculation and Experiment. G, f, and p correspond to good, fair, and poor agreement (see text). Numbers are percent difference, (Calc-exp)/exp. Reaction ratios are for center of assembly.

| Cross-section Set | ZPR-3 Assembly 11 | | ZPR-3 Assembly 48 | | | | GODIVA |
|---|---|---|---|---|---|---|---|
| | k | $\frac{239f}{235f}$ (1%)[b] | k | $\frac{239f}{235f}$ (1%)[b] | $\frac{238c}{239f}$[a] (6%)[b] | $\frac{238c}{235f}$ (5%)[b] | k |
| ENDF/B | p<br>-2.4 | p<br>-7 | p<br>-1.3 | f<br>-5 | f<br>+8 | G<br>+3 | p (G)[c]<br>+2.1 (+0.8) |
| Set 1 | p<br>-3.4 | f<br>-5 | G<br>-0.1 | f<br>-3 | f<br>+10 | f<br>+6 | |
| Set 2 | p<br>-6.2 | p<br>-7 | p<br>-4.2 | f<br>-5 | p<br>+12 | f<br>+6 | |
| Set 3 | p<br>-5.9 | p<br>-7 | p<br>-4.5 | p<br>-6 | f<br>+10 | G<br>+4 | |
| Set 4 | p<br>-4.7 | p<br>-7 | p<br>-2.7 | f<br>-5 | f<br>+10 | G<br>+5 | p<br>-2.7[c] |
| Set 4 Adjusted | p<br>-3.4 | G<br>-1 | G<br>±0.5 | G<br>-1 | G<br>+2 | G<br>+1 | |
| Set 4 Adjusted B | G<br>-1.1 | f<br>-5 | G<br>+0.8 | f<br>-3 | G<br>+2 | G<br>-1 | G<br>+0.1 |
| ENDF/B except U-238-c Set 4 | G<br>-0.8 | p<br>-7 | G<br>-0.3 | f<br>-5 | G<br>+5 | G<br>0 | |

[a] "Experimental" value derived from ratio of both these reactions to $^{235}U$ fission.

[b] Experimental accuracy.

[c] ENDF/B cross-section values for $^{235}U$ and $^{238}U$ above 2.2 MeV changed to those of W. G. Davey, Nucl. Sci. Eng. 32, 33 (1968).

For the ENDF/B set and Sets 1-4, the ratios of $^{238}U$ $\sigma_c$ to the important fission cross sections are about the same. For Assembly 48, Set 4 Adjusted, which increases the ratio of $^{239}Pu$ $\sigma_f$ relative to $^{238}U$ $\sigma_c$, gives greatly improved agreement compared to the previous sets. Set 4 Adjusted B, for which the ratio of $^{235}U$ $\sigma_f$ to $^{238}U$ $\sigma_c$ was also increased over the previous sets, also gives good agreement for the $k_{eff}$ of Assembly 11 (a $^{235}U$ core). The last line of Table I.B.2 gives results for calculations in which only the $^{238}U$ $\sigma_c$ was lowered from the ENDF/B values. Although for this case the important fissile element cross sections were all 5-10% higher than for Set 4 Adjusted B, the ratios of the $^{238}U$ capture cross section to the important fission cross sections for this calculation were about the same as for Set 4 Adjusted B, and the agreement with experiment was about as good.

Thus the calculations to date indicate that the ratio of $^{238}U$ capture to $^{235}U$ and $^{239}Pu$ fission in ENDF/B is too high. It cannot, of course, be firmly concluded that this ratio is too high, since the calculations to date were only for three assemblies. To gather more evidence, calculations are now underway with several consistent sets for the ten critical assemblies designated for the next phase of the ENDF/B testing, described in the next section.

(b) Testing of ENDF/B Data. For the next phase of the integral data testing of the ENDF/B cross sections, ten fast reactor critical experiments were selected.[See Sect. I.B.2.a.(ii)]. Cross-section sets for these assemblies have been calculated with $MC^2$, and the transport theory calculations of the assemblies are now being performed. These assemblies will also be used for the testing of consistent cross-section sets for the fissile elements.

b. Fast Critical Experiments--Theoretical Support (R. G. Palmer)

Last Reported: ANL-7518, p. 11 (Nov 1968).

(i) Empirical Approach to Self-shielding in ZPR Lattices. In ANL's ZPR assemblies, isotopes in which resonance absorption occurs exist in more than one form, e.g., uranium occurs as $U_3O_8$, U, and Pu-U-Mo alloy, and these are often arranged in uneven spacing. Such complicated lattices are not amenable to direct treatment by the two-region equivalence approximations which includes black-absorber Dancoff factors allowing only one type of absorbing plate per unit cell. No analytical techniques have been derived for multiple absorber systems, and the problem does not seem tractable. Numerical methods are available, for example, the computer codes RABID and RABBLE, but these are too time-consuming for general use.

An empirical approach to the problem is being investigated using numerical RABID calculations to test the quality of the empirical

calculations. To simplify the problem, the range of absorber concentrations is being limited to those in the range of the ZPR component plates, i.e., ratios of 10 to 1. Good results have been achieved for a two-absorber plate system of the form AMBMAMB..., where A and B are the two absorber plates of differing concentrations, and M is a diluent. The rationale of this approach is to fine the AM'AM'A... lattice which produces the identical flux shadowing on an A plate that it receives in the actual lattice with unit cell AM BM. For example, if the absorber concentration in B is greater than that in A, the diluent region M' would be correspondingly reduced in thickness compared to M. The approach is now being extended to three types of absorber plates.

(ii) Heterogeneity Code. The heterogeneity effect in plate-type fast reactor cells may be obtained by a perturbation calculation starting with homogeneous fluxes, adjoints, and group-dependent bucklings. The CALHET Code can be used for this task. In the original code, collision probabilities are obtained by numerical integration (Simpson's Rule). A revised version is now available for the CDC-1604 computer; standard XLIBIT cross-section sets are accepted, and collision probabilities (using Gauss Quadrature and Euler's Summation Formula) can be calculated more than one hundred times more accurately and more than one hundred times faster using techniques developed for the RABID code. A 24-group, 10-region problem has the following computing times on the CDC-1604:

| | Collision Probabilities (sec) | All Other Calculations (sec) | Total (sec) |
|---|---|---|---|
| Original | 8000 | 345 | 8345 |
| Modified | 65.5 | 345 | 410.5 |

(iii) Resonance Absorption in Multiplate Reactor Cells by Integral Transport Theory. A tractable approach to the computation of resonance absorption, average neutron fluxes, and group cross sections for multiplate fast reactor cells of the ZPR-3 type has been recently developed.* It is the purpose of this summary to show how two important restrictions on the method of calculation of collision rates of monoenergetic neutrons in infinite slab geometry can be relaxed or eliminated.

If scattering is assumed to be isotropic in the laboratory system, the neutron current at a distance $\tau$ mean free paths from an infinite plane parallel plate of optical thickness $\tau_1$ within which the source of uncollided monoenergetic neutrons varies linearly as

*Olson, Arne P., Trans. Am. Nuc. Soc. 11(1), 301 (1968).

$$S(x) = \bar{S} + (x - \bar{t}_1)\frac{\Delta S}{t_1}$$

is

$$\vec{J}(\tau,\tau_1) = \frac{1}{2t_1}\int_0^{t_1} S(x)E_2\left[\tau + \frac{\tau_1}{t_1}(t_1 - x)\right]dx = \frac{\bar{S}}{2\tau_1}[E_3(\tau) - E_3(\tau_1 + \tau)]$$

$$+ \frac{\Delta S}{2\tau_1}[1/2\{E_3(\tau) + E_3(\tau_1 + \tau)\} - \frac{1}{\tau_1}\{E_4(\tau) - E_4(\tau_1 + \tau)\}], \tag{1}$$

where $t_1$ is the plate thickness and

$$E_n(z) = \int_1^{\infty} \frac{\exp(-zu)}{u^n}\,du$$

is the exponential integral of order n. From Eq. (1), the collision rate in a second slab of optical thickness $\tau_2$ separated by $\tau$ mean free paths from the first slab is

$$C(1 \to 2) = \vec{J}(\tau,\tau_1) - \vec{J}(\tau + \tau_2,\tau_1). \tag{2}$$

The assumption of an infinite array of unit cells of optical thickness h leads to

$$C_\infty(1 \to 2) = \sum_{k=0}^{\infty} [\vec{J}(\tau + kh,\tau_1) - \vec{J}(\tau + \tau_2 + kh,\tau_1)]. \tag{3}$$

Evaluation of Eq. (3) is enabled by the asymptotic behavior of the $E_n$ functions:

$$E_n(z) \to \frac{\exp(-z)}{z + n}, \qquad z \gg 1. \tag{4}$$

For example, the summation formula for a geometric series gives

$$\sum_{k=0}^{\infty} E_n(z + kh) \simeq \frac{E_n(z)}{1 - R}, \tag{5}$$

where

$$R = (z + n)\exp(-z)/(z + n + h) \tag{6}$$

is the asymptotic ratio of successive terms.

In contrast to the exact result given by Eq. (3), the approximate method used by Olson assumes a spatially flat source within a given region. It also assumes that the angular neutron current at slab interfaces has the form

$$j(\theta) = A_1 \cos\theta + A_2 \cos^2\theta, \tag{7}$$

where $\theta$ is the polar angle.

For simple unit cells composed of a few plates, subdividing each plate effectively eliminates errors due to the flat-source assumption. On the other hand, many fast reactor core mockups have had very complicated unit cells. Limitations on core storage may necessitate fewer spatial regions and inclusion of a linear source variation to retain and improve computational accuracy.

A simple test problem has been examined in some detail in order to evaluate errors in relative thin-foil activations as obtained by different degrees of approximation. The 5.08-cm-wide unit cell consisted of a 0.635-cm $^{239}$Pu plate, the remainder being graphite, with a resonant absorber foil centered 1.905 cm from the $^{239}$Pu plate and foil 2 placed adjacent to the $^{239}$Pu plate. The results compiled in Table I.B.3 indicate average errors in foil-activation ratios of about 3.5% for the Kier method, using the two-term current approximation. The small errors given for the one-term approximation are fortuitous. Other problems indicate errors in excess of 4%. Although these errors are not large, relative experimental foil activations can be obtained to 1% accuracy. The exact treatment of collision rates yields a significant gain in accuracy with only a 20% increase in computation time for this test problem.

TABLE I.B.3. Foil-activation Ratio $R_1/R_2$ from 35.9 to 46.4 eV (% error)

| Method: | $A_1 \cos\theta$ | $A_1 \cos\theta + A_2 \cos^2\theta$ | | | Exact | | | |
|---|---|---|---|---|---|---|---|---|
| No. of Regions: | 20 | 4 | 10 | 20 | 5 | 7 | 10 | 13 |
| Foil Thickness (cm) | | | | | | | | |
| 0.01016 | | 0.5758 (4.4) | 0.5738 (4.1) | 0.5749 (4.3) | 0.5555 (0.7) | 0.5542 (0.5) | - | 0.5514 (0) |
| 0.00508 | | 0.5819 (4.0) | 0.5800 (3.6) | 0.5817 (3.9) | 0.5631 (0.6) | 0.5628 (0.6) | - | 0.5597 (0) |
| 0.00254 | 0.5689 (0.4) | 0.5913 (3.5) | 0.5894 (3.2) | 0.5920 (3.6) | 0.5746 (0.6) | 0.5750 (0.6) | 0.5717 (0.1) | 0.5714 (0) |
| 0.00127 | 0.5821 (0.1) | 0.5981 (2.6) | 0.5962 (2.3) | 0.5998 (2.9) | 0.5846 (0.3) | 0.5855 (0.5) | 0.5821 (0.1) | 0.5827 (0) |

## 2. Experimental Reactor Physics

### a. Fast Critical Experiments--Experimental Support (Idaho) (W. G. Davey)

Last Reported: ANL-7527, pp. 7-8 (Dec 1968).

(i) Neutron Spectrometry. The data from the proton-recoil neutron spectrum measurement with ZPR-3 Assembly 55 have been compared in Fig. I.B.3 with the results of an $MC^2$ calculation. The output of the $MC^2$ code has smoothed through a Gaussian window corresponding to the resolution of the proportional counter and was normalized to the data over the energy range of 1 keV to 1 MeV. There is general agreement between the theory and experiment except at 30 keV and above 1 MeV. The discrepancy at 30 keV was also seen in a comparison for Assembly 53.

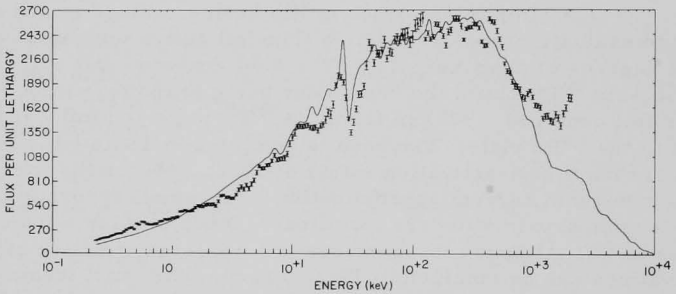


Fig. I.B.3. Comparison of Experimental and Calculated Neutron Spectrum of ZPR-3 Assembly 55

(ii) Integral Studies of Cross Sections. Efforts continued in behalf of the Cross Section Evaluation Working Group for the integral data testing of ENDF/B with fast reactor critical data. Specifications for the ten fast reactor benchmarks were finalized. These include critical dimensions for homogeneous spheres, central fission ratios, and central worths of materials. Results of analyses of two of the benchmarks, Assemblies 48 and 11, are being received from a number of national laboratories and industrial contractors, and a review of these results is underway. There are preliminary indications of satisfactory agreements between the multigroup libraries prepared from ENDF/B at the various agencies, but also some anomalies occur between the results of the reactor calculations.

b. Fast Critical Experiments--Experimental Support (Illinois) (R. Gold)

(i) Neutron Spectrometry

Last Reported: ANL-7500, p. 15 (Sept 1968).

(a) Calibration of Ionization Scale for Proportional Counters. A basic requirement for neutron spectroscopy with proportional counters is the establishment of a calibration of ionization (ion pairs) versus pulse amplitude. For a fixed amount of ionization produced initially in the gas, the amplitude of the resulting pulse will depend upon all of the variables associated with counter design.

Studies relating gas multiplication A to these variables have been partially successful over limited ranges of each of the relevant parameters; the problem is one of considerable complexity, however, and no entirely adequate prescription exists. Usually, all of the mechanical features of a counter will be fixed during measurements. These include anode and cathode radii, and gas type and pressure. Voltage V may be permitted to vary, however, and an accurate relationship between A and V is indispensable.

In order to provide a calibration, some known source of ionization may be introduced and the amplitude of the resulting pulse (proportional to multiplication) observed as a function of counter voltage. If the source is highly ionizing, as is the case when the exoergic reaction (615 keV) of nitrogen with thermal neutrons is used, it will not be possible to follow the increase in A above about 500, at which appreciable space-charge saturation occurs. A complete mapping of A versus V will then have to be obtained from an extrapolation or, preferably, continued by use of a more weakly ionizing source.

In past experiments, a fit of calibration data to a function of the form $(\log A)/V$ versus $\log V$ was used to extend multiplication upward from the region of measurement with nitrogen. This representation was originally suggested by Diethorn.* However, subsequent work** revealed both the origin and approximate nature of this representation. Consequently, in using the Diethorn formula, one must expect an extrapolation error that increases as the range of extrapolation increases.

A better calibration can be achieved by using both a nitrogen source (615 keV) and an argon (electron emission at approximately 3 keV) source. When this is done and the entire result is plotted as

*Diethorn, W., A Methane Proportional Counter System for Natural Radiocarbon Measurements, NYO-6628 (1956).

**Gold, R., and Bennett, E. F., Electron Multiplication Process in Proportional Counters, Phys. Rev. 147, 201-213 (1966).

(log A)/V versus log V, an apparent discrepancy is observed. Multiplication increases more rapidly with voltage than predicted.

Joint argon-nitrogen calibrations have been made for a variety of counter types. No simple extrapolation law correlates all of these results, but an empirical approach, specifically determined for each counter, can be found that will permit an adequate extrapolation from low-A to high-A values.

The approach consists of fitting the data with a function of the form $(\log A)/V^x$ versus V. The joint argon-nitrogen results are used to find the value of x that minimizes mean square residuals. This "voltage power factor" is retained for fitting to nitrogen-only calibrations taken with counters of the same type (design, pressure, etc.).

For example, a counter (of 2.54-cm diameter with a 0.0254-mm-dia anode) filled with 80 psi of hydrogen containing 0.6% of both methane and nitrogen was calibrated with both a nitrogen and an argon source. The voltage power factor for minimized mean square residuals was 0.70. Using the value $x = 0.70$, that portion of the calibration made with nitrogen ($A < \sim 600$) was fit (by least squares) and the extrapolation to a multiplication of 8000 was made. Multiplication predicted by this extrapolation was within 1% of that measured.

In addition, a "Diethorn" formula fit was made using the $^{14}N$-produced region of the calibration and the extrapolation evaluated at higher values of A. At $A = 8000$ results were in disagreement with the measured multiplication by 14% (the "Diethorn" plot underpredicting A). At a somewhat lower value, $A = 1600$, the discrepancy was reduced to 4%, and it diminished further as multiplication decreased.

In summary, the Diethorn extrapolation causes a significant systematic underestimation of gas multiplication in extrapolating to high values of A. Lacking an adequate understanding of the multiplication process, one should use only calibrations that have been verified experimentally over the whole range of use to avoid systematic errors at high A.

c. Planning and Evaluation of FFTF Critical Assembly Experiments (D. Meneghetti)

Last Reported: ANL-7527, pp. 9-10 (Dec 1968).

(i) The Effect of Self-shielding on the Spatial-dependent Small-sample Worth of $^{10}B$. In Table I.B.4 of the August 1968 Monthly Report, ANL-7487, the experimental worth of $^{10}B$ in Ih/kg was reported as a function of radial position in the 2-P row in half 1 of ZPR-3 Assembly 51. Values of

worth were listed for two orientations of the fuel in the 2-P drawers. These values (for positive positions) are restated in columns two and three of Table I.B.4 for comparisons with calculations.

TABLE I.B.4. Comparison of Calculated and Experimental Radial Worths of $^{10}B$ in ZPR-3 Assembly 51

| Radial Distance from Reactor Centerline (cm)[a] | Experimental Worth[b] (Ih/kg) | | Calculated Worth (Ih/kg) | |
|---|---|---|---|---|
| | 2-P Row Normal | 2-P Row Rotated 90° | Diffusion-theory Perturbation | Self-shielding Included |
| 0 | -9647 | -9695 | -10940 | -10381 |
| 2.54 | -9597 | -9652 | -10859 | -10304 |
| 6.35 | -9193 | -9274 | -10508 | -9965 |
| 12.70 | -7939 | -8091 | -9288 | -8782 |
| 15.24 | -7276 | -7445 | -8718 | -8221 |
| 17.78 | -6574 | -6748 | -8078 | -7583 |
| 20.32 | -6024 | -6112 | -7449 | -6944 |
| 25.40 | -4710 | -4763 | -6475 | -5842 |
| 30.48 | -3988 | -4037 | -6514 | -5449 |
| 33.02 | -3643 | -3907 | -7378 | -5826 |
| 35.56 | -3439 | -3835 | -7773 | -5807 |
| 38.10 | -2733 | -3380 | -5481 | -4132 |
| 40.64 | -1901 | -2540 | -3229 | -2495 |
| 43.18 | -1113 | -1619 | -1902 | -1506 |
| 45.72 | -573 | -902 | -854 | -701 |
| 50.80 | -112 | -189 | -179 | -158 |
| 57.15 | 129 | 65 | -31 | -28 |
| 63.50 | 148 | 144 | - | - |
| 76.20 | 0 | 0 | - | - |

[a]Mean experimental core radius, 33.5 cm. Experimental radial core-reflector interface position at position of traverse, 35.9 cm.
[b]See ANL-7487.

The worth of $^{10}B$ as a function of radius has been computed by a perturbation method using the MACH 1 code and cross-section set 29001. These values appear in column four of Table I.B.4.

Group-dependent self-shielding factors were derived for the $^{10}B$ sample. It was considered to be an infinitely long, thin, hollow cylinder with an isotopic nonspace-dependent neutron flux impinging on its surface. The self-shielding factor was obtained for each energy group.* The worth values for $^{10}B$ corrected in this manner are given in column five of Table I.B.4. It can be seen that self-shielding is not negligible, especially in the relatively soft spectrum of the reflector.

*Dwark, J., Hoffmann, P. L., Hurwitz, H., Jr., and Clancy, E. F., Self-Shielding Factors for Infinitely Long Hollow Cylinders, KAPL-1262 (1955).

3. ZPR-3 Operations and Analysis (W. G. Davey and R. L. McVean)

Last Reported: ANL-7527, pp. 11-13 (Dec 1968).

a. Basic Studies of Plutonium Systems

(i) Assemblies 53 and 54. Reduction of data from experiments with Assemblies 53 and 54 is complete except for the Doppler measurements with Assembly 53. The results for the two assemblies indicate good consistency and no apparent problems.

Cross-section sets for heterogeneity studies of Assemblies 53 and 54 are being developed. A study of the effects of different delayed-neutron parameters in the two assemblies has been indicated. To this end, 24-group fluxes were obtained from MACH 1 for a spherical model of Assembly 53, and a test case for program SPECB (spectrum weighting of delayed neutron fractions) is being prepared.

b. Mockup Studies

(i) FFTF Critical Program. The loading of Assembly 56A has been completed. This assembly consists of a 91.59-cm-high cylindrical core surrounded by a 27.9-cm-thick axial blanket and two nominally 15-cm-thick radial reflector regions. The outer radial reflector was composed of iron loaded directly into the matrix. The inner radial reflector, axial reflector, and core have the composition of the FTR Resumed Phase-B Critical Program, Assembly I. These reflector regions contained a combination of nickel and sodium plates. The core contains plates of ZPPR fuel, $U_3O_8$, $Fe_2O_3$, sodium, and $Na_2CO_3$. The nominal compositions have been given in Progress Report for January 1968, ANL-7419, p. 11, and ANL-7527, p. 12.

The outline of the critical loading is shown in Fig. I.B.4. The core contained 374.2 kg plutonium and 333.5 kg of the fissile isotopes Pu-239, Pu-241, and U-235. There were three divergences from a uniform loading. First, the critical loading contained five drawers of core compositionless fuel (two on half 1 and three on half 2). The initial loading of the core consisted of drawers containing all materials except fuel, with the number of drawers in the core being the number expected to be needed to achieve criticality. The approach to criticality was made by adding the fuel in a stepwise enlargement of the fueled region. The five fuel-depleted core drawers in the final loading resulted when criticality was reached before the substitution had been made in all of the fuel-depleted drawers.

The second variance from the uniform loading consisted of the safety rods and three of the drawers surrounding each of them. It was necessary to load the safety rods more heavily than the normal drawers to

ensure that their total worth satisfied the $1\frac{1}{2}\% \Delta k/k$ requirement. This was done in such a way as to maintain the same average composition, as nearly as possible, in the affected drawers. The normal loading in drawer columns containing the safety rods included one axial column of fuel, whereas the adjacent columns each contained two columns of fuel. The loading of the safety rods was increased to four fuel columns by transferring one column from each of the adjacent drawers labeled "lightly loaded drawers." The compositions of each of the drawers will be published when the exact compositions of each region are determined.

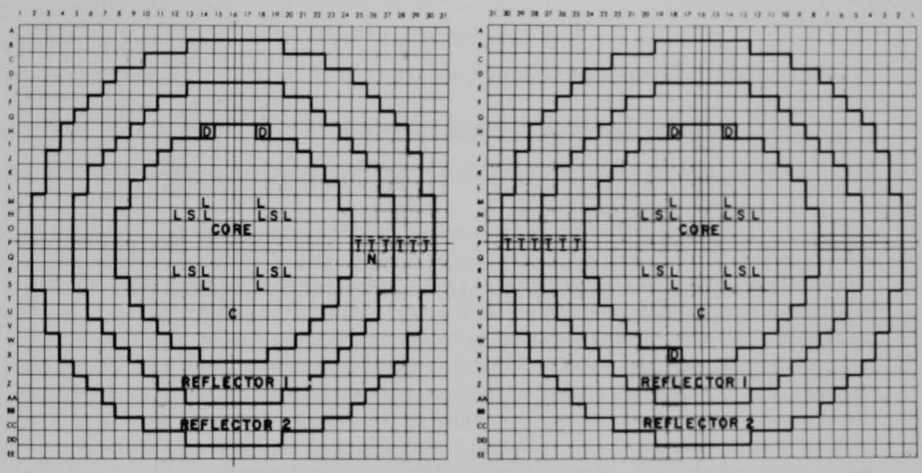


LOADING 56-9

S = SAFETY ROD C = CONTROL ROD L = LIGHTLY LOADED DRAWERS N = NEUTRON LEVEL DETECTOR
T = SOURCE TUBE DRAWERS D = CORE DRAWERS WITH NO FUEL

Fig. I.B.4. Critical Loading for ZPR-3 Assembly 56A

The final variation from a uniform loading is the presence of the startup source tubes in the radial blanket and the neutron-level detector in the inner reflector of half 1.

The primary purposes of Assembly 56A are to verify the prediction that the critical mass is below the 430-kg limit for ZPR-3 loadings and that the experimental program for Assembly 1 could proceed with ZPR-3 after the entire radial reflector is loaded to Assembly-1 specifications. The only measurement other than that of the critical loading was of the worths of the safety and control rod. The analysis of these data is awaiting the determination of the kinetics parameters.

The assembly is being modified by the substitution of the Ni-Na combination for the iron outer reflector, and the change of the safety rod and "lightly loaded" drawers to the normal loadings for their columns. It is predicted that adequate safety-rod worth will be obtained by moving two of the drawers, containing two columns of fuel, with each safety-rod mechanism. Approval is pending for this modification. The outer ring of the core was replaced by radial reflector prior to making these changes. Upon their completion, the core size will be increased in a normal approach-to-critical determination of the critical loading, and the experimental program on Assembly 1 of the Resumed Phase B Critical Experiments will proceed.

## 4. ZPR-6 and -9 Operations and Analysis

### a. Integral Studies of Large Systems (W. Y. Kato)

Last Reported: ANL-7527, pp. 22-29 (Dec 1968).

Three different small-zoned critical assemblies, designated Assemblies 19, 21, and 22, were constructed with ZPR-9. All were basically cylindrical, and contained a central test zone surrounded by concentric buffer, driver, inner reflector, and outer reflector regions. Steel was used in the inner reflector regions to reduce the critical mass. Equivalent regional radii and the average homogeneous concentrations are given in Table I.B.5. The materials in the test zones and the drivers in the three assemblies are all the same. Assembly 21 differs from Assembly 19 only in that the test zone is considerably smaller and the driver thickness is somewhat increased. Assembly 22 differs from Assembly 19 only in that the material in the buffer region is different; this change results in a reduction in critical mass.

TABLE I.B.5. ZPR-9 Assemblies 19, 21, and 22

| Assembly | Region | Outer Radius (cm) | Atom Densities x $10^{-21}$ | | | | | | | | |
|---|---|---|---|---|---|---|---|---|---|---|---|
| | | | Fe | Ni | Cr | Na | C | O | Al | $^{238}U$ | $^{235}U$ |
| 19 | Core | 25.88 | 14.694 | 1.202 | 3.035 | 9.323 | - | 14.563 | - | 5.813 | 1.156 |
| 21 | | 14.27 | 14.694 | 1.202 | 3.035 | 9.323 | - | 14.563 | - | 5.813 | 1.156 |
| 22 | | 25.88 | 14.694 | 1.202 | 3.035 | 9.323 | - | 14.563 | - | 5.813 | 1.156 |
| 19 | Buffer | 32.52 | 7.010 | 0.793 | 2.00 | - | - | 21.732 | 18.708 | 8.259 | 0.017 |
| 21 | | 20.89 | 7.010 | 0.793 | 2.00 | - | - | 21.732 | - | 8.259 | 0.017 |
| 22 | | 32.52 | 7.010 | 0.793 | 2.00 | - | - | - | 49.927 | - | - |
| 19 | Driver | 43.35 | 28.819 | 3.536 | 8.196 | - | 30.331 | - | - | 0.325 | 4.553 |
| 21 | | 32.06 | 28.819 | 3.536 | 8.196 | - | 30.331 | - | - | 0.325 | 4.553 |
| 22 | | 41.31 | 28.819 | 3.536 | 8.196 | - | 30.331 | - | - | 0.325 | 4.553 |
| 19 | Steel | 56.87 | 77.77 | 0.891 | 2.036 | - | - | - | - | - | - |
| 21 | Reflector | 56.87 | 77.77 | 0.891 | 2.036 | - | - | - | - | - | - |
| 22 | | 56.87 | 77.77 | 0.891 | 2.036 | - | - | - | - | - | - |
| 19 | Depleted | 73.45 | 4.332 | 0.540 | 1.140 | - | - | - | - | 39.93 | 0.081 |
| 21 | Reflector | 73.45 | 4.332 | 0.540 | 1.140 | - | - | - | - | 39.93 | 0.081 |
| 22 | | 73.45 | 4.332 | 0.540 | 1.140 | - | - | - | - | 39.93 | 0.081 |

The specific drawer-loading patterns for each assembly in the test zone, buffer, and driver regions are as follows, with plate dimensions given in inches:

| | |
|---|---|
| Test Zone | 1/4 $U_3O_8$, 1/2 Na, 1/8 $Fe_2O_3$, 1/16 SS, 1/16 E, |
| Assemblies 19, 21, and 22 | 1/8 D, 1/8 $Fe_2O_3$, 1/2 Na, 1/4 $U_3O_8$. |
| Buffer | 1/4 $U_3O_8$, 1/4 Al, 1/4 $U_3O_8$, 1/8 Al, 1/4 $U_3O_8$, |
| Assemblies 19 and 21 | 1/8 Al, 1/4 $U_3O_8$, 1/4 Al, 1/4 $U_3O_8$. |
| Buffer | 2 Al (full drawer of aluminum) |
| Assembly 22 | |
| Driver | 1/8 C, 1/8 SS, 1/8 C, 1/8 E, 1/8 SS, 1/8 C, |
| Assemblies 19, 21 and 22 | 1/8 SS, 1/16 SS, 1/8 C, 1/16 SS, 1/8 SS, 1/8 C, |
| | 1/8 SS, 1/8 E, 1/8 C, 1/8 SS, 1/8 C. |

The symbols E and D designate, respectively, enriched and depleted uranium, C refers to graphite (carbon), and SS to stainless steel.

The calculated real and adjoint centerline fluxes are included in Table I.B.6. The appropriate reference spectra for each of the zoned assemblies is also included for comparison. The calculations were made

TABLE I.B.6. Comparison of Calculated Real and Adjoint Centerline Fluxes for ZPR-6 Assembly 6 and ZPR-9 Assemblies 19, 21, and 22[a]

| Group | Lower Energy Limit of Group (keV) | Centerline Flux for ZPR-6 Assembly 6 (Reference) | Centerline Flux for ZPR-9 Assembly 19 | Centerline Flux for ZPR-9 Assembly 21 | Centerline Flux for ZPR-9 Assembly 22 | Centerline Adjoint Flux for ZPR-6 Assembly 6 (Reference) | Centerline Adjoint Flux for ZPR-9 Assembly 19 | Centerline Adjoint Flux for ZPR-9 Assembly 21 | Centerline Adjoint Flux for ZPR-9 Assembly 22 |
|---|---|---|---|---|---|---|---|---|---|
| 1 | 3679 | 1.20 | 1.19 | 1.16 | 1.15 | 4.80 | 4.79 | 4.72 | 4.80 |
| 2 | 2231 | 2.74 | 2.72 | 2.68 | 2.72 | 4.77 | 4.76 | 4.70 | 4.76 |
| 3 | 1353 | 4.45 | 4.41 | 4.41 | 4.13 | 4.46 | 4.47 | 4.46 | 4.47 |
| 4 | 821 | 5.69 | 5.68 | 5.81 | 5.18 | 4.11 | 4.15 | 4.18 | 4.14 |
| 5 | 500 | 10.23 | 10.25 | 10.50 | 10.21 | 4.09 | 4.13 | 4.19 | 4.12 |
| 6 | 302 | 9.40 | 9.45 | 9.71 | 9.59 | 4.13 | 4.19 | 4.30 | 4.20 |
| 7 | 183 | 11.89 | 11.98 | 12.21 | 12.55 | 4.12 | 4.17 | 4.31 | 4.20 |
| 8 | 111 | 12.05 | 12.11 | 12.08 | 11.73 | 4.10 | 4.15 | 4.30 | 4.19 |
| 9 | 67.4 | 10.22 | 10.22 | 10.10 | 10.62 | 4.11 | 4.13 | 4.28 | 4.16 |
| 10 | 40.9 | 8.60 | 8.58 | 8.40 | 8.51 | 4.12 | 4.13 | 4.27 | 4.11 |
| 11 | 24.8 | 6.44 | 6.41 | 6.32 | 6.67 | 4.18 | 4.16 | 4.27 | 4.08 |
| 12 | 15.0 | 6.12 | 6.09 | 5.94 | 6.06 | 4.25 | 4.22 | 4.30 | 4.10 |
| 13 | 9.12 | 3.96 | 3.93 | 3.82 | 3.97 | 4.37 | 4.34 | 4.33 | 4.17 |
| 14 | 4.31 | 2.89 | 2.87 | 2.83 | 3.14 | 4.52 | 4.49 | 4.44 | 4.27 |
| 15 | 2.61 | 0.622 | 0.619 | 0.616 | 0.607 | 4.77 | 4.73 | 4.67 | 4.56 |
| 16 | 2.03 | 0.779 | 0.777 | 0.795 | 0.369 | 4.78 | 4.74 | 4.67 | 4.66 |
| 17 | 1.23 | 1.400 | 1.402 | 1.379 | 1.302 | 4.80 | 4.77 | 4.69 | 4.69 |
| 18 | 0.961 | 0.427 | 0.428 | 0.408 | 0.458 | 4.67 | 4.65 | 4.55 | 4.75 |
| 19 | 0.583 | 0.507 | 0.505 | 0.462 | 0.569 | 5.04 | 5.01 | 4.90 | 5.17 |
| 20 | 0.275 | 0.307 | 0.303 | 0.271 | 0.346 | 5.23 | 5.21 | 5.09 | 5.58 |
| 21 | 0.101 | 0.084 | 0.083 | 0.075 | 0.095 | 5.15 | 5.15 | 5.04 | 5.49 |
| 22 | 0.0290 | 0.0081 | 0.0079 | 0.0076 | 0.0096 | 5.45 | 5.46 | 5.37 | 5.33 |

[a]The spectra were computed in cylindrical geometry by the MACH-1 code using the cross-section sets generated by the $MC^2$ code. ENDF/B cross sections were not used.

with the one-dimensional diffusion code, MACH-1,* in cylindrical geometry. The cross-section sets used for the calculation of the fluxes and other parameters are identified in the appropriate tables. Generally, the cross-section sets were generated by the $MC^2$ code;** however, some of the analysis was completed before the ENDF/B cross sections were available. No heterogeneity corrections have been included in the calculations.

Calculated and measured parameters for the assemblies are included in Table I.B.7. As before, most of the calculations were performed using the MACH-1 code. The control-rod calculations were made

TABLE I.B.7. Measured and Calculated Parameters for Assemblies 19, 21, and 22

| | Assembly[a] | | |
|---|---|---|---|
| | 19 | 21 | 22 |
| Measured critical mass, kg | 480.3 | 340 | 439.3 |
| Calculated critical mass, kg | 560 | 329 | 418 |
| Mass of U-235 in central core, kg | 87 | 26 | 87 |
| Total volume (excluding reflector), liters | 540 | 295 | 490 |
| Volume of central core, liters | 192 | 58 | 192 |
| Core height (excluding reflector), cm | 91.4 | 91.4 | 91.4 |
| Axial reflector thickness, cm | 15.2 steel<br>15.2 U | 15.2 steel<br>15.2 U | 15.2 steel<br>15.2 U |
| Calculated reflector savings, cm | Core 18.2<br>Driver 8.2 | Core 18.2<br>Driver 8.2 | Core 18.2<br>Driver 8.2 |
| Calculated effective delayed-neutron fraction | $6.89 \times 10^{-3}$ | $6.89 \times 10^{-3}$ | $6.76 \times 10^{-3}$ |
| Calculated prompt-neutron lifetime, sec | $4.07 \times 10^{-7}$ | $4.66 \times 10^{-7}$ | $4.41 \times 10^{-7}$ |
| Calculated Ih/% reactivity (Ih/% $\delta k/k$) | 435.5 | 429.5 | 435.2 |
| Calculated perturbation denominator[b] | $4.72 \times 10^5$ | $2.99 \times 10^5$ | $4.36 \times 10$ |
| Dual-purpose (fuel) control rods:[c] | | | |
| Averaged measured worth/rod, % $\delta k/k$ | 0.243 | 0.300 | 0.255 |
| Calculated worth/rod, % $\delta k/k$ | 0.220 | 0.370 | 0.238 |
| Boron safety rods: | | | |
| Measured worth/rod, % $\delta k/k$ | -0.180 | - | d |
| Calculated worth/rod, % $\delta k/k$ | -0.335 | -0.570 | d |
| Calculated Doppler coefficient for U-235 heating, $\delta k/k/°C$ | $+0.96 \times 10^{-6}$ | $+0.79 \times 10^{-6}$ | d |
| Calculated U-235 temperature expansion coefficient, $\delta k/k/°C$ | $-4.86 \times 10^{-6}$ | $-5.19 \times 10^{-6}$ | d |

[a]Cross sections used in the calculations are defined in the footnote of Table I.B.6.

[b]The values are normalized such that $\sum_i (\nu\Sigma_f)_i \phi_i = 1$ and $\sum_i \chi_i \phi_i^* = 1$ at the center of the core.

[c]Control rod drawers with triple columns of fuel measured 0.327% $\delta k/k$.

[d]Some of the calculations for Assembly 22 are omitted, since it was a slight variation of Assembly 19.

*Meneley, D. A., et al., ANL-7223 (1966).

**O'Shea, D. M., et al., ANL-7318 (1967).

by a first-order perturbation subroutine to the MACH-1 code, DEL, by perturbing the control-rod material throughout the region. Good agreement between the calculated and measured rod worths has been obtained for the dual-purpose fuel rods. The calculations generally overpredict the worth of the boron rods, due to self-shielding in the boron.

Doppler difference cross sections as a function of equivalent $\sigma_p$ for the different Doppler isotopes have been generated.* The Doppler cross sections with the appropriate equivalent $\sigma_p$ values were used with the DEL subroutine to calculate the Doppler coefficients. Only the Doppler effect in the fissionable isotope was considered. For example, the U-238 Doppler effect was ignored both for the U-238 in the depleted plates (because they were assumed not to heat) and for the U-238 in the fuel plates (because it is too dilute to have significant Doppler effect). Measurements with the same samples were also made in the reference ZPR-6 Assembly 6.** The comparison listed in Table I.B.8 indicates that the spectra in the two assemblies are reasonably well-matched.

TABLE I.B.8. Central Reactivity Worths in ZPR-9 Assembly 19 Compared with Results for ZPR-6 Assembly 6

| Sample Material | Weight of Sample (g) | Can Type | Can Weights (g) | Gross Sample Worth (Ih) | Net Sample Worth (Ih) | Specific Sample Worth (Ih/kg) | Worth Assembly 19, ZPR-9 / Worth Assembly 6, ZPR-6 |
|---|---|---|---|---|---|---|---|
| $(CH_2)_n$ | 58.986 | bare | - | 17.513 ± 0.009 | 17.513 ± 0.009 | 296.9 ± 0.2 | 1.421 |
| Be | 114.308 | bare | - | 1.801 ± 0.007 | 1.801 ± 0.007 | 15.76 ± 0.06 | 1.381 |
| $^{10}B$ | 29.29 | SS | 55.73 | -39.312 ± 0.070 | -39.195 ± 0.071 | -1338.2 ± 2.4 | 1.689 |
| C | 102.0 | bare | - | 0.459 ± 0.007 | 0.459 ± 0.007 | 4.50 ± 0.07 | 1.254 |
| Na | 51.38 | SS | 56.42 | -0.095 ± 0.005 | 0.020 ± 0.007 | 0.39 ± 0.14 | 1.538 |
| Al | 165.33 | bare | - | -0.091 ± 0.007 | -0.091 ± 0.007 | -1.15 ± 0.04 | 1.566 |
| Fe | 488.0 | bare | - | -0.720 ± 0.007 | -0.720 ± 0.007 | -1.475 ± 0.014 | 1.600 |
| SS Can | 72.39 | bare | - | -0.153 ± 0.005 | -0.153 ± 0.005 | -2.11 ± 0.07 | - |
| SS Block | 480.9 | bare | - | -0.871 ± 0.007 | -0.871 ± 0.007 | -1.81 ± 0.02 | 1.643 |
| Ni | 546.0 | bare | - | -1.435 ± 0.007 | -1.435 ± 0.007 | -2.63 ± 0.02 | 1.725 |
| Zr | 406.0 | bare | - | -0.748 ± 0.007 | -0.748 ± 0.007 | -1.84 ± 0.02 | 1.688 |
| Nb | 481.2 | SS | 30.10 | -5.983 ± 0.007 | -5.920 ± 0.009 | -12.30 ± 0.02 | 1.679 |
| Mo | 599.0 | bare | - | -5.115 ± 0.075 | -5.115 ± 0.075 | -8.539 ± 0.125 | 1.642 |
| Ta | 924.7 | bare | - | -19.724 ± 0.007 | -19.724 ± 0.007 | -21.269 ± 0.008 | - |
| W | 1108.0 | bare | - | -8.945 ± 0.007 | -8.945 ± 0.007 | -8.074 ± 0.007 | 1.756 |
| Enriched | 18.17 U<br>16.93 U-235 | SS | 72.603 | 1.100 ± 0.007 | 1.254 ± 0.009 | 69.01 ± 0.50 | - |
| Depleted | 1153.8 | bare | - | -6.317 ± 0.007 | -6.317 ± 0.007 | -5.475 ± 0.006 | 1.678 |

Figure I.B.5 contains the results of U-235 foil activations and U-235 fission counter traverses along the radii of Assembly 19. The foil activation and the fission counter fission rate curves are generally in good agreement for Assemblies 19, 21, and 22. A one-dimensional diffusion calculation has been included for comparison. Figure I.B.6 contains the results of foil activations in the axial direction in Assembly 19. The axial activations were made at two locations in the central zone, one in the

*Till, C. E., et al., in Proceedings of International Conference on Fast Critical Experiments and Their Analysis, October 10-13, 1966, ANL-7320, pp. 319-333.

**Karam, R. A., et al., Trans. ANS 11, 597 (1968).

buffer region and two in the driver region. To a fairly good approximation all the cosine-fitted axial shapes extrapolated to the same point. The points near the edge of the reflector were not used in the fit. An extrapolated half-height of approximately 66.5 ± 2.5 cm was obtained from the fits. This is equivalent to a reflector savings of 20.8 cm, which is close to the value calculated (by one-dimensional slab calculations) for the central test zone (see Table I.B.7). The calculated reflector savings for the driver region are too small by over a factor of two when compared to the measurements. The measurements for Assembly 19 indicate that the calculated reflector savings for the central zone are appropriate for all the assembly regions.

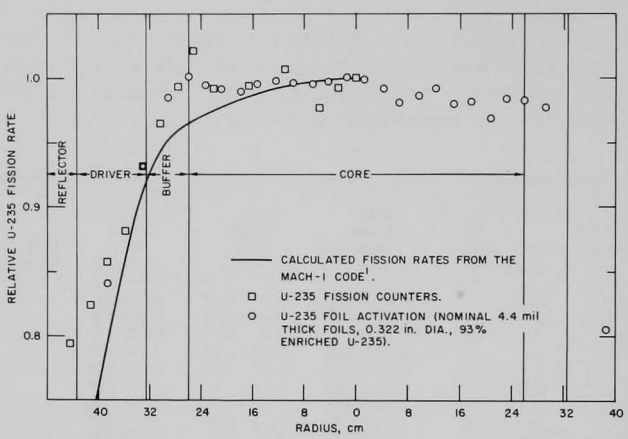


Fig. I.B.5. Measurement of Radial U-235 Fission Rate for ZPR-9 Assembly 19

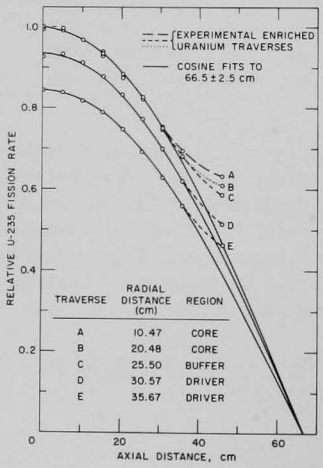


Fig. I.B.6

Axial Reflector Savings for ZPR-9 Assembly 19

b. Doppler Effect (C. E. Till)

Last Reported: ANL-7513, pp. 20-25 (Oct 1968).

A consistent analysis of measurements of U-235 and U-238 Doppler effect and central reactivity worth in four progressively softer reactor spectra, designated Assemblies 13, 14, 16, and 17, has been completed. These assemblies had central test-zone volume fractions of stainless steel (15.1%), sodium (38.9%), polyethylene (8.7%), enriched uranium (3.5%), and void (3.8%). Spectrum softening was accomplished by varying the amount of carbon and depleted uranium in each assembly. The carbon-depleted uranium volume fractions were, in Assembly 13, 14.1-15.9%; Assembly 14, 15.9-14.1%; Assembly 16, 19.4-10.6% and Assembly 17, 30.0-0.0%. These assemblies were modifications of the fast-spectrum Assembly 12 which contained no polyethylene, and had carbon and depleted uranium volume fractions of 15.9 and 22.9%, respectively. The other material volume fractions in Assembly 12 were the same as in Assemblies 13-17.

This analysis consisted primarily of using ENDF/B nuclear cross-section data in several standard computer codes. The exceptions were (1) in calculating the U-235 Doppler difference cross sections; J. Schmidt unresolved resonance parameters were used, and (2) in calculating central reactivity worths; the material cross sections for molybdenum, tungsten, tantalum, and boron were in part from Argonne cross-section set 224 and from I. Bondarenko self-shielded cross sections.

Reactor cross sections were calculated with the $MC^2$ code using the heterogeneous option. It is known that the heterogeneous calculation does not generate effective cell-averaged cross sections for the equivalent homogeneous case. Nevertheless, these $MC^2$ cross sections were used. Effort continues on comparisons that include better cell-averaged cross sections.

Doppler difference cross sections for U-235 were calculated in the unresolved resonance region (61 eV to 41 keV) with the RP-270 code. These cross sections were subsequently adjusted for estimated effects due to same- and intersequence resonance interference. The RABBLE code was used in the resolved region (below 61 eV). For U-238, the ERIC 2 code was used in both the resolved and unresolved resonance regions.

The one-dimensional diffusion-theory package MACH 1 was used to calculate the critical-assembly parameters using $MC^2$ cross sections. First-order perturbation theory, the DEL subroutine of MACH 1, was used (1) to calculate the Doppler effect using the Doppler difference cross sections and (2) the central reactivity worths. In addition, the latter worths were also calculated using a perturbed sample flux perturbation

formalization.* For purposes of comparison with the measured and calculated parameters in Assemblies 13-17, the corresponding parameters in Assembly 12 are also given in the subsequent discussion.

Measured critical masses in Assemblies 12-17 were 579.6, 402.8, 374.1, 333.1, and 126.7 kg of U-235, respectively. These correspond to calculated critical masses of 601.2, 374.9, 349.7, 294.4, and 136.1 kg of U-235. The present calculations overestimated the measured critical masses in Assemblies 12 and 17 by approximately 5%, and underestimated Assemblies 13, 14 and 16 by approximately 10%.

Table I.B.9 summarizes the calculated and experimental Doppler effects for U-235 and U-238 between room temperature and 500 or 1100°K. The Doppler samples used in these investigations were cylindrical, normally 1 kg $UO_2$, and highly enriched in either U-235 (97.7 wt % U) or U-238 (99.3 wt % U). The designation (FE) and (NNE) refers to the thermal-expansion characteristics of the experimental Doppler samples: FE means completely uninhibited expansion, and NNE complete axial constraint and partially inhibited radial expansion. As is evident from Table I.B.9, the U-235 expansion reactivity effect in Assembly 12 is negative, whereas in Assemblies 13-17 the thermal expansion is a positive reactivity effect.

TABLE I.B.9. Calculated and Experimental[a] Doppler Effects in Assemblies 12, 13, 14, 16, and 17 between 293°K and the Indicated Temperature (Ih/kg)

| | Assembly 12 | | Assembly 13 | | Assembly 14 | | Assembly 16 | | Assembly 17 | |
|---|---|---|---|---|---|---|---|---|---|---|
| Doppler Sample | 500°K | 1100°K | 500°K | 1100°K | 500°K | 1100°K | 500°K | 1100°K | 500°K | 1100°K |
| $^{235}U$ (FE) | +0.042 | +0.075 | +0.235 | +0.812 | +0.228 | +0.714 | +0.162 | +0.517 | -0.275 | -0.694 |
| $^{235}U$ (NNE) | +0.050 | +0.094 | +0.207 | +0.672 | +0.218 | +0.644 | - | - | -0.335 | -0.784 |
| $^{235}U$ (Calculated) | +0.089 | +0.202 | +0.427 | +1.023 | +0.398 | +0.945 | +0.307 | +0.700 | -0.300 | -0.918 |
| $^{238}U$ (FE) | -0.158 | -0.422 | -0.602 | -1.956 | -0.717 | -2.155 | -0.801 | -2.354 | -1.323 | -4.045 |
| $^{238}U$ (Calculated) | -0.101 | -0.246 | -0.914 | -2.592 | -0.981 | -2.788 | -1.131 | -3.226 | -1.527 | -4.411 |

[a]Diluent uranium isotope $^{238}U$ or $^{235}U$ subtracted based on $^{238}U$ (FE) or $^{235}U$ (FE), as appropriate.

As an indication of agreement of measurements and current calculations of the U-235 Doppler effect between 293 and 500°K, the percentage difference of the U-235 (calculated) from the experimental U-235 (NNE) are +78%, Assembly 12; +106%, Assembly 13; +83%, Assembly 14; -10%, Assembly 17. Similarly, for the U-238 Doppler effect, these percentages are -36, +52, +37, +41, and +15%, respectively, for Assemblies 12, 13, 14, 16, and 17.

Of particular note is the U-235 Doppler effect in Assembly 17. The reactor spectrum softening accomplished in Assembly 17 has turned

T *Till, C. E., in Reactor Physics Division Annual Report, July 1, 1966 to June 30, 1967, ANL-7310, pp. 143-51.

the U-235 Doppler effect strongly negative, and has shifted the relative contribution of Doppler effects for the unresolved and resolved resonance regions to the latter region. The improvement between measurement and calculation may be an indication of better knowledge of the parameters in the resolved region.

Table I.B.10 shows the experimental central reactivity worths in the assemblies. Table I.B.11 shows the corresponding calculated worths.

TABLE I.B.10. Measurements of Reactivity Worth

| Sample[a] | Weight (g) | Can Weight (g) | Assembly 12[b] (Net Ih/kg) | Assembly 13[c] (Net Ih/kg) | Assembly 14[d] (Net Ih/kg) | Assembly 16[e] (Net Ih/kg) | Assembly 17[f] (Net Ih/kg) |
|---|---|---|---|---|---|---|---|
| Mo | 598.8 | - | -8.059 ± 0.017 | -19.41 ± 0.05 | -20.28 ± 0.00 | -21.43 ± 0.01 | -24.87 ± 0.12 |
| Ni | 546.1 | - | -2.992 ± 0.018 | -11.60 ± 0.03 | -11.99 ± 0.02 | -12.79 ± 0.00 | -14.44 ± 0.01 |
| Fe | 484.3 | - | -2.110 ± 0.021 | -6.186 ± 0.03 | -6.084 ± 0.015 | -6.040 ± 0.002 | -3.494 ± 0.008 |
| Be | 114.3 | - | +12.20 ± 0.09 | +39.20 ± 0.06 | +46.13 ± 0.11 | +56.89 ± 0.03 | +128.69 ± 0.03 |
| C | 102 | - | +1.578 ± 0.109 | +10.52 ± 0.04 | +13.66 ± 0.08 | +17.74 ± 0.01 | +48.81 ± 0.31 |
| Al | 167.1 | - | -2.561 ± 0.060 | -1.143 ± 0.150 | -0.325 ± 0.006 | +0.993 ± 0.000 | +10.64 ± 0.04 |
| Na | 51.39 | 56.42 (SS) | -1.376 ± 0.200 | -1.323 ± 0.720 | +0.108 ± 0.049 | +1.693 ± 0.078 | +13.90 ± 0.33 |
| W | 1108 | - | -7.340 ± 0.009 | -23.07 ± 0.32 | -27.53 ± 0.32 | -30.01 ± 0.32 | -42.19 ± 0.32 |
| Ta | 924.7 | 27.54 (SS) | -17.982 ± 0.016 | -49.04 ± 0.38 | -57.58 ± 0.38 | -62.16 ± 0.38 | -89.23 ± 0.38 |
| B | 75.2 | 20.6 (SS) | - | -824 ± 6 | -975 ± 3 | -1090 ± 5 | -1660 ± 5 |
| Poly ($CH_2$) | 58.988 | - | +443.40 ± 0.25 | +436.65 ± 0.08 | +487.39 ± 5.93 | +488.2 ± 3.9 | +707.8 ± 4.2 |
| Poly ($CH_2$) | 13.70 | 72.32 (SS) | - | +469 ± 3.1 | +512.2 ± 3.1 | +550.1 ± 0.9 | +905.7 ± 1.3 |
| SS-304 | 481 | - | -2.364 ± 0.021 | -7.958 ± 0.029 | -8.059 ± 0.004 | -8.281 ± 0.019 | -7.029 ± 0.023 |
| SS Can | 72.38 | - | -2.542 ± 0.138 | -8.994 ± 0.041 | -9.600 ± 0.034 | -9.837 ± 0.111 | -8.635 ± 0.290 |
| $B_4C$ | 59.62 | 64.70 (SS) | - | -713.2 ± 5.9 | -757 ± 5.9 | -837.1 ± 5.9 | -1295 ± 6 |
| Depleted Uranium | 1155 | - | -4.674 ± 0.009 | -8.510 ± 0.005 | -8.911 ± 0.012 | -9.191 ± 0.001 | -11.88 ± 0.04 |
| Al Can | 26.36 | - | - | - | - | +1.328 ± 0.076 | +10.85 ± 0.27 |
| Enriched Uranium | 18.11[g] | 72.38 (SS) | +70.12 ± 0.88[h] | - | - | - | - |
| Enriched Uranium | 18.24[g] | 72.34 (SS) | - | +134.5 ± 0.5[h] | - | - | - |
| Enriched Uranium | 18.17[g] | 72.34 (SS) | - | - | +137.4 ± 0.3[h] | +143.6 ± 0.0[h] | +135 ± 0.7[h] |
| Pu | 119.24[i] | 22.27 (SS) 6.85 (Al) | +93.05 ± 1.68[j] | - | - | - | - |
| Pu | 121.55[i] | 19.77 (SS) 7.05 (Al) | - | - | - | +199.0 ± 2.0[j] | +228.1 ± 2.2[j] |

[a]All samples are nominal 1 x 2 x 2 in. except the enriched uranium, which is 1/16 x 1/2 x 2 in., and the plutonium, which is 1/4 x 2 x 2 in.
[b]Assembly 12: 1% Δk/k = 451.2 Ih.
[c]Assembly 13: 1% Δk/k = 438.86 Ih.
[d]Assembly 14: 1% Δk/k = 435.69 Ih.
[e]Assembly 16: 1% Δk/k = 428.07 Ih.
[f]Assembly 17: 1% Δk/k = 391.78 Ih.
[g]93.2 wt % $^{235}U$.
[h]U mixture.
[i]0.01 wt % $^{238}Pu$; 95.05 wt % $^{239}Pu$; 4.48 wt % $^{240}Pu$; 0.45 wt % $^{241}Pu$; 0.01 wt % $^{242}Pu$.
[j]Pu mixture.

TABLE I.B.11. Calculated Central Worths with and without Sample-size Effect (Ih/kg)

| Sample | Assembly 12[a] Without Size Effect | Assembly 12[a] With Size Effect | Assembly 13[b] Without Size Effect | Assembly 13[b] With Size Effect | Assembly 14[c] Without Size Effect | Assembly 14[c] With Size Effect | Assembly 16[d] Without Size Effect | Assembly 16[d] With Size Effect | Assembly 17[e] Without Size Effect | Assembly 17[e] With Size Effect |
|---|---|---|---|---|---|---|---|---|---|---|
| Mo | -9.543 | -9.080 | -29.52 | -27.56 | -30.81 | -28.82 | -33.25 | -31.25 | -32.97 | -31.80 |
| Ni | -2.585 | -2.364 | -9.177 | -8.221 | -9.336 | -8.396 | -9.422 | -8.560 | -5.964 | -5.868 |
| Fe | -2.478 | -2.309 | -5.209 | -4.895 | -5.083 | -4.799 | -4.557 | -4.365 | +0.506 | +0.130 |
| Be | +7.237 | +10.20 | +63.87 | +61.44 | +71.56 | +68.63 | +89.92 | +85.81 | +157.4 | +148.7 |
| C | -1.318 | -0.615 | +19.97 | +20.37 | +22.98 | +23.33 | +30.36 | +30.58 | +59.82 | +59.39 |
| Al | -2.818 | -2.682 | +0.418 | +0.603 | +1.297 | +1.458 | +3.639 | +3.728 | +15.99 | +15.64 |
| Na | -0.535 | -0.526 | +4.089 | +3.746 | +4.995 | +4.662 | +7.365 | +7.062 | +19.22 | +19.10 |
| W | -8.785 | -8.161 | -52.45 | -36.87 | -56.04 | -39.20 | -63.91 | -44.21 | -82.70 | -54.54 |
| Ta | -24.45 | -20.36 | -124.3 | -82.95 | -132.8 | -88.39 | -151.5 | -100.2 | -196.4 | -126.5 |
| B | -273.4 | -244.9 | -4541 | -1154 | -4956 | -1239 | -5909 | -1428 | -8937 | -1930 |
| Poly ($CH_2$) | +314.7 | +532.7 | +652.2 | +854.1 | +710.2 | +904 | +845.9 | +1013 | +1193 | +1175 |
| Poly ($CH_2$) | +314.7 | +409.5 | +652.2 | +710.9 | +710.2 | +766.7 | +845.9 | +895 | +1193 | +1189 |
| SS (304) | -2.609 | -2.399 | -6.677 | -6.261 | -6.631 | -6.247 | -6.267 | -5.982 | -1.397 | -1.774 |
| $B_4C$ | -214.2 | -200.3 | -3549 | -1103 | -3873 | -1187 | -4618 | -1374 | -6981 | -1889 |
| Depleted Uranium | -5.679 | -5.725 | -15.41 | -13.81 | -16.10 | -14.37 | -17.46 | -15.44 | -18.11 | -15.17 |
| Enriched Uranium | +64.84 | +65.92 | +135.4 | +130.8 | +138 | +134 | +140.6 | +138.5 | +103.3 | +113.7 |
| Pu | +88.40 | +96.11 | +125.5 | +205.4 | +120.9 | +212.9 | +104.6 | +226.4 | -30.63 | +207.5 |
| Pu[f] | +87.87 | +95.26 | +251.9 | +220.8 | +259.9 | +229.6 | +272.6 | +246.2 | +231.2 | +245.6 |

[a]Assembly 12: 1% Δk/k = 445.76 Ih.
[b]Assembly 13: 1% Δk/k = 428.71 Ih.
[c]Assembly 14: 1% Δk/k = 425.41 Ih.
[d]Assembly 16: 1% Δk/k = 417.53 Ih.
[e]Assembly 17: 1% Δk/k = 385.02 Ih.
[f]Pu sample worth without the $^{240}Pu$ component.

The column marked "without size effect" is the usual first-order perturbation calculation; "with size effect" gives the result of the calculation made using the calculated perturbed sample flux. Generally, the material worths calculated when sample-size effects are considered are in better agreement with the experimentally measured worths. (Plutonium sample cross sections were infinitely dilute and therefore probably do not represent accurate estimates of the plutonium worths.)

It is to be expected that unit cell averaging corrections to the present $MC^2$ cross sections would show overall improvement in the current calculations. Such work is continuing.

5. ZPPR Operations and Analysis (W. G. Davey and P. I. Amundson)

Last Reported: ANL-7527, pp. 29-33 (Dec 1968).

a. Doppler Effect

(i) Design. The bid package has been issued for construction. The vacuum capsule containment for the Doppler element is included in the package. This completes the items which must be built to special design for the complete Doppler system.

(ii) Equipment. The drive motor and control system have been completely set up. The oscillator is working satisfactorily. Preliminary tests indicate that the repeatability of any particular position is 0.001 in.

Remote control has been completed for the entire vacuum system and is working satisfactorily. Remote control for the drive system is in the final checkout stage.

The cooling air blower and temperature-control sensors have been received for the cooling air system and the Doppler element. Equipment which has been ordered but not yet received are: a) the Doppler controller for the cooling air system and Doppler element, and b) the special-design thermocouple for measuring the Doppler-element temperature.

(iii) Activation Doppler Experiment. The smaller of two activation Doppler ovens has been successfully benchtested under vacuum and at elevated temperatures. Heating elements and thermocouples operated properly. No major vacuum leaks were detected.

(iv) Reactivity Doppler Analysis. Some errors in the 1100°K cases involving resolved resonances in U-238 were detected and corrected. Problems arose in the unresolved range, where statistically selected subgroups of 20 resonances were used as RABBLE input. Five such subgroups, in the range from 5.53 to 9.12 keV, gave very inconsistent results in a comparison of $\delta\sigma_a$ between 300 and 500°K. Additional runs using subgroups of 40, 60, and 80 resonances are planned.

b. Reactor Equipment Development

(i) Automation of Data Acquisition

(a) Data-collection System. The Control Equipment Corporation Data-Logger for this system has been received and is being evaluated. Several minor discrepancies with the specifications have been found. These will be corrected by the supplier or by modification to our system, whichever is most expeditious.

Construction has begun on the DCS signal cabinet. This unit provides remote switching between the 60 thermocouples in the core and the 15 inputs to the data-logger.

Work is in progress on a routine to read and decode the information from the Incremental Magnetic-Tape System. Routines will be available for both the SEL-840 and the CDC-1604.

(b) ZPPR Computer. The preparation for the ZPPR on-line computer is continuing. Discussions have been held with Systems Engineering Laboratories regarding acceptance tests, and agreement has been tentatively reached. The revised procedures for acceptance test will be ready for examination at Fort Lauderdale during Argonne's witness of the factory-acceptance tests.

Preliminary design of the remote I/O terminal is nearing completion, and major components for one terminal have been ordered. Some programs for collecting data from the terminals have been written. These will be assembled and partially debugged during the factory-acceptance test.

A detailed description of the 24-bit counter-register module (one of the modules for use in the I/O terminal) has been prepared.

c. Heterogeneity. Considerable effort has been directed toward operational familiarity of the counting-room computer (SEL-810A). An exploratory program has now been written and is operational.

The order for two additonal sample changers has been made, and specification for a CRT display are being formulated.

An inverse kinetics code and a small Monte Carlo code are ready to be checked out on the 840 MP, as well as a plot routine.

d. Mockup Studies. The entire radial Ni + Na reflector region was removed to supply the nickel necessary to complete the ZPR-3 Assembly-56 reflector. The axial Ni + Na reflector is of the FTR composition except for eighty drawers from which one piece of nickel was removed.

ZPPR is in operational readiness awaiting approval for operation. The past month has been spent in personnel training and systems operation familiarization.

## C. Component Development--LMFBR

### 1. Reactor Mechanism and Instrumentation

#### a. Instrumentation Development (T. P. Mulcahey)

##### (i) Out-of-core Neutron Flux Detection System (Intermediate Range Neutron Flux Monitor) (G. F. Popper)

Last Reported: ANL-7527, pp. 35-37 (Dec 1968).

Wide-range and intermediate-range circuits are being developed and will be tested with detectors installed in a special thimble in EBR-II. Environment and performance requirements for FFTF and future LMFBRs serve as development and test goals.

(a) Detectors and Cables. The Westinghouse high-temperature (850°F max) fission-counter chambers, compensated ionization chambers, and mating cables have been completed and accepted. The Reuter-Stokes fission-counter chambers (850 and 1400°F max) and mating cables have been completed and accepted; completion of the compensated ionization chambers awaits cable delivery. The manufacturers have begun programs to test partially and qualify all these detector-cable combinations at temperatures up to the maximum ratings.

The malfunction of the test system consisting of a Westinghouse WX-4036 detector and Bostrad-22 cable has been traced to a voltage breakdown in either the cable-connector assembly or the detector when 500 V was applied. Reduction of the detector excitation voltage to about 50 V eliminated the breakdown phenomenon, and the system performed as expected at this reduced voltage. However, because the detector could not be kept in saturation at 50 V, the tests at 700°F were terminated temporarily.

To see if permanent damage to either the detector or cable had occurred or whether this was the same reversible breakdown phenomenon experienced while testing the cable-connector in a furnace at 800°F, the 01-thimble temperature was reduced to the normal cooled condition of about 100°F. The system operated normally at all voltages up to 700 V, the maximum applied.

Reactor-startup data with the detector cable operating at 100°F were taken (see Fig. I.C.1) in the presence of the largest gamma flux ($>7 \times 10^3$ R/hr) available in the 01 thimble immediately after shutdown and after ~4 days of EBR-II operation at 50 MWt. The data show greater than a two-decade overlap between the log counting channel and the true-rms log channel; for comparison purposes, data from the conventional EBR-II linear flux channel are also shown.

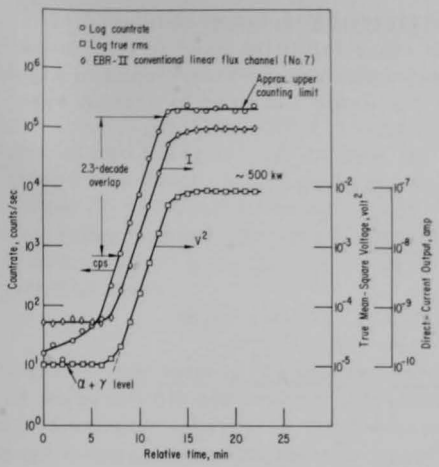


Fig. I.C.1. Response of WX-4036 Detector with Bostrad-22 Cable (at 100°F in 01 Thimble of EBR-II) to Reactor Startup. Response of conventional channel is shown for comparison. Gamma flux was >7 x $10^3$ R/hr, chamber sensitivity: 0.21 cps/nv and 2.88 x $10^{-9}$ $V^2$/nv.

Preliminary gamma-flux measurements, taken at 700 and 100°F in the EBR-II 01 thimble with the fission-counter-chamber test system, indicate that the gamma sensitivity increased at most by 10% at 700°F. The data from which this figure was deduced are sparse, so further data are being taken to verify this conclusion. No change in neutron sensitivity was noted over the entire temperature range from 100 to 700°F; this supports the conclusions reached when the detector-cable was tested in a furnace previously.

(ii) Circuits. The Milletron block diagrams of the source-, intermediate-, and power-range systems have been approved for construction. Detailed circuit drawings are being furnished; acceptance testing of the entire wide-range channel is expected during February.

The elimination of spurious noise signals in the Gulf General Atomic wide-range neutron monitor is continuing during the extended shutdown of EBR-II. It is hoped that adequate system performance can be achieved before the reactor is restarted late in February. The shielded twisted-wire pairs being used to supply the preamplifier with low-voltage power and to extract the linear-power-range and high-voltage-monitor signals will be changed to coaxial cables. The preamplifier will also be fitted with an adapter to accept these new cables.

The Argonne test system has indicated that spurious electrical noise need not be a serious problem in nuclear detection systems. Such noise did not contribute at all to the dc current signal or to the mean-square-voltage signal being measured with a true-rms-logarithmic voltmeter; only a few extra counts were injected into the log-countrate meter being used. These pulses are believed to be mainly caused by transients produced from the silicon-controlled rectifiers used in the main EBR-II tank-heater controllers. More careful overall electrostatic shielding of the detector and cable systems should substantially reduce the number of noise pulses being counted from this source. It is apparent that noise-suppression techniques used in low-level-counting neutron-detection systems must be adequately fieldtested in typical LMFBR-building environments to ensure

satisfactory overall performance. The electrical noise encountered at EBR-II is far greater than that found at other facilities used to test these systems, and thus more effective techniques to reduce these types of signals must be found. Typical noise could be simulated and used to pretest systems prior to reactor installation.

b. FFTF Instrumentation (R. A. Jaross)

(i) In-core Flowmeter Development (G. F. Popper and F. Verber)

Last Reported: ANL-7527, p. 37 (Dec 1968).

(a) Prototype Permanent-magnet Flowmeter Tests. As a result of redirection of FFTF requirements, work on the flowthrough (centerflow) permanent-magnet flowmeter will be deferred. Emphasis will be on investigation of the feasibility of eddy-current and permanent-magnet probe-type flow sensors. Dimensional limitations of 7/8-in. OD (with a possible maximum of 1.3-in. OD) and a maximum length of 10 in. for the probe-type flow sensors are being imposed because of the curvature of the instrument-guide tubes (through which the sensors are to be removable) above the subassemblies of the FFTF reactor.

Magnets for two flowmeter designs (see ANL-7527) will be procured in both Alnico-5 and -8. These will be temperature-stabilized for 1200°F operation and will be used to determine the external field effects of one magnet upon another. Tests will also be made to determine the ability of the magnets to withstand temperature cycling.

(b) Eddy-current Flowmeter Tests. As a result of redirection of FFTF requirements, work on the flowthrough (centerflow) flowmeter is being deferred pending results of a feasibility study to be made on eddy-current and permanent-magnet probe-type flow sensors described above. However, high-temperature ceramic-insulated nickel-coated magnet wire will be procured in various sizes to accommodate the needs of both the eddy-current probe-type flow sensors and the larger centerflow flowmeter. Physical Science Corp. has advised us that it can supply Durock-coated nickel-clad silver wire in AWG sizes from approximately 36 to 21 (~5- to 28.5-mil diameter) for operation at 1200°F in an inert-gas atmosphere. Another source of high-temperature magnet wire is Anaconda Wire and Cable Co., which manufactures Anacote magnet wire (which is rated for 1200°F use) about once a year. Several firms with precision-type coil-winding capability and experience in winding high-temperature coils have indicated interest in supplying our coil needs. None of these firms, however, possess a universal-type coil-winding machine or have a source for 1200°F magnet wire in the sizes discussed, namely, AWG 26 to 16 (16- to 50-mil diameter).

(ii) Signal Lead Connectors for Sodium Service (A. P. Grunwald)

Last Reported: ANL-7527, p. 38 (Dec 1968).

The FFTF prototype connector coupling under test has been opened and reclosed three times without difficulty. However, the torque required to unlatch the coupling has increased to about 100 ft-lb (previously, values of ~50 ft-lb were observed). A tool to perform this operation without removing the connector from the furnace has been designed; exact measurements of the torque and visual inspection of the lock will be attempted in latching tests.

The pin-to-pin resistance has been measured several times in three locations of the 36-pin connector. The values were fairly consistent at about 9.9 microhms, and no significant relationship of resistance and temperature has been discovered up to approximately 500°F.

The leakrates of the gas through the flux-wire-tube nipples continue to be quite consistent and satisfactory. The trend toward gradual decrease of leakage with time under load seems to continue, but is now quite weak. As expected, the nipples seem to stabilize near an optimal value for each specimen.

Tests at temperatures above 550°F (the highest so far) and at pressures above 5 psig will be undertaken.

(iii) Failed-fuel Location Method Development (E. S. Sowa)

Last Reported: ANL-7527, p. 38 (Dec 1968).

(a) Sodium Test Loop. The welding of the loop was completed, and the gas-disengagement-chamber detection loop was installed in position. The dump-tank connection and gas-equalization lines were installed, after which the loop was pressuretested and leakchecked. All leaks were corrected. The control consoles were wired and installed; installation of Calrod and tracing heaters has begun.

A second gas-detection loop will be installed on the surge tank as requested by the FFTF Project. Parts for this second loop will be scavenged from other systems.

A program schedule has been prepared for the remainder of the fiscal year; it reflects redirected emphasis to accomplish the objectives of the program and delineates additional costs.

A brief theoretical analysis indicates that an experimental determination of bubble-size distribution can be performed in 1200°F sodium. Although such an experiment would require additional effort, it

would produce data on bubble-size distribution after injection of the sample and would lead to a better understanding of the hydrodynamical model of bubble behavior.

2. Fuel Handling, Vessels, and Internals--Core Component Test Loop (CCTL) (R. A. Jaross)

Last Reported: ANL-7527, pp. 38-39 (Dec 1968).

The pressure differential across the FFTF prototype subassembly under flowtest has remained constant at 45.9 psig.

From December 15, 1968 through January 23, 1969 the CCTL has been in continuous operation for 956.7 of the 960 hr available (the pump was off for 3.3 hr). The cumulative total operating time at any temperature is 3079.3 hr, of which 1699.1 hr were at 1060°F and 400 gpm.

Data related to sodium purity (see also Progress Report for November 1968, ANL-7518, pp. 33-34), are shown in Table I.C.1.

TABLE I.C.1. Quality of Sodium in CCTL

| Date | Loop Temp (°F) | Minimum Cold-trap Coolant Temp (°F) | Plugging Temp (°F) |
|---|---|---|---|
| 11/15/68 | 550 | 242 | 249[a] |
| 11/20 | 650 | 195 | <215 |
| 11/22 | 700 | 198 | 219 |
| 11/25 | 750 | 200 | 218 |
| 11/26 | 800 | 207 | 231 |
| 11/27 | 850 | 200 | 230 |
| 12/2 | 900 | 214 | <215 |
| 12/3 | 955 | 214 | <215 |
| 12/4 | 997 | 200 | <215 |
| 12/5 | 1060 | 224 | <252 |
| 12/9 | 1060 | 190 | <215 |
| 12/11 | 1060 | 180 | <252[b] |
| 12/13 | 1060 | 196 | <215 |
| 12/23 | 1060 | 200 | 225 |
| 12/24 | 1060 | 184 | 220 |
| 1/2/69 | 1058 | 189 | 260 |
| 1/3 | 1060 | 175 | 255 |
| 1/7 | 1060 | 157 | 296 |
| 1/8 | 1060 | 153 | 248 |
| 1/13 | 1060 | 229 | 250 |
| 1/14 | 1060 | 224 | 260 |
| 1/16 | 1060 | 200 | 255 |
| 1/17 | 1060 | 229 | 250 |
| 1/20 | 1060 | 212 | 235 |

[a]Analysis of sodium sample taken 11/15/68 showed 7 ppm oxygen and 10 ppm carbon.

[b]Analysis of sodium sample taken 12/11/68 showed 8 ppm oxygen and 10 ppm carbon; a second analysis by a different laboratory showed 14 ppm carbon.

Leakage of oil through the face seal of the mechanical pump was measured hourly from December 15 to January 23. These leakage rates to an external collection vessel were measured with the pump and associated face seal at equilibrium temperatures corresponding to loop speed for 400 gpm. The average leakage was 3.2 $cm^3/hr$, the maximum was 4.7 $cm^3/hr$, and the minimum value was 2.5 $cm^3/hr$. These data at 1060°F are consistent with previous data (see Progress Report for October 1968, ANL-7513, p. 41) that showed leakage at room temperature to be 1.9 $cm^3/hr$ and are acceptable.

Between December 15 and January 23, the measured average consumption of inert gas for the CCTL was 1.4 $ft^3/hr$ at 3.0-5.0 in. of water pressure. Other CCTL data that were recorded included temperature profiles for the test vessel, valves, pumps, drain line, and overflow tank as related to liquid levels. All were consistent with design control temperatures.

## D. Systems and Plant--LMFBR

### 1. 1000-MWe Plant

#### a. Contract Management, Technical Review, and Evaluation (L. W. Fromm)

Last Reported: ANL-7527, pp. 39-40 (Dec 1968).

The final edited copy of the Westinghouse Task-I report has been received and is being reviewed by ANL. The Task-I reports of the other contractors are being published and are expected to be distributed within a few months.

(i) Babcock & Wilcox Co. Subcontract. B&W is editing and reproducing the Task-II and -III final report, which describes the B&W reference concept, and the Task-IV report, which describes the requirements for research and development.

(ii) Westinghouse Electric Corp. Subcontract. The reports on the plant-availability and the Task-V safety studies have been completed and are being reviewed within Westinghouse. The final design of the primary and secondary pumps has been completed. The architect-engineer has submitted partial drafts of the design descriptions of the conceptual systems. All material for the Task-IV report is being integrated for the final report.

(iii) General Electric Co. Subcontract. A draft of the Task-III report has been received; it is complete except for some additional overall design work being done on the carbide-fuel core. Most material for the Task-IV report is complete and is being integrated for the final report.

(iv) Combustion Engineering, Inc. Subcontract. Work on the follow-on study has been completed, except for publication of the Task-IV report describing the requirements for research and development.

(v) Atomics International Subcontract. The thermal-hydraulic analysis of the Task-III reference reactor and revision of the reactor structural drawings have been completed, but static nuclear analysis is still in progress. The Task-II and -III reports, which will be issued in several volumes, are being edited. Drafts for all but two sections of the Task-IV report have been completed. Completion of the follow-on study is still scheduled for March 1969.

## E. EBR-II

### 1. Research and Development

#### a. Reactor Experimental Support--Reactor Analysis and Testing (R. R. Smith)

Last Reported: ANL-7527, pp. 40-43 (Dec 1968).

(i) Nuclear Analysis and Safety

(a) The Origin of the September 9, 1968, Fission-product Release. During the startup of Run 30B on September 7, 1968, the equilibrium activity levels for $^{133}Xe$ and $^{135}Xe$ in the cover gas of the primary system were found to be approximately double those established during Run 30A. From the shape of the buildup curves for these species, the conclusion was reached that: (1) a fission-product release had occurred, and (2) the release was characteristic of one which permitted bond sodium to extrude through a cladding defect (see Progress Report for September 1968, ANL-7500, p. 44).

Throughout the remainder of Run 30, and during Runs 31 and 32, attempts were made to locate the source of the release by removing and replacing groups of suspect subassemblies and restarting the reactor (see ANL-7527, p. 42). All driver-fuel elements and all fueled irradiation experiments were demonstrated not to be the source of the activity. The source was then sought in the eleven control rods of the reactor.

The equilibrium activity levels of $^{135}Xe$ with a given control rod fully inserted and fully withdrawn were established. On December 8, a definite decrease in the $^{135}Xe$ activity was noted when control rod No. 2 (Subassembly L462) was withdrawn. Reinsertion caused an increase, and a final withdrawal caused a decrease. Subassembly L462 was removed from the core on December 17 and disassembled in the air cell of the Fuel

Cycle Facility. From measurements of sodium level and visual inspections, the cladding defect located approximately 2.65 in. above the top of the fuel column. Procedures used in locating the defect and details relevant to the defect are given in Sect. I.E.2.b.(iii)(c).

Location of the defect made it possible to postulate a mechanism to explain the basic nature of the fission-product release. Until Subassembly L462 was removed, the $^{133}Xe$ and $^{135}Xe$ activities equilibrated at values approximately twice those established during Runs 29 and 30A. Because the buildup of activity was gradual (rather than stepwise) and because no increase was noted in the FERD and FGM signals, the release was attributed to the extrusion of bond sodium from a cladding defect. Such a mechanism explained the gradual buildup because the bond sodium would preferentially carry iodine parents which would decay into the $^{133}Xe$ and $^{135}Xe$ activities. The short-lived iodine and bromine species, which directly and indirectly are sensed by the FERD and FGM systems, could not survive long enough to diffuse from the place of their release, through the sodium annulus, and to the defect.

Although such a mechanism is still considered valid, it met with one principal objection. From a knowledge of the signal-to-noise ratio obtained from the exposed-fuel calibration studies done in November 1968, it was possible to estimate with an acceptable degree of reliability the sodium leakrate that would be needed to give signals of the intensity noted. On several occasions, however, the reactor was operated long enough for the entire bond sodium to be extruded from the element. No evidence of a gas release was ever noted. Because of this, the conclusion was reached that either the leakrate calculations were in error or that some other mechanism existed for the intermittent transfer of bond sodium through the defect.

The original calculations of leakrates based on exposed-fuel studies appear to be reliable, but such rates were effective rates that did not consider the possibility of intermittent extrusion of the sodium bond.

Observations of sodium level in the leaking element of Subassembly L462 permit the postulate that the leak was intermittent and that the driver force for such a leak is short-term fluctuations in coolant pressure. Such fluctuations are believed to be caused by turbulent flow through the subassembly or normal variations in pump output, or both. When the pressure is momentarily higher on the coolant side, sodium is forced inward through the cladding perforation. Conversely, when the pressure is lower on the coolant side, bond sodium and chemically fixed halogen fission products are forced out. Because the extruding sodium is swept away by the coolant flow, the net result is a delivery of halogen fission products to the primary system.

Because of the pressure produced by the pump [see Sect. (d) below], the bond level is held at some point above the cladding perforation. The level oscillates with coolant pressure, but presumably cannot drop to the level of the defect while the pumps are on. This postulated mechanism can be made to be consistent with the leakrate model previously used by redefining the previously calculated leakrate as an effective leakrate.

The postulated intermittent-leakrate mechanism is consistent with the results of other analyses. As illustrated in Sect. (d), the radial and axial pressure profiles in the EBR-II core have significant bearing on the nature of bond leaks. For the elevation of the cladding perforation of the fuel element in Subassembly L462, it is now understood that the sodium could be released on a pump shutdown and forced back in on a pump startup. Inferential experimental evidence of such a phenomenon is given in Sect. (b).

(b) Sodium Release through a Cladding Perforation on Pump Shutdown. The intermittent-leak model postulated in Sect. (a) predicts that when communication between primary and bond sodium is permitted by a cladding defect, a pump shutdown may lead to the extrusion of bond sodium through a defect. Re-examination of the $^{135}Xe$ activity following the shutdown of Run 30A on September 5 reveals that the leak, apparent during Run 30B, could very likely have been active during the final portion of Run 30A, because some evidence of bond extrusion was indicated after the shutdown. In principle, the $^{135}Xe$ activity resulting from bond extrusion after shutdown may be estimated by subtracting calculated values of the activity from those established experimentally. A graphical illustration of this subtraction is given in Fig. I.E.1. In processing the information presented in Fig. I.E.1, the equilibrium value for $^{135}Xe$ was assumed to be $3.55 \times 10^{-3}$ $\mu$Ci/ml (actually an average value for September 4 and 5 when the $^{135}Xe$ activity had reached equilibrium). Multiplication of this value by the appropriate buildup and decay factors gave the values for plotting the curve that is second from the top in the figure. Subtraction of these values from experimental values (top curve) gave the growth curve for $^{135}Xe$ following shutdown (marked the "difference curve"). From the evidence indicated in the figure, the conclusion may be made that $^{135}I$ was released to the primary coolant following the shutdown of Run 30A. In this instance, power was reduced to 500 kW at 1850 and the primary pumps were turned off at 1940.

Subsequent releases of $^{135}I$ during Run 30B and throughout Runs 31 and 32 are understandable in terms of a model which postulates that, when the coolant pumps are turned off, the associated reduction in pressure causes bond sodium to be forced through the defect. When the pumps are restarted prior to the following startup, the pressure gradient

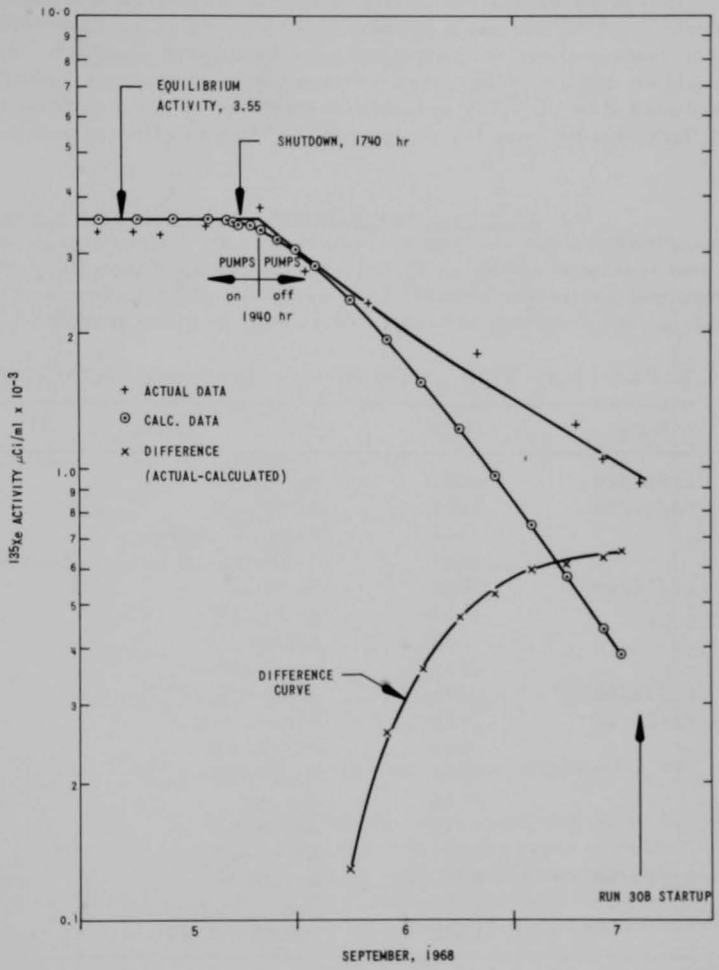


Fig. I.E.1. $^{135}$Xe Activity at Time of Fission-product Release in September 1968

is reversed; primary sodium is forced back into the leak and up past the level of the defect. Although the gas pressure in the plenum of the fuel element increases during the ascent to power, the increase is more than compensated for by the pump pressure. Accordingly, the bond level is expected to remain above the defect until the next pump shutdown. As discussed above, the communication between bond and primary sodium permits a net outward flow of $^{135}I$ by possible fluctuations in the instantaneous pressure differential between the gas plenum of the fuel element and the primary coolant.

(c) Fission-product Release of December 24, 1968. Another fission-product release having characteristics similar to those described above was indicated on December 24. In this instance the effect of pump shutdown was particularly marked. A summary of pertinent events preceding, during, and following the indicated release is given in Table I.E.1.

TABLE I.E.1. Time-Power History, December 17-24, 1968

| Date | Time | Event |
|---|---|---|
| 12/16/68 | 0745 | At 50 kW |
| 12/17/68 | 0109 | At 50 MW |
| | 0344 | Began shutdown |
| | 1245 | Transferred L462 to basket |
| 12/18/68 | 0604 | At 50 kW |
| | 1533 | At 30 MW |
| | 1615 | Scram |
| | 2115 | At 50 kW |
| 12/19/68 | 0250 | At 50 MW |
| 12/23/68 | 0110 | Scram |
| | 0245 | At 500 kW |
| | 0710 | At 50 MW |
| | 1035 | Scram |
| | 1510 | At 500 kW |
| | 1751 | At 50 MW |
| 12/24/68 | 0903 | Scram |
| | 1110 | Pumps turned off |
| | 1450 | Fuel handling |

A graphical summary of the $^{135}Xe$ activity data for the period December 20-26 is given in Fig. I.E.2. Although only four cover-gas samples were taken and analyzed on December 24, it is apparent, from an inspection of the data, that a fission-product release occurred, presumably following the pump shutdown at 1110. A separation of the $^{135}Xe$ activity resulting from the leak was effected by subtracting calculated values of the $^{135}Xe$ activity from measured values after the shutdown. In this instance,

too, the buildup of $^{135}Xe$ after shutdown is evident. Control-rod Subassembly L462 was not suspect because it had been removed from the core approximately one week earlier (on December 17). During this time the $^{135}Xe$ inventory in L462 had decayed by a factor of approximately $6 \times 10^5$.

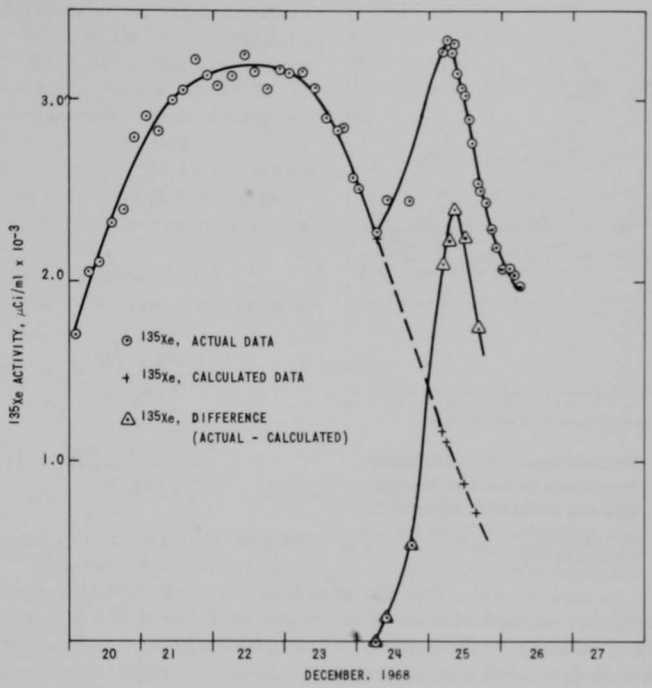


Fig. I.E.2. $^{135}Xe$ Activity at Time of Fission-product Release of December 24, 1968

Since the December 24 release, two other releases have been noted: one following a scram and subsequent pump shutdown on December 27, and the other following normal reactor and pump shutdowns on January 2. In both cases $^{133}Xe$ and $^{135}Xe$ activities appeared to be normal during power operation and increased only after reactor and pump shutdowns.

(d) An Analysis of Several Modes of Cladding Penetration in Mark-IA Fuel Elements in EBR-II. Several cladding-penetration modes in Mark-IA fuel elements have been analyzed to predict probable consequences. In Fig. I.E.3 are given the estimated dynamic (pumps on) pressures at various radial and axial locations in the core. These pressures and the following assumptions constitute the basis for the following calculations reported.

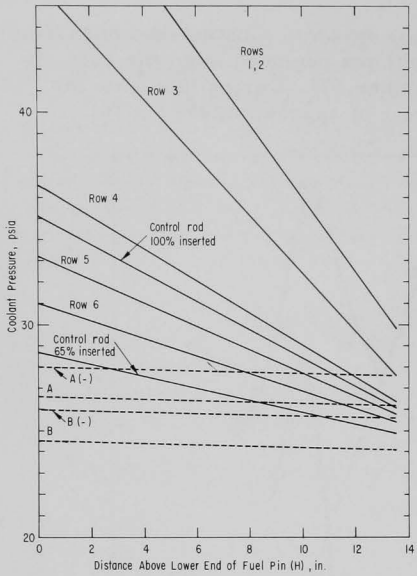


Fig. I.E.3. Coolant Pressures at Which Sodium Bond Could Be Extruded through a Cladding Perforation (Interpretation and application of figure are explained in text)

(1) The coefficient of thermal expansion for steel was taken to be $10 \times 10^{-6}/°F$

(2) The coefficient of thermal expansion for uranium in the absence of firm information on irradiated metal was set at $10 \times 10^{-6}/°F$. This value is more conservative for these purposes than the usual value of $8 \times 10^{-6}$ The effective fuel temperature at 50 MW was taken to be 1000°F, which corresponds to an 840°F coolant outlet temperature.

(3) Growth for irradiated low-silicon fuel were set as

$$\frac{V_{0.95\%\ burnup}}{V_{fresh}} = 1.064;$$

$$\frac{V_{1.20\%\ burnup}}{V_{fresh}} = 1.139,$$

where V denotes fuel volume.

(4) The dimensional data and calculated dimensional characteristics of fuel elements as shown in Table I.E.2 were used. (The term "free" volume means that volume within the normal jacket which can be filled with fuel, sodium, or argon; it does not include the volume occupied by the restrainer.)

Of primary concern are the questions: Under what circumstances is it likely that a leak will lead to operation with "dry" (unbonded) fuel? Would the resultant melting of the fuel create abnormal pressures within the jacket? From the results of bare-pin experiments and the recent cladding penetration in L462, the release of fission products from unmelted driver fuel has been shown to be low.

No perforation above the top of the fuel pin can lead to unbonded uranium. If the perforation is above the level of the bond sodium, the fuel element, when immersed in the bulk sodium, will expel nonrecoverable gas when there is a positive pressure differential, and will inhale sodium when there is a negative differential. This process continues until the sodium level stabilizes near the cladding penetration. If the cladding perforation is below the original level of the sodium bond, however, bond

sodium may be expelled until it reaches the level of the perforation. The level of the bond sodium at no time can fall below the level of the perforation, regardless of the variations of temperature and pressure.

TABLE I.E.2. Dimensions of Low-silicon, High-expansion Fuel Pin as a Function of Burnup

| Fuel Condition | Length of Fuel Pin (in.) | Pin Diameter (in.) | Pin Vol ($cm^3$) | Growth in Fuel Vol (%) | Free Vol of Jacket ($cm^3$) | Sodium Vol ($cm^3$) | Plenum Vol ($cm^3$) | Plenum Pressure (psia) | Annular Vol ($cm^3$/in in.) | Total Annular Vol ($cm^3$) | Vol of Sodium over Pin ($cm^3$) | Total Free Vol over Pin ($cm^3$) | Pressure When Gas Occupies Free Vol over Pin (psia) |
|---|---|---|---|---|---|---|---|---|---|---|---|---|---|
| At 70°F | | | | | | | | | | | | | |
| Fresh | 13.5 | 0.144 | 3.603 | | 5.952 | 0.796 (0.761)[a] | 0.633 (0.698) | 12.2 (12.2) | 0.0465 | 0.628 | 0.168 (0.133) | 0.831 | |
| 0.95% Burnup | 13.6 | 0.148 | 3.833 | 6.4 | 5.062 | 0.796 (0.761) | 0.433 (0.468) | 18.7 (18.2) | 0.0312 | 0.424 | 0.372 (0.337) | 0.805 | |
| 1.20% Burnup | 13.8 | 0.152 | 4.105 | 13.9 | 5.062 | 0.796 (0.761) | 0.161 (0.196) | 50.2 (43.5) | 0.0158 | 0.218 | 0.578 (0.543) | 0.739 | |
| At Operating Position--Reactor Down--Pumps Off--700°F | | | | | | | | | | | | | |
| Fresh | 13.58 | | 3.671 | | 5.158 | 0.891 (0.851) | 0.596 (0.636) | | | | | 0.847 | 29.0 (22.0) |
| 0.95% Burnup | 13.68 | | 3.905 | | 5.158 | 0.891 (0.851) | 0.362 (0.402) | | | | | 0.820 | 21.6 (22.7) |
| 1.20% Burnup | 13.88 | | 4.183 | | 5.158 | 0.891 (0.891) | 0.084 (0.044) | | | | | 0.753 | 23.5 (24.7) |
| Operating--840°F | | | | | | | | | | | | | |
| Fresh | 13.6 | | 3.703 | | 5.180 | | | | | | | 0.850 | 23.3 (24.6) |
| 0.95% Burnup | 13.7 | | 3.940 | | 5.180 | | | | | | | 0.824 | 24.1 (25.6) |
| 1.20% Burnup | 13.9 | | 4.220 | | 5.180 | | | | | | | 0.756 | 26.2 (27.6) |

[a]All numbers in parentheses refer to a pin erroneously filled with sodium to a level 0.15 in. below nominal.

Cases for cladding perforations occurring in the vicinity of the fuel are considered in Fig. I.E.3. The solid lines indicate the total absolute pressure at various elevations H above the bottom of the fuel pin and at several radial positions in the EBR-II core under conditions of full coolant flow. Dotted line A refers to a normal fuel element at 1.20 a/o burnup; it indicates for a leak at position H the external pressure which would just barely allow the sodium meniscus to reach the top of the fuel. Dotted line A(-) refers to the same situation except that the sodium loading was assumed to be erroneously 0.15 in. lower than nominal (i.e., 0.50 in. instead of 0.65 in.). (It should be noted that the underfilling of sodium assumed in preparing this graph is unlikely, considering the quality control of the production of fuel elements.) Line B and B(-) are parallel cases for fuel elements at 0.95% burnup. For fresh fuel, the values would be substantially lower than for B. The slight slope of the dotted lines takes into account the effect of the static head of sodium within the fuel element. Unbonding of fuel during pump operation can occur only in regions in which the solid line falls below the pertinent dotted line. Aside from cases of low-sodium filling, the regions of the reactor susceptible to fuel melting as a result of bond extrusion represent a fairly small part of the entire driver core.

Three hypothetical cases have been considered in which the coolant pressure falls below that necessary to keep the fuel covered.

Case I: Assume that a large leak occurs in a 1.20%-burnup pin (inadvertently lacking 0.15 in. of sodium) in Row 5 at H = 11.5. From Fig. I.E.3 the external pressure of the coolant is 26.9 psia. The original gas loading of 0.698 $cm^3$ (at 70°F and 12.2 psia) will expand to

$$V = 0.698\ cm^3 \times \frac{1300}{530} \times \frac{12.2}{26.9} = 0.776\ cm^3 \text{ at } 840°F,$$

of which 0.756 $cm^3$ can be accommodated in the free space above the fuel. The remaining 0.020 $cm^3$ will drive the sodium down the annulus 0.020/0.158 $\approx 1\frac{1}{4}$ in., where 0.0158 (from Table I.E.2) is the annular volume (in $cm^3$) per inch. The $1\frac{1}{4}$ in. (approximately 6 g) of unbonded fuel would melt almost instantaneously and freeze against the jacket wall. Assume that this frozen fuel plugs the annulus hermetically and that all fission-product gas is released to the plenum. Assuming that 27% of the fission-product atoms are gaseous and assuming 1.20% burnup to the very end of the pin, approximately 1.8 $cm^3$ (STP) of fission-product gas would be yielded. The volume constraint at the exit coolant temperature of 840°F yields a gauge pressure of about 100 psi.

Case II: Assume, as another example, a 1.20%-burnup pin in a control rod. Assume that this pin also has been underloaded with sodium by 0.15 in. and that a leak occurs at the midlength of the fuel (H = 6.75 in.) while the control rod is only 65% inserted in the reactor. Assume also that the temperature of the plenum is 840°F. From Fig. I.E.3, the external coolant pressure is 26.8 psia. With a sudden leak, the gas will expand to

$$V = 0.698 \times \frac{1300}{530} \times \frac{12.2}{26.8} = 0.780\ cm^3,$$

a volume almost identical to that obtained in Case I.

Case III: Assume a similar pin (1.20% burnup, underloaded with sodium) in Row 6 has a sudden leak at H = 12 in. The external pressure is 26.1 psia and the gas expands to

$$V = 0.698 \times \frac{1300}{530} \times \frac{12.2}{26.1} = 0.800\ cm^3.$$

However, the total volume of the jacket down to the leak is such that about 0.020 $cm^3$ (~$2\frac{1}{2}$%) of the gas will be expelled. About 7 g of fuel would melt, and the resulting pressure would be slightly higher than that in the two preceding cases.

The foregoing examples indicate that an unlikely linking together of unfavorable circumstances would be needed to unbond even a

small amount of fuel when the pumps are on. In the first place, an overload of argon (i.e., sodium low by 0.15 in.) has been assumed. Furthermore, the leak has been assumed to occur in the upper part of a pin in a low-flow channel and to be large and sudden, permitting the gas pressure to drive the bond down instantly to the equilibrium level, after which the molten uranium freezes into a hermetic plug. More realistically, the leak would probably cause a much slower ejection of bond. Consequently, the top of the pin would melt before much uranium was exposed and would form a plug higher up. This would mean that less bond would be expelled, much less uranium melted, and less gas evolved, and the plenum pressure would be much lower. Further, it was assumed that the pin is at 1.20% burnup to its very end and that it was fabricated from high-expansion fuel. Such material is no longer used for pin fabrication, although some pins made with high-expansion material are either in the reactor or in the fuel inventory.

(e) Blockage of Channel Flow when Operating with Oxide Fuel. To determine the probability of cladding failure being propagated from one rod to an adjacent rod, the temperature distribution was determined for a fuel rod subjected to two conditions of blocked flow.

In the first case, a fuel rod was assumed to have ruptured, and the dispersed fuel was assumed to have been deposited with a uniform thickness of 0.056 in. (the thickness of a spacer wire) on an adjacent fuel rod. The sodium coolant was assumed to remove the heat from both the uncovered surface of the fuel rod and the surface of the deposit. In the second case, the fuel was assumed to fill a coolant-channel triflute so that a 60° arc of the surface of the fuel rod was covered with fuel and the heat generated in the fuel deposit had to be transferred circumferentially to the coolant outside the filled triflute. In both cases, the fuel deposit was assumed to be at its original conditions of density and volumetric heat generation. The fuel was assumed to be $UO_2$-$PuO_2$ in both cases. Because of the low thermal conductivity and high melting point of the fuel, the stainless steel cladding possibly could be heated to the point of failure.

The fuel rod in both cases was assumed to be a 0.29-in.-OD by 0.015-in.-wall stainless steel rod that contained 80% $UO_2$-20% $PuO_2$ pellets. The rod was assumed to operate at a maximum heating rate of 16 kW/ft. The fuel was assumed to be composed of a central region of columnar grains at 99% of theoretical density, an annular region of equiaxed grains at 97% of theoretical density, and an outer region of the oxide at its original density. A void was assumed to be at the center with a volume equal to the porosity changes that occurred in the columnar and equiaxed grain regions. The columnar grains were assumed to form above 3900°F, and the equiaxed grains between 3000 and 3900°F. Because of the density variations possible in fuel, calculations were made for fuel at 92% and 82% of theoretical density. The calculated temperatures and radii of the fuel pellets are given in Table I.E.3.

TABLE I.E.3. Calculated Temperatures and Grain Radii of Oxide Fuel Rod Operating at 16 kW/ft

| | | |
|---|---|---|
| Fuel density (% of theoretical) | 92 | 82 |
| Maximum temperature (°F) | 4580 | 4360 |
| Surface temperature (°F) | 1530 | 1530 |
| Void radius (in.) | 0.022 | 0.039 |
| Columnar-grain radius (in.) | 0.066 | 0.071 |
| Equiaxed-grain radius (in.) | 0.092 | 0.097 |
| Original-density radius (in.) | 0.125 | 0.125 |

The fuel in both cases was assumed to have expanded and to be in contact with the cladding, and the fuel-to-clad contact conductance was set at 1500 Btu/(hr)(ft$^2$)(°F). The heat was assumed to be removed by 850°F sodium flowing at 12 ft/sec. Axial heat conduction was neglected.

In the first case, two-dimensional temperature distributions were obtained from the THTB program for different angles of fuel coverage. After a 100° arc of the fuel surface had been covered, the cladding temperature was found to increase to 2570°F for 92%-total-density fuel and to 2760°F for 82%-total-density fuel. As the melting temperature of Type 304 stainless steel is 2550-2650°F, the cladding of the fuel rod would melt.

In the second case, the maximum cladding temperatures calculated were 2100°F for 92%-total-density fuel and 2170°F for 82%-total-density fuel. Although the cladding would be below its melting temperature, its tensile strength would be low. For a tensile strength of 2000 psi at 2200°F (unirradiated Type 304 stainless steel), the bursting pressure would be approximately 300 psi. Therefore, if the internal gas pressure resulting from a fission-gas release is greater than 300 psi, the cladding would fail.

b. Nuclear Analysis Methods Development

Last Reported: ANL-7527, pp. 44-48 (Dec 1968).

(i) Analysis of Some ZPR-3 Assemblies. Preliminary analysis is being made of ZPR-3 Assemblies 2, 5, and 6F using the ENDF/B cross sections and cross-section set 238. These three assemblies have approximately the same size and material-volume fractions as the EBR-II core.

The point ENDF/B cross sections are being used in the MAC code by employing the isotopic-consistent $B_1$ approximation to generate 22-group cross sections for the core and blanket materials of each assembly. These cross sections are then used in the SNARG-1D code to calculate the critical mass for a spherical-geometry model of each assembly. Similar SNARG-1D calculations are being done with the 22-group set 238.

Initial results indicate that the ENDF/B cross sections for the materials in these assemblies may be overreactive by ~1.5% in $k_{eff}$ when compared with those in Set 238 and with the experimental results. However, the manner of generating $\Sigma_{tr}$ in the isotropic-consistent $B_1$ option may have introduced some uncertainty. An anistropic treatment may reduce the reactivity calculated with the ENDF/B data.

c. Equipment--Fuel Related (E. Hutter)

(i) New Control Rod Subassemblies (O. S. Seim and T. E. Sullivan)

Last Reported: ANL-7527, pp. 49-50 (Dec 1968).

(a) Greater-worth Control Rod. Fabrication of the new lower shield piece for the control rod was completed. Tests conducted on the increased-holddown-effect (IHE) control rod with the new shield piece installed showed a total pressure drop of approximately 41 psi, approximately 5 psi lower than the total pressure drop measured with the original shield piece installed. To reduce the total pressure drop further to the required 38.8 psi at 61 gpm, the top ends of the $B_4C$ tubes were modified to provide an exit taper to improve pressure recovery. Tests conducted using the modified $B_4C$ tubes showed a total pressure drop of approximately 38 psi.

Calculations were made of the orifice sizes for the orifice tube, using the apparent 0.8-psi maximum allowable pressure drop as the controlling factor. For the initial test of pressure drop through the orifice tube, the orifices were sized somewhat smaller in diameter than the calculated diameters; this permits approaching the correct total pressure drop by increasing the orifice diameters as required.

Effects of Fast-reactor Irradiation on Boron Carbide (J. H. Kittel)

Considerable interest has developed in the behavior of boron carbide under fast-reactor conditions because of the selection of the material for higher-worth control rods for EBR-II and for the FTR. The first significant US experience with irradiation of boron carbide in a fast reactor is being obtained with pellets taken from an oscillator rod used in EBR-II for approximately one year.

The pellets had been made by blending boron powder, 93.9% enriched in boron-10, in stoichiometric proportion with Thermax-brand carbon powder. The mixture was calcined in a closed graphite crucible at 2000°C for one hour, and the resulting $B_4C$ cake was ball-milled

to -325 mesh powder. The powder was hot-pressed in graphite dies at 2000°C into pellets 0.437 in. in diameter by 1.00 in. long. The densities of the pellets ranged from 90 to 93% of theoretical. The pellets were then centerless-ground and loaded as a 14-in.-long column into a sealed Type 304L stainless steel tube.

The oscillator rod was used in position 5A3 in EBR-II from April 10, 1967 to June 20, 1968. During this period it accumulated a total exposure of 5070 MWd, equivalent to 113 full-power days. The total $^{10}B$ burnup was 1.8 a/o; the total boron atom burnup was 1.7%. Under irradiation the rod operated at a peak linear power rating of 88 W/cm. The maximum calculated centerline temperatures ranged from 800 to 1000°F.

After this irradiation, the cladding of the rod was punctured to determine the extent of gas release. At room temperature the pressure increase within the rod resulting from gas release was 7 psi. From this it can be calculated that helium gas release amounted to 11% of the theoretical yield.

The pellets were removed from the cladding intact, except for the two pellets at the center, which had clean transverse fractures. None of the pellets showed significant diameter changes. The gamma activity of the pellets three months after removal from the reactor ranged from 2.3 to 9.0 R/hr at 4 in.

Postirradiation metallography revealed no unusual features in the microstructure of the boron carbide. Examination of a complete pellet cross section will be made with a shielded microprobe after carbon-coating equipment is installed in a hot cell.

Metallographic examination of the cladding is in progress. Of particular interest will be examinations for possible evidence of carburization of the inside surface of the cladding.

(ii) Oscillator Rod--Mark II (O. S. Seim and T. E. Sullivan)

Last Reported: ANL-7527, p. 50 (Dec 1968).

Fabrication drawings of the new design of the seal for the oscillator rod, have been completed and are now being checked. Fabrication of the Mark-IIA type-4 rod is complete except for stress relieving and balancing, which will be done after completing water flowtests.

d. New Subassemblies Design and Experimental Support (E. Hutter)

(i) Radial Blanket (O. S. Seim and W. R. Ware)

Last Reported: ANL-7478, p. 59 (July 1968).

The proposed design of the radial-blanket (nickel reflector) subassemblies for Rows 7, 8, 9, 10, and 11 is being revised to reflect the comments of reviewers. Investigation of the effect of heat generation in thick sections of stainless steel is being continued. Simplified methods of fabrication are being studied to reduce the unit cost of the subassembly.

e. Instrumented Subassembly (E. Hutter)

Last Reported: ANL-7527, pp. 52-54 (Dec 1968).

(i) Research and Development (A. Smaardyk and H. H. Hooker)

(a) Ball Screw and Nut Assemblies of Drive System. The elevator assembly that supports the instrumented-subassembly package is moved vertically by two special ball screw and nut assemblies. To prevent unequal wearing of the ball screws, each ball screw and nut assembly must share the 400-lb operating load approximately equally. The manufacturing tolerance for the ball screw allows ±0.002 in./ft of lead error in each screw. With this tolerance, a maximum of 0.032-in. difference in elevation between the two screws could result, causing one screw to carry the entire load. To avoid this potentiality, each screw is independently suspended from the drive system by spring supports. These supports compensate for the lead-error accumulation in the screws over the entire 8 ft of travel of the elevator.

The spring support consists of a series of Belleville spring washers on the top end of the ball-screw journal. The washers ride between the radial support bearing and the upper locking nut on the journal. With this arrangement, the ball screw can change its vertical position in the drive system as a function of the load imposed on it by the ball nut.

By using this arrangement for each ball screw, a relatively even distribution of the load between the two screws is ensured. This distribution is effected by compression of the spring support on the ball screw that has the greatest lead-error accumulation or the greater share of the operating load. As the bulk of operating load shifts to one screw, that screw is displaced downward by the application of the additional load on the spring-washer assembly. This displacement progresses until the load is again distributed equally between the two screws.

Operating tests have been made of the drive system to determine the amount of deflection of each ball-screw support assembly versus the lead-screw position (including lead-screw tolerance buildup). The results of these tests indicate a maximum variation of 0.0035 in. between the two ball-screw assemblies caused by the accumulated lead error over the 8 ft of vertical travel. This amount of variation results in a 0- to 30-lb load shift between the ball-screw units. This variation occurred with an 8.8-lb/mil spring constant for the Belleville spring assembly, using a 400-lb load. The maximum load variation (30 lb) occurs only within the last foot of travel. Over the remainder of travel, the load variation is less than 17 lb.

f. Packaged Loop (R. E. Rice)

Last Reported: ANL-7527, pp. 54-55 (Dec 1968).

Further engineering development effort on the loop has been deferred. An informal report summarizing the results of the work to date is being prepared for the files so that they can be reviewed if the task is reactivated in the future.

g. Process Chemistry (D. W. Cissel)

Last Reported: ANL-7527, pp. 55-58 (Dec 1968).

(i) Sodium Coolant Quality Monitoring and Control (W. H. Olson, C. C. Miles, E. R. Ebersole, and G. O. Haroldsen)

(a) Primary Sodium

(1) Radionuclides. The results of analyses for radionuclides in four samples of primary sodium are listed in Table I.E.4.

TABLE I.E.4. Radionuclides in Primary Sodium

| Sample Date | $^{137}I$ ($\mu Ci/g \times 10^4$) | $^{137}Cs$ ($\mu Ci/g \times 10^2$) |
|---|---|---|
| 12/13/68 | 2.64 | - |
| 12/26/68 | 3.43 | 1.34 |
| 12/27/68 | 3.70 | 1.30 |
| 1/6/68 | 1.65 | - |

(2) Trace Metals. A sample of primary sodium taken on December 13, 1968, was analyzed for trace metal impurities by atomic absorption spectrophotometry. Results of the analysis are listed in Table I.E.5.

TABLE I.E.5. Trace Metal Impurities in Primary Sodium

| Metal | Concentration (ppm) | Metal | Concentration (ppm) |
|---|---|---|---|
| Al | <0.6 | Mn | <0.05 |
| Bi | 1.8 | Mo | <0.02 |
| Cd | <0.02 | Ni | 0.1 |
| Co | <0.08 | Pb | 11.4 |
| Cr | 0.5 | Sn | 18.3 |
| Cu | 0.25 | | |

(3) Oxygen. Two primary sodium samples were analyzed for oxygen by the mercury amalgamation method. The results of the analyses are listed in Table I.E.6.

TABLE I.E.6. Oxygen Content of Primary Sodium

| Sample Date | No. Aliquots | Oxygen (ppm) |
|---|---|---|
| 12/12/68 | 3 | 5.0 ± 0.8 |
| 1/3/69 | 6 | 5.7 ± 0.6 |

(4) Carbon. A sample of primary sodium taken on December 12, 1968, was analyzed for total carbon by the oxyacidic flux method. The average carbon content in three aliquots was 2.1 ± 0.8 ppm.

(b) Secondary Sodium

(1) Radionuclides. A sample of secondary sodium taken on December 20, 1968, was analyzed for radionuclides. The $^{24}Na$ content was $2.5 \times 10^{-2}$ $\mu Ci/g$. No other isotopes were found.

(2) Trace Metals. A sample of secondary sodium taken on January 7, 1969, was analyzed for trace metal impurities by atomic absorption spectrophotometry. The results of the analysis are listed in Table I.E.7.

TABLE I.E.7. Trace Metal Impurities in Secondary Sodium

| Metal | Concentration (ppm) | Metal | Concentration (ppm) |
|---|---|---|---|
| Al | <0.6 | Mn | <0.05 |
| Bi | <0.1 | Mo | <0.3 |
| Cd | <0.02 | Ni | <0.08 |
| Co | <0.08 | Pb | 0.4 |
| Cr | 0.06 | Sn | <2.6 |
| Cu | <0.08 | | |

(3) Carbon. A sample of secondary sodium taken on January 6, 1969, was analyzed for carbon by the oxyacidic flux method. The average carbon content in 4 aliquots was 2.7 ± 0.9 ppm.

(c) Primary and Secondary Argon. Concentrations of hydrogen and nitrogen in the primary and secondary cover-gas systems are listed in Table I.E.8.

TABLE I.E.8. Hydrogen and Nitrogen in Primary and Secondary Argon (ppm)

| | Primary | | | Secondary | | |
|---|---|---|---|---|---|---|
| | High | Low | Avg | High | Low | Avg |
| $H_2$ | 192 | 0 | 16 | 0 | 0 | 0 |
| $N_2$ | 5,000 | 3,000 | 3,900 | 300 | 200 | 275 |

h. Experimental Irradiation and Testing (H. Lawroski)

Last Reported: ANL-7527, pp. 59-62 (Dec 1968).

(i) Experimental Irradiations (R. Neidner)

The five following experimental subassemblies completed their scheduled exposure during or at the completion of Run 32:

| Subassembly No. | Capsule Content and Number of Capsules ( ) | Experimenter | Approx Accumulated Burnup (fuels--a/o) (nonfuels--nvt x $10^{-22}$) | Disposition Plan |
|---|---|---|---|---|
| XO25 | Cladding Materials (19) | GE | 3.1 | Return to experimenter. |
| XO39 | $UO_2$-25 w/o $PuO_2$ ( 5) | PNL | 1.0 | Return to experimenter. |
| | UC-20 w/o PuC ( 1) | LASL | 1.5 | Return to experimenter. |
| | $UO_2$-20 w/o $PuO_2$ ( 1) | ANL | 5.2 | Return to experimenter. |
| | $UO_2$-20 w/o $PuO_2$ ( 7) | GE | 5.3* | Hold for reinsertion. |
| | Cladding ( 4) | GE | 1.0* | |
| | Cladding ( 1) | GE | 5.7* | Return to experimenter. |
| XO42 | Boron Carbide ( 4) | PNL | 0.9 | Return two to experimenter; reinsert two. |
| | Tantalum ( 3) | PNL | 0.9 | Hold for reinsertion. |
| XO52 | Mark-IA Fuel ( 3) | ANL | 2.9* | Return to experimenter. |
| XO53 | Mark-II Fuel (37) | ANL | 3.3* | Return some to experimenter; reinsert rest. |

*Had previous exposure in another subassembly.

i. FCF Equipment Improvement (M. J. Feldman)

(i) Process Equipment (N. R. Grant, J. P. Bacca, and V. G. Eschen)

Last Reported: ANL-7518, p. 54 (Nov 1968).

(a) Bond-testing Methods. A survey is being made of methods other than eddy-current techniques for testing the bonds of the experimental capsules and elements. So far, two methods have been found that appear to have promise. Both are based on the difference in the temperature of the surface of the capsule or element opposite the bonded and the unbonded area after the capsule or element has been heated under closely controlled conditions and for a predetermined time.

In one of these methods, a liquid organic chemical that changes color above a certain temperature is coated on the surface of the capsule or element. The area of the surface that is the hottest is identified by the color change. The second method makes use of infrared examination to determine the hottest area of the capsule or element; it is based on the principle used in the optical pyrometer.

After a thorough literature survey and personal contact with the people working with these techniques, the method which appears to have the best potential will be selected for further study.

(ii) Auxiliary Equipment (W. L. Sales and K. H. Kinkade)

Last Reported: ANL-7527, p. 63 (Dec 1968).

(a) Pneumatic Transfer System. The pneumatic sample-transfer system was placed in operation for carrying of samples from the FCF cells to the analytical caves.

j. Superheater and EM Pump Study and Test (R. A. Jaross and E. Hutter)

(i) Superheater Vibration Study (G. S. Rosenberg)

Last Reported: ANL-7518, pp. 54-56 (Nov 1968).

Tube-baffle impact was first studied by approximating the tube by a force-excited beam, clamped at both ends, with stops at the midpoint. For a given force amplitude and frequency, the amplitude of displacement can be determined. This approach is being pursued in greater detail under the structural dynamics studies of crossflow-induced vibrations (see Progress Report for December 1968, ANL-7527, pp. 117-119; and this Progress Report, Sect. III.C.1.d).

A computer code has been formulated to compute displacement, shearing force, and bending stress of a pinned-pinned beam with motion-constraint stops. It is planned to use this code to gain insight into the tube-baffle impact effects in the EBR-II superheater.

The distributed transverse force associated with vortex shedding can be written as

$$f(x,t) = C_k \tfrac{1}{2} \rho_f u^2 d \sin \omega_v t, \tag{1}$$

where $C_k$ is lift coefficient, $\rho_f$ is fluid density, d is tube diameter, u is crossflow velocity and $\omega_v$ is vortex-shedding frequency, which is related to the Strouhal number

$$N_s = \omega_v d / 2\pi u. \tag{2}$$

In the EBR-II superheater, the distribution of crossflow velocity along the length of the tube between baffles is not expected to be uniform; rather, there is some nonuniform distribution and

$$u = u(x).$$

This distribution can be expressed in the form

$$u(x) = \bar{u}_c \psi(\bar{x}), \tag{3}$$

where $\bar{u}_c$ is mean crossflow velocity, $\bar{x}$ is $x/\ell$, and $\psi(\bar{x})$ is a shape function defined such that $\int_0^1 \psi(\bar{x})\, d\bar{x} = 1$. If we assume the vortex-shedding frequency to be constant along the length of the tube and equal to that associated with the mean crossflow velocity, Eq. (1) can be written

$$f(x,t) = \alpha_1 \psi(\bar{x}) \sin \omega_v t. \tag{4}$$

For the EBR-II superheater, $\alpha_1 = 2.78$ lb/ft, $\omega_v = 55.2$ rad/sec ($N_s = 0.2$; single-tube value), and $\omega_v = 182.2$ rad/sec ($N_s = 0.66$; tube-bank value).

To gain insight into the influence of crossflow velocity distribution, we have selected the following three distributions:

$$\psi(x) = \begin{cases} 1 \\ \dfrac{\pi}{2} \sin \pi\bar{x} \\ 1 - \cos 2\pi\bar{x} \end{cases} \tag{5}$$

Considering a two-span section with motion restricted at the two extreme baffle locations, we are using the above-mentioned computer code to obtain the tube displacement, shearing force, and bending stress for the three distributions given in Eq. (5).

k. Feasibility Study of Fuel Failure Detection--Chemical and Mechanical Methods

(i) Trace Elements Analytical Techniques (C. E. Crouthamel)

Last Reported: ANL-7527, p. 65 (Dec 1968).

In evaluating the suitability of an element as a tag, the most important factors to be considered are: (1) solubility of the tag in sodium; (2) sensitivity of analytical detection methods; (3) chemical stability of the tag in sodium; (4) corrosiveness of the tag in the fuel environment; (5) trace element content of EBR-II primary sodium. To aid in tag selection, a survey has been made of the available data on pertinent chemical and physical properties of potential tags. As a result of this survey, many elements have been eliminated as possible tags. A considerable number, however, are still candidates; the most promising appear to be rubidium, antimony, silver, gold, gallium, and thallium.

Testing of methods for determining the isotopic ratio in natural antimony has been continued. The thermal-neutron-activation method was described previously (see ANL-7527). Currently, a spark-source mass-spectrometric method is being studied. In preliminary work, the $^{121}Sb/^{123}Sb$ ratio in natural antimony of 99.999% purity was determined by this method and found to be 1.348. The accepted literature value for the ratio is 1.339. Further work is required to determine the limits of accuracy and sensitivity of the spark-source mass-spectrometric analysis.

Preliminary studies have been started to test the corrosive characteristics of possible tags in a fuel-element environment. Mixtures of 2 w/o Cs-Na, 2 w/o Rb-Na, 2 w/o Sb-Na, and 2 w/o Au-Na were placed in separate capsules of Type 304L stainless steel, which were then sealed and rotated at 650°C for 500 hr. Preliminary metallographic studies indicated that the stainless steel was not attacked by any of the tag elements under these conditions. Additional corrosion studies are planned.

(ii) Sodium Loop--Tag Confirmation Study (F. A. Cafasso)

Last Reported: ANL-7518, p. 56 (Nov 1968).

Design, procurement, and assembly of components of the loop for evaluating the stability of isotopic tags in circulating sodium are continuing. Fabrication of support members for loop components is complete, and bending and welding of piping for the loop have been started.

1. Materials-Coolant Compatibility (D. W. Cissel)

Last Reported: ANL-7518, pp. 56-57 (Nov 1968).

(i) Materials Evaluation

(a) Creep-rupture Testing. A modification of an existing sodium test system allows simple creep-rupture tests of wires of various materials to be run. Initial experiments are being made with stainless steel wires to evaluate the effects of mild carburization at 500 and 550°C on lifetime and elongation.

(ii) Problems Identified due to Operations

(a) Bellows Failure in Valve SN-17. The search is being continued for possible causes of the failure of the bellows of valve SN-17 from the secondary sodium system. Sections of the bellows are being tested in a fatigue tester after being exposed at 550°C to sodium containing about 10 ppm oxygen. Similar specimens will be exposed at 550°C to sodium containing about 30 ppm oxygen, after which they will be fatigue tested. Metallographic sections will be examined to determine if the morphology of the failed section has been reproduced.

(iii) Surveillance Subassemblies

(a) SURV I Subassembly. A section of stainless steel from the can containing the graphite samples in the SURV I subassembly was examined for carbon attack. A hardened case, 0.03 to 0.04 mm deep, was evident on the steel. No sticking of the carbon to the stainless steel was noted during the separation operation. Because the attack zone is such a small fraction of the total cladding thickness, its presence probably has not significantly modified the mechanical properties of the stainless steel.

The lower adapter of the subassembly was sectioned to determine the extent of the sodium attack on the chromium-plated areas. The plate was still present to a depth of 0.065 mm, and the outer surface was smooth on a micro scale. Imperfections in the plating were quite similar to those noted on a control having no exposure. An attempt was made to distinguish the plated areas from the stainless steel by superficial hardness testing. This was unsuccessful both for the control and the exposed specimen, but microhardness traverses of the control clearly showed the increased hardness of the chromium plating.

The equipment for bend testing of SURV specimens is being checked and calibrated.

m. Driver Fuel Transient Performance Studies--TREAT Experiments

Last Reported: ANL-7518, p. 59 (Nov 1968).

(i) Mark IA Fuel TREAT Experiments. Two preirradiated Mark-IA driver-fuel elements fabricated from high-swelling fuel have been encapsulated remotely at TAN in a dry, transparent test assembly for photographic studies in TREAT of failure thresholds and failure mechanisms. These elements are E-34 from Subassembly C-169, having a nominal burnup of 1.2 a/o, and Element BF-05 from Subassembly XO17, having a nominal burnup of 2.5 a/o. Subsequent to assembly at TAN, both test capsules passed instrumentation and leaktests, were decontaminated, and were shipped to TREAT on January 20, 1969. On that date a second leaktest at TREAT revealed leakage through instrumentation connectors on the external surfaces of both test capsules. An attempt will be made to repair these leaks.

In addition to information from high-speed photography and from thermocouples attached to the outer periphery of these pins, information on axial fuel motion in each test assembly will be obtained from two eddy-current motion transducers located axially at the top and bottom extremities of the fuel. The performance of these transducers has been proved under similar test conditions with unirradiated fuel in TREAT (see Progress Report for August 1968, ANL-7487, pp. 65-66).

Neutron radiographs of the pin with 1.2 a/o burnup show a gap of approximately 200 mils between the fuel and the restrainer cap at the top. This gap should be ideal for the detection of fuel motion during transient tests.

The pin with 2.5 a/o burnup is interesting as a limiting case in studies of the transient behavior of Mark-IA fuel. The fuel is touching the top restrainer cap, but there is an axial gap of about 20 mils between the fuel and the bottom of the fuel jacket. Examination of sections from an element similar to this pin showed complete circumferential contact between the fuel and the stainless steel jacket at the midplane of the fuel, causing entrapment of sodium in the annulus between the fuel and jacket in the bottom half of the element. It will be of interest to note whether the pin fails at the restrainer cap or from expansion of trapped sodium.

n. Leak Detection and Location--Xenon Method (R. E. Rice and P. B. Henault)

Last Reported: ANL-7527, p. 69 (Dec 1968).

The first phase of the xenon-tagging program for identification of failed fuel has been implemented. Five Mark-II surveillance subassemblies

and approximately 20 experimental subassemblies containing ceramic fuel are included among those to be xenon tagged in CY 1969. Application of xenon tagging to encapsulated experiments also is being evaluated.

The first xenon tagging of unencapsulated mixed-oxide fuel elements was recently accomplished by General Electric (GE) with consultation from ANL. A 37-element subassembly was tagged with a unique xenon isotopic mixture having a nominal $^{124}Xe$ content of 5%. The tagging technique developed by GE employs a normal 10-cc hypodermic syringe with a 4-ft needle. The needle is filled by a Teppler pump system and operated from outside the glovebox in which the fuel elements are being seal-welded. The sequence of operations in the procedure is as follows:

(1) The hypodermic syringe is purged and filled with 10 cc of xenon tag from a Teppler pump system.

(2) The syringe needle is passed through a septum seal at the top of the welding glovebox.

(3) When a fuel element is ready to be seal-welded, the needle is inserted about 1 ft into the top of the element.

(4) Approximately 10 cc of tag is injected into the element, and the element is capped with its end plug to prevent diffusion of gas out of the element. This operation takes approximately 15 sec.

(5) The end plug is seal-welded to complete the tagging operation. This normally requires 3 to 8 min.

GE conducted a series of prototype tests to demonstrate the adequacy of their apparatus. Five uranium oxide fuel elements were tagged with 1.0 ± 0.1 ml of natural xenon, welded, allowed to stand overnight, and then opened. The gas from each element was analyzed for xenon to determine if it had diffused or otherwise been lost from the system. The results of the analyses are tabulated below:

| Pin | Amount of Tag Recovered (ml) | Time Xenon Remained in Syringe (min) | Time Lapse between Tagging and Seal-welding (min) |
|---|---|---|---|
| 1 | 0.75 | 2 | 36 |
| 2 | 0.75 | 8 | 42 |
| 3 | 0.82 | 15 | 83 |
| 4 | 0.74 | 2* | 7* |
| 5 | 0.72 | 15* | 8* |

*Estimates

In each case approximately 0.25 ml of xenon was lost. Most of the loss was concluded to be the result of unavoidable dilution of the xenon with residual helium. Calculations indicated that the volume of dead space in the 4-ft needle and the 10-cc syringe is approximately 1.5 cc. This volume would be filled with helium following the purge operation and would mix the 10 cc of xenon during fill.

Final seal-welding was delayed for as long as 83 min to determine if this would affect possible diffusion. Data indicate that this delay had no effect.

Two sets of five xenon tags each have been prepared and delivered to ANL. The first set was made by blending natural xenon with xenon enriched to ~12 a/o $^{124}Xe$; the enriched xenon was supplied by Mound Laboratory. These tags are being distributed to experimenters for injection into experimental fuel elements to be irradiated in EBR-II. The second set of tags was made by blending natural xenon and xenon enriched to 1 a/o $^{124}Xe$. These tags will be reserved for possible use in tagging the experimental Mark-II driver-fuel subassemblies for testing in EBR-II.

Arrangements are being made with Mound Laboratory for preparing a set of seven tags by blending natural xenon and xenon enriched to 5 a/o $^{124}Xe$. These tags are expected to be delivered to ANL in March 1969.

o. Oxide Driver

Not previously reported under this heading.

The scope of work on an oxide driver core for EBR-II covers the conceptual and engineering design of a configuration in which a predominant number or all of the driver elements use mixed-oxide fuel. Because the primary mission of EBR-II is to serve as a fast-flux irradiation facility in the AEC's LMFBR program, the design of the oxide-driver core will be based on conservative and realistic considerations of materials, neutronics, thermal-hydraulics, structural analysis, and safety. The objectives of this task are to determine the feasibility of partially or completely driving EBR-II with mixed-oxide fuel and to determine the extent to which such a modification will enhance the capability of EBR-II as a fast-reactor irradiation facility. Such enhancement could come from increased power level, increased flux density, longer fuel lifetime, improved system-safety characteristics, and increased irradiation space. A predominance of oxide-fuel driver elements in EBR-II will provide the system needed for meaningful tests of statistical models of fuel-element reliability as a function of burnup. Work done to date on the oxide driver core has been reported under Nuclear Analysis Methods Development (see Progress Report for December 1968, ANL-7527, p. 44 for last report under that task).

Further testing of the iteration model for group-dependent bucklings against the preliminary oxide-core design tends to confirm the applicability of the model for making scoping calculations of the core. Power distributions predicted by this model were used to make scoping thermal-hydraulics calculations for the 91-subassembly preliminary design. At a power of 62.5 MWt, a core inlet temperature of 700°F, and a core $\Delta T$ of 190°F, the maximum temperatures of the fuel and of the cladding (with hot-spot corrections) were calculated to be 4340 and 1030°F, respectively. The corresponding maximum linear power was calculated to be 13.0 kW/ft, the maximum sodium velocity 22.1 ft/sec, the primary flowrate 8700 gpm, and the core frictional $\Delta P$ 19 psi. These results suggest that there will be no serious thermal-hydraulics problems connected with the preliminary design, even when account is taken later of the fact that not all the 91 subassemblies in the reactor will be fully fueled (i.e., the reactor contains a number of experimental subassemblies that contain nonfueled experiments).

A thermal-hydraulics analysis was also made of a 67-subassembly core operating at the same conditions. The calculated maximum fuel temperature was found to exceed the melting point of the fuel under the hot-spot conditions postulated, and the maximum sodium velocity was calculated to be 33.4 ft/sec. It thus appears that a fuel enrichment should be sought which corresponds to a core somewhat smaller than the one in the preliminary design.

## 2. Operations

### a. Reactor Plant (G. E. Deegan)

Last Reported: ANL-7527, pp. 69-79 (Dec 1968).

#### (i) Operations (J. R. Davis)

Run 32B was concluded on December 24 after a total of 1101 MWd in Run 32. After fuel handling had been accomplished and the primary pumps restarted for Run 32C, the cover-gas activity in the primary tank increased. During subsequent 50-MW operation in Run 32C, the presence of a small source of fission-product release in the reactor was indicated. The four most suspect experimental subassemblies were removed.

During Run 32D, which was completed on January 2 after an accumulation of 1397 MWd in Run 32, cover-gas activity was apparently normal. A detailed analysis of the activity following shutdown, however, revealed that the source of the fission-product release was probably still in the reactor.

The scheduled shutdown of the reactor for maintenance and installation of plant modifications was begun after Run 32D. Required fuel

handling was performed before starting to cool the primary tank for the shutdown. The tank was cooled to 350°F, and the secondary and steam systems were drained and cooled to ambient temperature. Scheduled maintenance and modifications are being made.

Table I.E.9 shows the loading changes made in EBR-II during the current reporting period.

TABLE I.E.9. Loading Changes in EBR-II since December 1, 1968

| Date | Position | Removed[a] | Installed[a] | Comments |
|---|---|---|---|---|
| 12/17/68 | 3D2 | C-2120 | C-2181 | For Run 32B |
| | 5D3 | L-462 | L-473 | |
| | 2D1 | XO00 | C-2008 | |
| | 3B1 | C-2171 | C-2136 | |
| | 4E1 | C-2027 | C-2182 | |
| | 3A2 | C-2167 | XO51 | New experimental subassembly |
| 12/24/68 | 3F1 | C-2148 | C-2167 | For Run 32C |
| | 5C2 | C-2116 | C-2148 | |
| | 3B2 | C-2147 | C-2116 | |
| | 5A2 | C-2103 | C-2147 | |
| | 4F1 | C-2174S | C-2168 | Removal of 70%-enriched subassembly |
| | 4B1 | C-2175S | C-2170 | |
| | 3B1 | C-2136 | C-2171 | |
| | 3C2 | XO39 | C-2183 | Irradiation completed |
| 12/28/68 | 6D2 | XO19 | B-3054 | Removal of subassemblies for investigation of fission-product release. For Run 32D |
| | 6B5 | XO20 | B-3002 | |
| | 5E2 | XO33 | C-2010 | |
| | 4F2 | XA08 | C-2006 | |
| | 6D1 | B-3039 | A-773 | |
| 1/2/69 | | | | End of Run 32D |
| 1/3/69 | 1A1 | C-2112 | N-15 | |
| | 4E2 | XO25 | C-2009 | Irradiation completed |
| | 2C1 | C-2185S | XO00 | |
| | 7D5 | XO42 | A-748 | Irradiation completed |
| | 5B3 | L-465 | CRTGA | Gauging of control-rod thimble |
| | 5B3 | CRTGA | L-460 | |
| | 5C3 | L-466 | CRTGA | Gauging of control-rod thimble |
| | 5C3 | CRTGA | L-461 | |
| | 5B1 | L-464 | CRTGA | Gauging of control-rod thimble |
| | 5B1 | CRTGA | L-459 | |
| | 5F3 | L-463 | CRTGA | Gauging of control-rod thimble |
| | 5F3 | CRTGA | Vacant | Position vacant for installation of instrumented subassembly (now postponed to a later date) |
| | 6C1 | B-3036 | A-896 | |

[a]Subassembly Type:

| | | | |
|---|---|---|---|
| B | Row-6 driver fuel subassembly | X | Experimental Subassembly |
| C | Driver-fuel subassembly | CRTGA | Control-rod thimble gauge |
| L | Control-rod subassembly | A | Depleted uranium inner-blanket subassembly |

The reactor was operated for 99 MWd in January, bringing its cumulative total to 22,765 MWd.

(ii) Operations Maintenance

(a) Cathodic Protection System for EBR-II Containment Shell. The EBR-II steel containment shell was examined for evidence of corrosion after measurements of ground potential indicated the possibility of such attack. The area examined was pitted where the corrosion-resistant coating had been scraped off, apparently during the placement of the earth backfill around the building during construction. A specialist was contracted by the Laboratory to evaluate the problem and recommend an appropriate solution.

The cathodic protection system for the containment shell was installed in November 1968 and energized on December 3, 1968. It was designed by the Harco Corporation. Although the system was originally installed on a temporary basis, it is to be converted into a permanent system for the entire site during 1969. The system consists of an anode ground bed energized by a rectifier unit. The anode bed contains 10 Durichlor cast iron anodes, each 2 in. in diameter and 60 in. long. The rectifier unit has a capacity of 24 V and 50 A dc.

Measurements of structure-to-soil potential were taken at representative locations around the containment shell. Interference testing also was made of the nearby cast iron waterline to determine if it was being affected by the cathodic system. The measurements were obtained with a portable copper/copper sulfate reference electrode and a permanent zinc reference electrode buried on the west side of the containment shell at a depth of approximately 25 ft. The electrodes were used as references in obtaining potentials on the structures. All measurements were taken with the potentiometer-voltmeter circuit of a Miller Multi-Combination Meter Model B3. This meter is designed for corrosion-engineering work.

At the time of the testing, the rectifier unit was adjusted to provide an output of 10.5 V and 45 A dc. (The unit normally should be operated to provide a dc output between 40 and 50 A.) The rectifier settings for the test were: coarse--2; fine--5. Structure-to-soil electrical potentials that were obtained in the tests are listed in Table I.E.10.

TABLE I.E.10. Structure-to-soil Electrical Potentials

| Location | Structure-to-soil Potential (mV) | |
|---|---|---|
| | Current Off | Current On |
| Reactor shell, Southwest | | -1120 |
| Reactor shell, West (at zinc electrode) | | |
| Zinc-to-copper/copper sulfate | -935 | -1500 |
| Shell-to-zinc | +430 | +200 |
| Shell-to-copper/copper sulfate | | -1300 |
| Reactor shell, Northwest | | -1400 |
| Reactor shell, North | | -1200 |
| Reactor shell, Northeast | | -1240 |
| Reactor shell, East | | -970 |
| Reactor shell, Southeast | | -950 |
| Reactor shell, South (sump under passageway) | | -960 |
| Hydrant west of reactor | -470 | -470 |

The measured reactor-shell potentials with respect to the copper/copper sulfate portable reference electrode exceeded -850 mV, the normally accepted value which indicates full cathodic protection of buried steel. The measured potential of the reactor shell with respect to the permanent zinc electrode was +200 mV, which then computed with respect to copper/copper sulfate is equivalent to -1300 mV. (This can be checked by comparing the zinc-to-copper/copper sulfate potential to the shell-to-zinc potential listed in the table.)

Although the measurements indicated that the shell is receiving full cathodic protection, three small areas of the containment shell that are shielded from the cathodic protection current were found during the tests. One of these is immediately behind the valve pit at the southeast side of the shell; a potential of -450 mV was obtained at that point. The other two shielded areas are at the east passageway; a potential of approximately -400 mV was obtained at each of those points. These areas of the shell are shielded from the protection current by adjacent metallic structures. The exact sizes of the shielded areas could not be determined, but they are estimated to be small. The effects of long-term polarization on the shell may reduce the shielding effect and thereby improve the protection of the shielded areas. Recommendations have been made to retest the system within six months to determine if long-term polarization has produced any effects.

Measurement of pipe-to-soil potential taken at the hydrant west of the reactor building indicated that the temporary cathodic protection system is not affecting the electrically discontinuous cast iron waterlines, and that the system will not damage adjacent metallic structures not connected into the system.

Voltages and amperages of the system since it was placed into operation are provided in Table I.E.11.

After startup, the current showed a tendency to increase. Because the opposite reaction would normally be expected, the matter was discussed with the designer. The designer believed that the tendency was due to some secondary effect related to other structures, and he recommended reducing the current output pending further observations. The resetting to reduce the current output was made on December 6. When the current had stabilized, the rectifier was returned to its former setting on December 10. The current output peaked during the period from December 10-13, and then started to decrease. The designer believes that the polarization of the reactor shell is now complete, but that the current, although decreased, is still high because of the effect of surrounding structures. The designer also pointed out that those structures, although outside the protected area, are receiving partial protection from the system.

TABLE I.E.11. Voltage and Amperage Readings of Cathodic Protection System for EBR-II Containment Shell

| Date | Time | System Current (A) | System Voltage (V) | Remarks |
|---|---|---|---|---|
| 12/3/68 | 1030 | | | Started system |
| 12/3 | 1500 | 45 | 10.9 | |
| 12/4 | 0830 | 46+ | 10.9 | |
| 12/5 | 0900 | 46+ | 11 | |
| 12/6 | 0900 | 48 | 10.9 | |
| 12/6 | 1430 | 48 | 11 | Changed setting |
| 12/6 | 1430 | 42 | 8 | |
| 12/7 | 1900 | 42 | 8 | |
| 12/9 | 0830 | 42 | 8 | |
| 12/10 | 0830 | 42 | 7.9 | |
| 12/10 | 1130 | 48 | 9 | Changed setting back to original |
| 12/11 | 1030 | 48 | 9 | |
| 12/12 | 0915 | 48 | 9 | |
| 12/13 | 0845 | 48 | 9 | |
| 12/16 | 1030 | 47.5 | 9 | |
| 12/18 | 0900 | 47 | 9 | |
| 12/19 | 1530 | 47 | 9 | |
| 12/24 | 0930 | 47.5 | 9 | |
| 12/26 | 0930 | 47 | 9 | |
| 12/27 | 1430 | 47.5 | 9 | |
| 12/30 | 1300 | 47 | 9 | |
| 1/2/69 | 1300 | 45 | 9 | |
| 1/3 | 1400 | 44 | 9 | |
| 1/6 | 1300 | 45 | 9 | |
| 1/13 | 1300 | 44 | 9 | |

b. Fuel Cycle Facility Operations (M. J. Feldman)

Last Reported: ANL-7527, pp. 70-78 (Dec 1968).

(i) Fuel Production

(a) Hot Line (N. R. Grant)

Table I.E.12 summarizes the production activities for the first 15 days in January. The initial steps have been taken to phase out remote fuel processing and fabrication in the air and argon cells.

Processing of fuel from the reactor in the hot line was initiated in September 1964 and has continued essentially without interruption since then. During this period, the two major objectives of the program were accomplished: (1) to develop and demonstrate the equipment and procedures required for the remote pyrochemical processing and refabrication of irradiated metallic driver fuel; (2) to supply the EBR-II with driver fuel at an adequate rate to ensure that no interruptions in the reactor operating schedule would result from a lack of fuel supply, and in conjunction with this program, to receive spent subassemblies from the reactor at a rate adequate to maintain sufficient storage and transfer capacity in the storage

basket within the primary tank of the reactor. Information gained from these years of experience will be summarized in a final report of the reprocessing and refabrication activities.

TABLE I.E.12. Production Summary for FCF Hot Line

| | 1/1/69 through 1/15/69 |
|---|---|
| Subassemblies received: | |
| Core, control, and safety | 2 |
| Other | 0 |
| Subassemblies transferred to ICPP for storage | 0 |
| Subassemblies dismantled for surveillance | 11 |
| Subassemblies dismantled for examination, etc. | 0 |
| Subassemblies fabricated | 2 |
| Subassemblies transferred | |
| To reactor | 0 |
| To L&O vault and interbuilding corridor for storage | 0 |
| Elements decanned | |
| From irradiated subassemblies | 130 |
| Rejects | 46 |
| Other | 0 |
| Total decanned | 176 |

Melt Refining

| | Irradiated Fuel | Recycle Material | New Fuel |
|---|---|---|---|
| Number of runs | 5 | 1 | 0 |
| Average pour yield, % | 92.4 | 91.8 | 0 |

Processing

| | 1/1/69 through 1/15/69 |
|---|---|
| Injection-casting runs | 3 |
| Elements processed | |
| Accepted | 131 |
| Rejected | 48 |
| Elements welded | 40 |
| Elements rewelded | 0 |
| Elements leaktested | |
| Accepted | 0 |
| Rejected | 0 |
| Elements bonded (including recycle) | 183 |
| Elements bondtested | |
| Accepted | 129 |
| Rejected | 54 |
| Elements to surveillance | 547 |
| Number of subassemblies | 10 |

Waste Shipments

| | |
|---|---|
| Cans to burial ground | 4 |
| Oxide and glass scrap to ICPP | 2 |

Fuel for EBR-II will be produced in the FCF cold line and by Aerojet-General Corp., a commercial vendor. The fuel discharged from the reactor will be transferred to a water basin at ICPP for additional postirradiation cooling before reprocessing. The fuel now in the argon cell will be fabricated into subassemblies, but no additional fuel will be processed. The FCF will be emphasizing postirradiation examinations, experimental support, and reactor support.

(b) Cold-line Production and Assembly (D. L. Mitchell)

Normal production of Mark-IA driver-fuel elements and subassemblies is continuing in the cold line. A summary of the production in the first half of January is given in Table I.E.13.

TABLE I.E.13. Production Summary for FCF Cold Line

| | 1/1/69 through 1/15/69 |
|---|---|
| Alloy-preparation runs | |
| New fuel | 0 |
| Remelts | 0 |
| Total | 0 |
| Injection-casting runs | 5 |
| Pins processed | |
| Accepted | 489 |
| Rejected | 19 |
| Elements welded | 509 |
| Elements rewelded | 0 |
| Elements leaktested | |
| Accepted | 0 |
| Rejected | 0 |
| Elements bondtested | |
| Accepted | 81 |
| Rejected | 15 |
| Elements available for subassembly fabrication (cold-line fuel) | 486 |
| Subassemblies fabricated (cold-line fuel) | 0 |
| Elements received from vendor* | 866 |
| Inspected and accepted | 971 |
| Inspected and rejected | 2 |
| Elements available for subassembly fabrication (vendor fuel) | 4055 |
| Subassemblies fabricated (vendor fuel) | 0 |

| | |
|---|---|
| *Total vendor elements received to date | 5551 |
| Inspected and accepted | 4495 |
| Inspected and rejected | 697 |

The final design of Mark-II driver-fuel elements has been completed, and preparations are being made to modify the equipment in the cold line to produce sufficient elements to fabricate five prototype subassemblies that will be used to obtain surveillance data.

(ii) Inspection of Vendor Fuel (D. L. Mitchell)

The acceptance rate for vendor fuel has continued to improve; the rate for several recent batches was 100%.

One subassembly (C-2183) was assembled with vendor-produced elements to aid in evaluation of the vibratory test reported in ANL-7527. This test simulated the vibrational forces that normally occur within the flowing sodium in the primary tank. Subassembly C-2183 contains 48 vendor elements that had been subjected to the vibratory test, 39 vendor elements that had been accepted but not subjected to the test, and 4 cold-line elements. Of the 48 elements, 8 had voids in the bonding sodium. By current specifications, the voids in one of these 8 elements would have made it rejectable. The subassembly will be irradiated, after which the effect of defects produced by the vibratory test will be compared with the effect of any defects that might be produced by reactor operations.

(iii) Surveillance

(a) Chemical Analyses (E. R. Ebersole)

The number of fuel-product analyses on hot-line, cold-line, and vendor fuel samples made during the reporting period, together with the average values and ranges, are as follows:

| Analyzed for | Number of Analyses | Average Value | Range |
|---|---|---|---|
| Total U | 17 | 94.40 w/o | 94.05-95.01 |
| $^{235}U$ (% of total U) | 17 | 52.09 w/o | 51.84-52.33 |
| $^{239}Pu$ | 12 | 1172 μg/g | 813-1354 |
| Mo | 19 | 2.54 w/o | 2.30-2.60 |
| Ru | 19 | 1.91 w/o | 1.81-2.08 |
| Rh | 16 | 0.267 w/o | 0.231-0.288 |
| Pd | 19 | 0.186 w/o | 0.164-0.218 |
| Zr | 37 | 0.063 w/o | 0.029-0.110 |
| Nb | 15 | 0.0085 w/o | 0.004-0.011 |
| Si | 46 | 374 ppm | 93-541 |
| Al | 15 | 94 ppm | 53-162 |
| Cr | 17 | 53 ppm | 27-116 |
| Fe | 24 | 310 ppm | 59-666 |
| Ni | 20 | 189 ppm | 125-449 |
| C | 6 | 305 ppm | 156-410 |
| Total Analyses | 299 | | |

Analyses made for surveillance of irradiated pins from the reactor during the reporting period are tabulated below:

| Analyzed for | Number of Analyses | Average Value | Range |
|---|---|---|---|
| Mo | 1 | 2.57 w/o | |
| Zr | 23 | 0.108 w/o | 0.074-0.159 |
| Nb | 21 | 0.009 w/o | 0.006-0.013 |
| Si | 36 | 376 ppm | 72-974 |
| Al | 6 | 193 ppm | 131-371 |
| C | 22 | 421 ppm | 215-776 |
| Fe | 1 | 887 ppm | |
| Tc | 4 | For burnup determination | |
| Total Analyses | 114 | | |

(b) Postirradiation Analysis of EBR-II Fuel (J. P. Bacca)

(1) Surveillance of Mark-I Fuel. Mark-IB Subassembly C-2136, the fifth and final subassembly of this surveillance program, reached a maximum burnup of 1.19 a/o during EBR-II Run 32. The subassembly was transferred to the FCF where postirradiation examinations of the fuel elements are being made.

(2) Surveillance of Cold-line Fuel. Subassembly C-2120, the fifth and last subassembly of the first phase of the cold-line surveillance program, reached a burnup of 1.25 a/o during Run 32. The subassembly was transferred to the FCF where postirradiation examinations of the fuel elements are being made.

In the second phase of the cold-line surveillance program, ten subassemblies (five C type and five B type) will be irradiated to maximum burnups near 1.2 a/o to gain adequate data for statistical treatment of the performance of the fuel. These subassemblies are in the reactor.

(3) Surveillance of Vendor-produced Fuel. Irradiation of Subassembly C-2183, which contains 87 fuel elements manufactured by Aerojet-General Corp. (AGC) and 4 elements manufactured in the FCF cold line, began in EBR-II during the last part of Run 32. This subassembly and three others (C-2178, C-2181, and C-2182) will be among those used to assess the performance of AGC-produced fuel.

Subassembly C-2183 contains several fuel elements having minor voids in their sodium thermal bonds. The effects of these voids on the irradiation performance of the fuel elements will be evaluated after the subassembly reaches a burnup of 1.2 a/o.

(4) 50-MWt Surveillance Program. The third subassembly of this program (C-2103) reached a maximum burnup of 1.18 a/o during Run 32, approximately 0.6 a/o of which was accumulated during 50-MWt operation of the reactor. Postirradiation examinations of the elements from the subassembly indicated an average fuel swelling of 5.2% and a range from 3.2 to 7.1%. These values are in close agreement with those exhibited in the past by similar types of U-Fs alloy irradiated under 45-MWt reactor operation. Table I.E.14 summarizes the fabrication information and irradiation performance data for elements from C-2103. These results, as well as those obtained earlier for Subassemblies C-2049 and C-2072, indicate that driver fuel can be safely irradiated to a burnup level of 1.2 a/o ± 0.05 a/o in any grid position in the EBR-II core.

TABLE I.E.14. Fabrication and Irradiation Performance Data for 50-MW Surveillance Driver-fuel Subassembly C-2103

| Injection-casting Batch No. | Silicon Content of Fuel (ppm) | Number of Elements | Range of Element Burnup[a] (a/o) | Total Volume Swelling of Fuel (ΔV/V, %) | | Calculated Centerline Temp of Fuel (°F) | |
|---|---|---|---|---|---|---|---|
| | | | | Average | Range | Maximum | Range |
| 4225 | 110 | 9 | 1.08-1.14 | 6.0 | 4.7-7.1 | 1044 | 982-1044 |
| 4226 | 250 | 43 | 1.08-1.14 | 5.1 | 3.2-6.3 | 1050 | 993-1050 |
| 4227 | 290 | 36 | 1.08-1.14 | 5.0 | 4.1-6.0 | 1040 | 970-1040 |
| 4228 | 260 | 1 | 1.11 | 6.5 | - | 1026 | - |
| 0444 | 180 | 1 | 1.11 | 5.4 | - | 1042 | - |

[a]Max burnup 1.18 a/o; avg burnup 1.00 a/o.

To gain adequate data for statistical treatment of the performance of the fuel, postirradiation examinations of three additional subassemblies will be conducted after irradiation. One element will be irradiated to approximately 0.8 a/o, one to approximately 1.0 a/o, and the third to approximately 1.2 a/o. In these subassemblies, the entire burnup of the fuel elements will be accumulated during 50-MWt reactor operation.

(5) 70%-Enriched-fuel Experiment. Subassemblies C-2174 and C-2175, each containing 91 elements of 70% enrichment, reached a maximum burnup of 1.0 a/o during Run 32. Subassembly C-2174 was transferred to the FCF for postirradiation examinations while C-2175 remains in the reactor grid for additional irradiation to 1.2 a/o during Run 33. This burnup level should be attained by the middle of the run.

Table I.E.15 presents pertinent fabrication and performance data for the 70%-enriched elements of C-2174. The average swelling of the fuel elements of the subassembly was 6.1%, and the range was from 4.1 to 7.9%. These swellings, like those observed for earlier 70%-enriched subassemblies following lower burnups, are only slightly higher than those observed in the past for similar types (similar silicon content) of 52%-enriched driver fuel. Apparently, the higher-temperature,

higher-power irradiation conditions experienced by the 70%-enriched U-5 w/o Fs fuel cause only slight increases in the swelling rate during irradiation, at least to 1 a/o burnup. Temperatures at the centerline of the fuel during irradiation are not yet available.

TABLE I.E.15. Fabrication and Irradiation Performance Data for Subassembly C-2174 Containing 70%-enriched Fuel

| Injection-casting Batch No. | $^{235}U$ Enrichment of Fuel (w/o) | Silicon Content of Fuel (ppm) | Number of Elements | Range of Element Burnup (a/o) | Total Volume Swelling of Fuel (ΔV/V, %) | |
|---|---|---|---|---|---|---|
| | | | | | Average | Range |
| 0700 | 69.78 | 260 | 15 | 0.91-1.0 | 6.2 | 5.2-7.2 |
| 0701 | 69.63 | 496 | 32 | 0.91-1.0 | 6.0 | 4.1-7.9 |
| 0702 | 70.02 | 362 | 20 | 0.91-1.0 | 6.3 | 4.9-7.0 |
| 0703 | 70.10 | 407 | 24 | 0.91-1.0 | 5.8 | 4.2-7.7 |

(6) Driver-fuel Extended-burnup Program. Elements from Subassembly C-2027, the "lead" subassembly of this program, were given postirradiation examinations in the FCF after irradiation to 1.49 a/o maximum burnup. Table I.E.16 summarizes pertinent fabrication and irradiation performance data for the elements. The average fuel swelling for the subassembly was 6.1%, and the range was from 4.6 to 8.0%. These data indicate that driver fuel of this type (silicon greater than 200 ppm) continues to show low irradiation-swelling characteristics. These data are also consistent with the data resulting from earlier examination of elements from companion Subassembly C-291 following irradiation to 1.31 a/o burnup. The fuel in both of these subassemblies was made from the same casting batches. Precision diameter surveys of elements from C-2027 failed to show evidence of cladding straining resulting from internal pressurization and fuel swelling.

TABLE I.E.16. Fabrication and Irradiation Performance Data for Extended-burnup Driver-fuel Subassembly C-2027

| Injection-casting Batch No. | Silicon Content of Fuel (ppm) | Number of Elements | Range of Element Burnup[a] (a/o) | Total Volume Swelling of Fuel (ΔV/V, %) | | Calculated Centerline Temp of Fuel (°F) | |
|---|---|---|---|---|---|---|---|
| | | | | Average | Range | Maximum | Range |
| 4148 | 250 | 45 | 1.35-1.50 | 6.3 | 4.6-8.0 | 1069 | 961-1069 |
| 4153 | 310 | 46 | 1.35-1.50 | 5.9 | 4.6-7.9 | 1069 | 961-1069 |

[a]Max burnup 1.49 a/o; avg burnup 1.26 a/o.

The very satisfactory performance of elements in C-2027 after burnup to approximately 1.5 a/o has led to the decision to irradiate another subassembly (B-362) to a maximum burnup of 1.75 a/o. This burnup should be attained at the end of Run 34. Subassembly B-362 is the last of three companion subassemblies fabricated for this program. The fuel in B-362 is the same as that in Subassembly B-364, which was examined several months ago. The fuel in B-364, following maximum burnup of 1.16 a/o, displayed low irradiation-swelling characteristics--in the range from 3.1 to 5.8%. Silicon content of this fuel ranged from 290 to 370 ppm.

To gain adequate data for statistical treatment of the higher-burnup characteristics of low-swelling fuel similar to that utilized in C-2027, several subassemblies are being designated for irradiation to 1.5 a/o. These irradiations should be completed by the end of Run 34.

To extend this test of higher-burnup acceptability to subassemblies containing fuel with silicon contents less than 200 ppm, another subassembly (C-2065) will be irradiated to 1.5 a/o during Run 33. This subassembly, containing fuel elements with silicon contents ranging from 110 to 270 ppm, will be the "lead" subassembly of the program during Run 33.

(7) Driver-fuel Silicon Surveillance Program. The last five subassemblies of this program (B-3030, C-2163, C-2164, C-2112, and C-2119) reached target burnup at the end of Run 32, and will be transferred to the FCF for postirradiation examinations when fuel-handling operations are resumed in the reactor plant.

(8) Encapsulated Mark-IA Driver-fuel Experiment. Three encapsulated Mark-IA driver-fuel elements attained a maximum burnup of 2.9 a/o in Subassembly XO52 at the end of Run 32. These encapsulated elements (BF-04, BF-08, and BF-11) will be subjected to postirradiation examinations in the FCF when fuel-handling operations are resumed in the reactor plant.

(9) Encapsulated Mark-II Driver-fuel Experiment. Irradiation of Subassembly XO53, containing 37 encapsulated Mark-II prototype driver-fuel elements, was continued during Run 32 and is tentatively scheduled to continue through Run 34, at which time a maximum burnup of approximately 4 a/o will be attained by most of the elements in the subassembly.

Precision diameter surveys are being made of Capsules 201, 212, and 251, and the elements contained therein. These capsules were removed from Mark-II irradiations Subassembly XO29 after approximately 2.4 a/o burnup and replaced with three unirradiated elements to make up Subassembly XO53.

(c) Failure Analysis (J. P. Bacca and R. V. Strain)

(1) Examination of Suspect Subassembly L462. Control-rod Subassembly L462, suspected of containing an element which was releasing fission products during reactor operation, was transferred to the FCF for examination. The subassembly was not given a standard wash to remove the sodium on it; instead, it was subjected to humidified argon and dry air to oxidize the sodium. After this treatment, the subassembly was dismantled in a routine manner, but examination of the individual

elements at that time was hindered by the presence of a heavy coating of sodium reaction product on the surfaces of many of the elements. This coating could not be removed by wiping with a dry cloth, and it was not readily soluble in methanol.

Rather than attempting to clean all of the 61 elements of the subassembly individually with water before carrying out any tests, the bonds of the elements were eddy-current tested with the coating on them. The bond tester did not "see" the coating and produced sodium-bond recordings very similar to those produced when testing clean irradiated elements. Bondtesting results for the elements indicated that two elements (E-8 and E-34) had unexpectedly low sodium levels and that one element (E-57) had an unusually high sodium level. Although the sodium levels of Elements E-8 and E-34 were higher than those in elements as fabricated, they were lower than expected for this burnup level. This indicated that very little, if any, swelling of the fuel pins had occurred during irradiation. The sodium level of Element E-57 was approximately 2.65 in. above the fuel pin. This level corresponds to the position of the weld joining the element spacer wire to the cladding tube near its top end.

Subsequent visual examination of Element E-57 showed that a very short section of the spacer wire was bent away from the jacket (see A of Fig. I.E.4). The coating of sodium reaction product was removed from the element with water, after which a re-examination of the element indicated the possible existence of a hole in the cladding tube under the spacer wire at the weld joining the spacer wire to the tube (see B of Fig. I.E.4). The element was then heated to 450°C for about 5 min and examined again. This examination indicated that the thermal expansion of the bonding sodium in the element during heating had forced a small amount of this sodium through the hole in the jacket, thus confirming the existence of a hole (see C of Fig. I.E.4).

A neutron radiograph of Element E-57 made at TREAT shows the sodium level in the element and the region of the hole in the jacket as dark areas. (See Fig. I.E.5.) Apparently, at some time while the element was exposed to the humidified argon, to water during the cleaning operations, or to the air during heating, small amounts of the bonding sodium inside of the element were converted to sodium hydroxide or sodium bicarbonate. The carbon or hydrogen present then acted as strong neutron attenuators during neutron radiography operations and became identifiable in the radiograph. Additional examinations of this element are being continued to determine the size of the hole and its other characteristics.

The position of Element E-57 in Subassembly L462, the location of the hole in the cladding, and the condition of the spacer wire indicate that the hole probably was made during fabrication of the subassembly. It appears that the hexagonal tubing caught on the element spacer wire

A

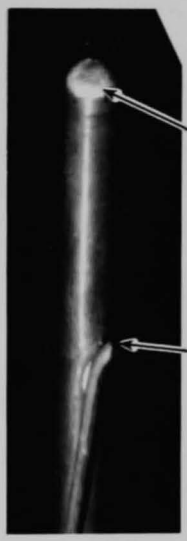


B

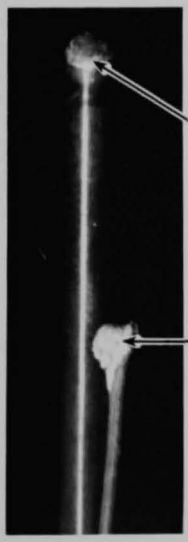


C

Fig. I.E.4

Macrophotos of the Suspect Area of Element E-57 from Sub-assembly L462. A. Top of the element prior to removing the sodium reaction products that resulted from the modified sodium-removal wash (humidified argon and dry air). B. Top of the element after it had been washed with methanol and water. C. Top of the element after it had been heated to 450°C. The thermal expansion of the sodium during heating forced a small amount of the sodium out through the hole.

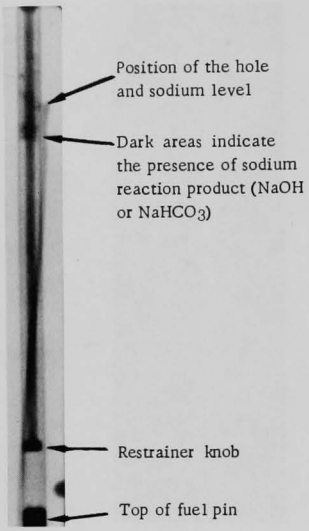


E-57

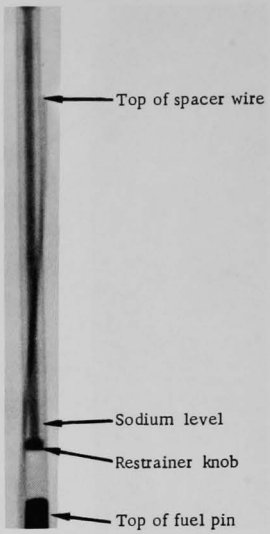


E-34

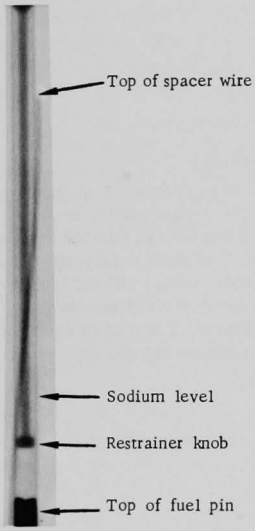


E-8

Fig. I.E.5

TREAT Neutron Radiographs of the Plenum Area of Elements E-57, E-34, and E-8 from Subassembly L462. (The sodium levels indicated are those measured by the bond tester; the change in density of the radiographs at the sodium level is not obvious.)

(even though the end of the spacer wire is beveled), tearing the wire-to-tube weld, as it was lowered over the fuel bundle of the subassembly during fabrication. Further examination (including neutron radiographs) of Elements E-8 and E-34 revealed no evidence of leaks (see Fig. I.E.5). At the present time, no explanation can be made for the low sodium levels found in these two elements.

(d) Materials Surveillance and Compatibility Studies
(J. P. Bacca, R. V. Strain, C. L. Meyers, and S. T. Zegler)

(1) Postirradiation Examination of Safety-rod Thimble 3D1. During November 1968, at the end of Run 31G, the safety-rod guide tube (thimble) was removed from EBR-II core grid position 3D1. The thimble consists of a thin-walled hexagonal tube made of Type 304L stainless steel, 57.31 in. long and 2.290 in. across the flats (initially), and is welded to a lower adapter for accommodation in the reactor core. The overall length of the thimble, including the lower adapter, is 90.87 in. Although fluence measurements have not yet been made for the thimble, the peak value has been estimated to be near $1 \times 10^{23}$ n/cm$^2$ (fast). An operating temperature for the thimble has been estimated by examining EBR-II core-loading diagrams for Runs 3 through 31 to determine the types of subassemblies which surrounded the thimble during its irradiation lifetime and for how long. Two sides of the thimble were located adjacent to driver-fuel subassemblies for 100% of the time, one side for 93% of the time, one for 75% of the time, one for 67% of the time, and one for 40% of the time (see Table I.E.17).

Because the temperature distribution surrounding the thimble was not held constant throughout the period of service of the thimble in EBR-II, a nominal temperature distribution was estimated for the case in which driver-fuel subassemblies completely surround the thimble. The lower of the two temperatures shown for each thimble situation in Table I.E.17 is that of the coolant at the hexagonal tubing wall at the top of the fuel region. The higher temperature is that of the coolant at the hexagonal tubing wall 6 to 12 in. above the top of the fuel. The temperatures show that the three sides of the thimble adjacent to the fourth-row driver-fuel subassemblies (grid positions 2, 3, and 4) operated at temperatures as much as 54°F higher than the temperature at the three sides adjacent to the second- or third-row subassemblies (grid positions 1, 5, and 6). Slightly lower temperatures would occur in sides of the thimble adjacent to experimental subassemblies. However, as most of the core operating time was accumulated with driver fuel in the fourth-row positions, a calculated temperature distribution with driver fuel in the six surrounding positions should best describe the actual temperature distribution of the thimble.

In addition to the visual examination of the thimble for deformation and surface damage reported last month, a dimensional survey was made to detect axial bowing and radial swelling or bulging. The

orientation of the sides of the thimble with respect to the center of the core has been determined to be as shown in Table I.E.17. The results of the bowing measurements also are summarized in this table. Bowing was determined by measuring the distance from a fixed reference point to a given side, or flat, of the thimble at a number of locations along its axial length. The maximum deviation or bow at midlength of a flat was 0.033 in.

TABLE I.E.17. Summary of In-reactor Data and Bowing Measurements for Safety-rod Thimble 3D1

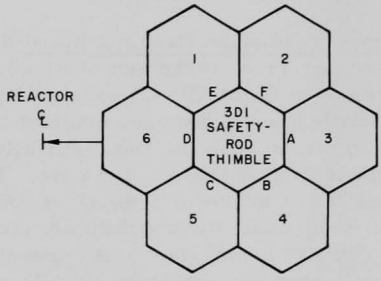


| Driver-fuel Grid Position | Thimble Flat Adjacent to Grid Position | % of Time Driver Fuel in Grid Position | Coolant Temp Assuming Driver Fuel in All Adjacent Locations[a] (°F) | Thimble Bowing at Midlength of Flat (in.) |
|---|---|---|---|---|
| 1 | E | 93 | 800 and 864 | 0.033 toward position 4 |
| 2 | F | 66 | 835 and 904 | Slight bowing |
| 3 | A | 100 | 826 and 886 | 0.029 toward position 3 |
| 4 | B | 75 | 835 and 904 | 0.027 toward position 4 |
| 5 | C | 100 | 800 and 864 | Slight bowing |
| 6 | D | 40 | 795 and 850 | 0.027 toward position 3 |

[a]The first value is the temperature of the coolant at the wall of the hexagonal can at the top of the fuel region. The second value is the temperature of the coolant at the wall of the hexagonal can at 6 to 12 in. above the top of the fuel region.

The flat-to-flat distance across the thimble increased at a relatively uniform rate from the bottom of the hexagonal tube upwards to a region 25 to 40 in. below the top of the thimble. At that point, the distance was 0.020 to 0.025 in. longer than the normal as-fabricated dimension (2.290 in.). The distance decreased progressively from that point to the top of the thimble. These data do not indicate whether the increases in flat-to-flat distances are caused by swelling of the stainless

steel in the thimble wall or of bulging of the thimble in this region. Future destructive examinations (density measurements and electron microscopy) will provide this information.

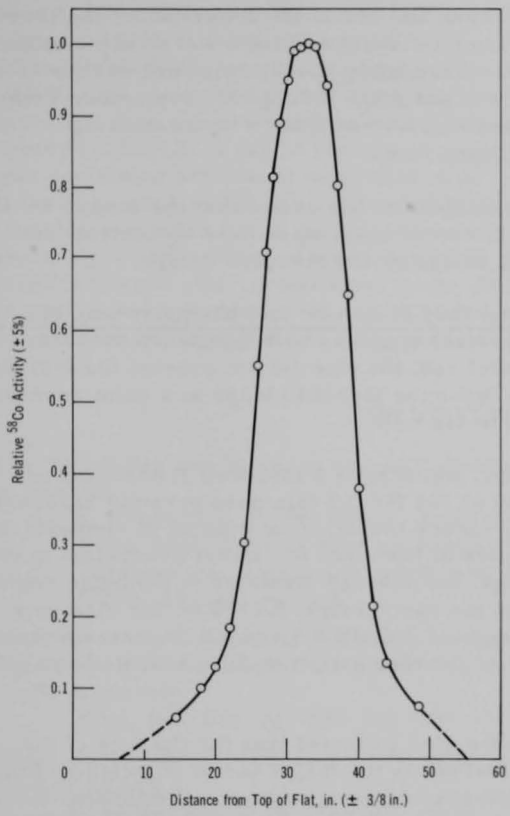


Fig. I.E.6. Relative $^{58}Co$ Activities Observed during Gamma Scan along Flat A of Safety-rod Thimble from Grid Position 3D1 (activity at midlength of flat = 1.0)

The results of an axial survey of the residual gamma activity in flat A, shown in Fig. I.E.6, indicate a peak activity approximately 30-35 in. below the top of the thimble. Gamma scans of the other flats were also made. A steel tube was inserted in the thimble during these measurements to reduce the gamma-energy contributions from the remainder of the thimble. The results of the gamma scans of the other flats are in good agreement with the results of the gamma scans of flat A. The relatively small differences in peak activities of the respective thimble flats indicate that the reactor neutron flux is rather uniform across the thimble location (3D1). This result was as expected.

Additional analyses and correlation of these data are being made and will be reported when completed.

The machining needed to separate the individual flats of the thimble have been completed. A full-length gamma scan will be made of each flat. Samples from selected flats will be taken for fluence determination before they are distributed for detailed examination by ANL, PNL, ORNL, and GE-NSP.

(2) Examination of Bushings from Subassembly L498. Continued metallographic examination of Ampco 18-13 (aluminum-bronze) bushing rings from control-rod Subassembly L498 has shown no evidence of loss of material following reactor service. The geometrical shape of the cross section of the ring and the microstructure of the ring have remained the same as those observed for unirradiated reference samples.

Subassembly L498 is the first of the IHE (increased-holddown-effect) design to be employed in the EBR-II. The IHE design incorporates a third set of bushings located below the top set of bushings near the top of the lower adapter shank. The standard control rod has only two sets of bushings, one above the shank and one at the lower end of the lower adapter component. The irradiation conditions of L498 were very similar to those experienced by another subassembly (L457) examined earlier (see ANL-7487, pp. 75-76, August 1968, and ANL-7500, p. 88, September 1968). Subassembly L457 was a standard control rod fitted with alternating Ampco 18-13 and Berylco 25 bushing rings.

This examination has shown that the Ampco 18-13 rings stand up well in the EBR-II environment when used on control-rod subassemblies of either the IHE design or the standard design.

(3) Bonding Test of Driver-fuel Elements with Special Tips. In a bonding test of driver-fuel elements with tips fabricated from 1/4-hard, Type 304 stainless steel rod, the tips did not prevent the fuel pin from deforming the plug end to cause the jacket to bulge at a point approximately 1/8 in. above the tubing-to-tip weld.

The tips, which have a Rockwell B hardness of 98 and a Vickers microhardness of 228 HV 0.5 (diamond pyramid hardness using a 500-g load), did slightly reduce the extent of bulging of elements as compared with the two softer types of tips used for jacket production in the past. After 3000 bonding impacts, the average diameter in the bulge region was 0.1765 in. for elements with the special tips, 0.1770 in. for elements with tips having a surface hardness of 200 HV 0.5 and a bulk material hardness of 148 HV 0.5, and 0.1790 in. for elements with fully annealed tips (microhardness of 145 HV 0.5).

The tests also indicated that the flatness of the shear on the bottom end of the fuel pin is the major factor in bulging of the elements during bonding. Metallographic examinations and microhardness measurements of all three types of tips after impact bonding indicate that considerable work hardening occurs near the ends of all tips during bonding. All Type 304L stainless steel tips probably harden and offer more resistance to deformation after a number of impacts. If the end of the fuel pin has a good shear, this resistance to deformation is sufficient to prevent swelling, regardless of which of the three types of tips is used. If the pin has a bad shear, the harder tips will cause slightly less swelling than the other two types.

No austenitic stainless steels, however, appear to be hard enough to eliminate swelling when the pins are badly sheared. Loading of the end of the fuel pin with the best shear down, which has been standard practice, should be continued as a means of minimizing swelling. Preferential loading of the pins has been effective in reducing swelling of the elements during impact bonding to an acceptable level.

(iv) Experiment Handling and Interim Examination
(V. G. Eschen and N. R. Grant)

During the reporting period, four experimental subassemblies (XO25, XO21A, XO42, and XO39) were dismantled in the air cell. Nineteen Mark-B19 capsules from XO25 were returned to the experimenter. Subassembly XO21A contained samples of structural material. One of its capsules was returned to the experimenter, and the balance of the Mark-B7 capsules, plus one new capsule, are being stored for refabrication as Subassembly XO21B. Four of the seven capsules from XO42, also a Mark-B7 type containing structural materials, will be returned to the experimenter and will be replaced in the subassembly by new capsules. Two of the four capsules contained boron carbide; these were neutron radiographed. Subassembly XO39, a Mark-A type containing fueled capsules, had been fabricated in the air cell. It contained some elements from Subassembly XO11 as well as ten new mixed-oxide and mixed-carbide elements. Measurements and neutron radiographs are being made of most of the elements from XO39.

## PUBLICATIONS

The Objectives and Status of the AEC-Sponsored 1000 MWe LMFBR Follow-on Studies
L. W. Fromm, J. P. Burelbach, D. E. Lutz, and D. H. Thompson
Proc. Natl. Topical Mtg. on Fast Reactors Systems, Materials, and Components, Cincinnati, April 2-4, 1968. USAEC Report CONF-680419, pp. 3-8

Analysis of the Dieaway of Prompt Neutrons with Two-Group Time-Dependent Diffusion Equation in Reflected Reactors
R. A. Karam
Nucl. Sci. Eng. 35, 285-289 (Feb 1969) Note

Monte Carlo Interpretation of a $^{238}$U Spherical Shell Transmission Experiment at 23 keV
L. B. Miller and W. P. Poenitz
Nucl. Sci. Eng. 35, 295-297 (Feb 1969) Note

Reactor-Noise Analysis: The Convariance Method via Polarity Detection
N. Pacilio
Nucl. Sci. Eng. 35, 249-258 (Feb 1969)

Live-Timer Method of Automatic Dead-Time Correction for Precision Counting
K. G. Porges and S. J. Rudnick
Rev. Sci. Instr. 40, 1-8 (Jan 1969)

Design and Analysis of Instrumented Subassembly System for EBR-II
A. Smaardyk, C. J. Divona, R. H. Olp, and E. Hutter
ANL-7423 (June 1968)

# II. OTHER FAST REACTORS--CIVILIAN--OTHER FAST BREEDER REACTORS

## A. Fuel Development

### 1. Other Fuel Jacket Alloy Studies

#### a. Mechanical Properties of Fuel Jacket Alloys (F. L. Yaggee)

Not reported previously.

(i) Effect of Temperature and Strain Rate on the Fracture Mode of Type 304 Stainless Steel. The fracture surfaces of tensile specimens of Type 304 stainless steel were studied by means of optical microscopy to determine the effect of temperature and strain rate on the transition point from transgranular to intergranular failure. The specimen material came from the same heat as that used in the EBR-II control-rod thimble currently undergoing postirradiation examination at ANL. The tensile tests were conducted at temperatures of 22, 450, 550, 650, and 750°C and at strain rates of 1, 10, 100, and 1000%/min.

Preliminary results indicate that specimen failure occurs by transgranular fracture at all strain rates up to 100%/min and at temperatures below 550°C. At these strain rates, evidence of intergranular fracture begins to appear at about 550°C, and at 750°C the failure is entirely due to intergranular fracture. At the highest strain rate of 1000%/min, evidence of failure by intergranular fracture does not appear until 650°C, and at 750°C failure is again entirely due to intergranular fracture. In all tests the specimen had sustained a true uniform strain of 15% at the start of the transition from transgranular to intergranular fracture.

These results suggest that the intergranular-type fracture could occur at lower values of true uniform strain and at temperatures below 550°C: at strain rates in the creep range ($\dot{\epsilon} < 10^{-4}$%/min). This possibility will be investigated by a similar study of fractured creep-specimens of the same material.

These studies are being conducted in cooperation with similar studies of specimens that have suffered radiation damage, and the results for the irradiated material will be reported at a future date.

#### b. Fabrication Development of Fuel Jacket Alloys (N. J. Carson, Jr.)

Last Reported: ANL-7513, pp. 92-93 (Oct 1968).

One of the efforts of the Fabrication Technology Group has been the study of techniques for the fabrication of vanadium alloys. Data are

needed to determine (1) the response of vanadium alloys to room-temperature working, (2) the effect of heat treatments on the strain-hardened alloys, and (3) the influence of cooling rate on the properties and structures of the alloys. The alloys being investigated are V-15 w/o Cr-5 w/o Ti, V-15 w/o Ti-7.5 w/o Cr, and V-20 w/o Ti; data are also being gathered for unalloyed vanadium for comparison purposes and for binary alloys of vanadium and chromium because of their superior resistance to corrosion in sodium contaminated with oxygen.

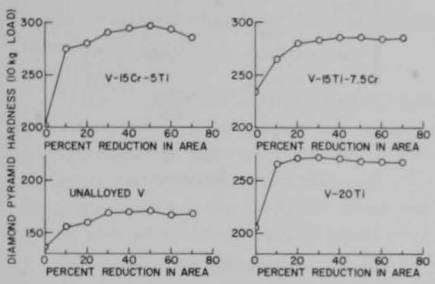


Fig. II.A.1. Hardness of Selected Vanadium Alloys as a Function of the Percent Reduction at Room Temperature (alloy composition in w/o)

Alloy hardness is plotted as a function of room-temperature reduction in Fig. II.A.1. The curve for the V-15 w/o Cr-5 w/o Ti alloy has appeared in Progress Report for July 1957, ANL-7357, and is included for comparison. Initially, each alloy was worked at a temperature above ambient, and then heat treated to obtain equiaxed grains and uniform second-phase distribution, as well as to make the alloys workable at room temperature. In all cases, reduction was accomplished by rolling and was calculated on the basis of percent reduction in cross-sectional area. Metallographically polished surfaces were measured for hardness with an Avery hardness tester under a constant load of 10 kg, and each hardness value is an average of three measurements.

All of the alloys tested were reduced more than 70% at room temperature, all achieved maximum hardness by 50% reduction, and all have a tendency to soften with additional reduction. The V-15 w/o Cr-5 w/o Ti and V-20 w/o Ti alloys achieved most of their hardening in the first 10% reduction.

The response of these strain-hardened alloys to heat treatment is shown in Figs. II.A.2 and II.A.3. Again the curves for V-15 w/o Cr-5 w/o Ti reproduce data published previously. The alloys were heat treated for 1 hr at temperature in vacuo, and all reached minimum softness when heat treated between 800 and 950°C. For most alloys the last sharp downward break in the curve marks the temperature at which the recrystallization rate became rapid. The one exception is the curve for 50% reduced V-20 w/o Ti alloy. Significant recrystallization was observed in the samples heated at 600°C and higher.

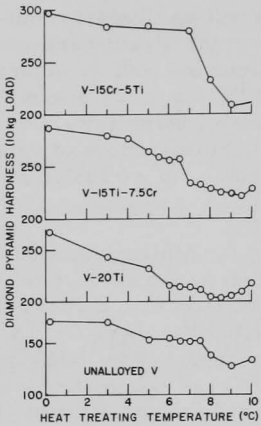


Fig. II.A.2

Hardness of Selected Vanadium Alloys Reduced 50% at Room Temperature and Heat Treated for 1 hr (alloy composition in w/o)

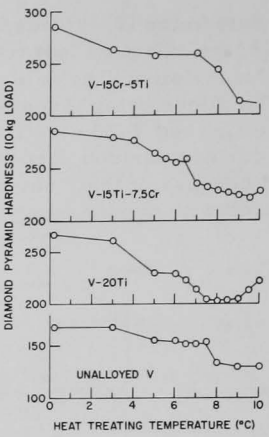


Fig. II.A.3

Hardness of Selected Vanadium Alloys Reduced 70% at Room Temperature and Heat Treated for 1 hr (alloy composition in w/o)

Quenching studies of the V-15 w/o Cr-5 w/o Ti alloy have been completed. Specimens of the alloy were heat treated for 1 hr at temperatures ranging from 900 to 1600°C. At each test temperature, one specimen was heat treated in a resistance-heated vacuum furnace and cooled in the furnace after heat treatment, and a second specimen was heat treated at the same temperature in an inert atmosphere and oil quenched. The results obtained are illustrated in Fig. II.A.4.

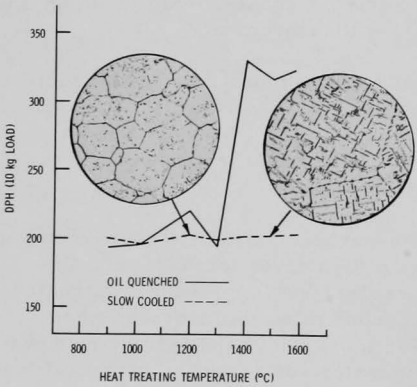


Fig. II.A.4. Effect of Cooling Rate on the Hardness of V-15 w/o Cr-5 w/o Ti Alloy

All heat-treated V-15 w/o Cr-5 w/o Ti specimens that were furnace cooled gave comparable hardness values. Both the furnace-cooled and the quenched specimens of V-15 w/o Cr-5 w/o Ti that were heat treated between 900 and 1200°C had equiaxed grains with small uniformly distributed particles of a second phase. However, when samples of this alloy were heat treated above 1200°C, several significant effects occurred:

(1) The particles of second phase began to dissolve. This dissolution was observed in the photomicrographs of the quenched specimens, which revealed structures with increasingly less second-phase particles as the heat-treatment temperature was increased.

(2) The rate of grain growth increased and became particularly high above 1350°C.

(3) The hardness of the quenched specimens also increased.

These last two observations also give evidence of some second-phase dissolution.

All the samples that were slowly cooled from the higher temperatures showed second-phase precipitates, but the precipitates were found as platelets on preferred atomic planes. The makeup of these platelets has not been completely determined. Our best information to date is that the platelets are predominantly titanium carbonitrides. In any case, heat treatments intended to promote platelet formation should be carried out at 1200°C or above and should include a relatively slow cooling rate. The platelets should be formed near the end of the fabrication process since they make the alloy very difficult to work at room temperature.

The joint vanadium-alloy fabrication effort with Westinghouse Electric Corporation was completed in December 1968. The purpose of the program was to supply a stockpile of fabricated shapes with known histories and properties from which qualified experimenters can draw, and to compare the fabricability of Westinghouse alloys with ANL alloys.

Fifty-eight kilograms of vanadium alloys in the form of extrusion-billet cores were prepared by Westinghouse personnel. The cores were fabricated into rod stock, sheet bar, and tube blanks at ANL. Five alloys were processed: one full billet each of V-15 w/o Cr-5 w/o Ti, VANSTAR 7, 8, and 9 alloys plus half billets each of V-20 w/o Ti, and VANSTAR 8 alloys. Thirty-seven extrusions were made, either primary or secondary, in this program to obtain the extrusion constants shown in Table II.A.1.

TABLE II.A.1. Extrusion Constants of ANL and VANSTAR Alloys at 1150°C

| Alloy | Product | Extrusion Constant (ksi) | Alloy | Product | Extrusion Constant (ksi) |
|---|---|---|---|---|---|
| V-15 w/o Cr-5 w/o Ti | 2-in.-dia bar | 81.6 | VANSTAR 7 | 2-in.-dia bar | 77.9 |
| | Tube Blank | 64.8-66.6 | | Tube Blank | 51.7-54.7 |
| | 5/8-in.-dia rod | 58.4-62.2 | | 5/8-in.-dia rod | 46.7-51.9 |
| VANSTAR 9 | 2-in.-dia bar | 85.2 | VANSTAR 8 | 2-in.-dia bar | 82.3 |
| | Tube Blank | 52.2-59.7 | | Tube Blank | 50.7-57.7 |
| | 5/8-in.-dia rod | 53.6-54.0 | | 5/8-in.-dia rod | 54.4-59.5 |

# III. GENERAL REACTOR TECHNOLOGY

## A. Applied and Reactor Physics Development

### 1. Theoretical Reactor Physics--Research and Development

#### a. Reactor Computations and Code Development (B. J. Toppel)

Last Reported: ANL-7487, pp. 77-78 (Aug 1968).

(i) Fuel-cycle Package. In addition to the procedure for microscopic-cross-section collapse already available in the Fuel-cycle Package (see ANL-7487), a module which creates collapsed-region-dependent macroscopic group cross sections has been added to the Fuel-cycle Package. This ARC-system module uses linear flux weighting in the following manner: In every region of the problem, the macroscopic cross sections of the various materials are collapsed to any number of groups with the average group flux in that region. This module collapses the minimal material-level cross-section data contained in XS.M.MIN,* and it generates the data set B.HOMOG* for the collapsed minimal material-level cross-section data. Since the active isotope microscopic cross sections are included in XS.M.MIN by the burn path, these are available for subsequent burnup calculations. The mode of operation is to carry out one multigroup flux calculation with approximate atom-density distributions, collapse to fewer groups, and then solve the fuel-cycle problem with the collapsed group structure. Considerable improvement in problem run time may be obtained by this method.

Documentation of the Fuel-cycle Package is now being carried out. This documentation entails the definition of all variables used in the Fuel-cycle Package and the declaration of the function of all subroutines. Presently, the documentation is 70% complete.

A startup procedure, which estimates the burn step time satisfying the desired burnup and the enrichment giving the desired multiplication constant at the specified time in the cycle, has been included in the Fuel-cycle Package. In this startup procedure, one burn-step subinterval is utilized in obtaining the cyclic mode** with an enrichment and burn-step time specified as input. At this point the burn-step time, which would give the desired burnup, is estimated. By use of this burn-step time and a second enrichment specified in the input, the cyclic mode is again obtained. A linear search of enrichment versus the multiplication constant is then initiated until an enrichment is obtained which gives the desired multiplication constant at the specified time in the cycle. This startup

* Toppel, B. J., ANL-7332 (Nov 1967).

** Reactor Physics Division Annual Report, ANL-7310 (Jan 1968), pp. 493-501.

procedure is intended to reduce the range of enrichment and burn-time adjustments that must be made by the more accurate but slower final search procedure.

Debugging and testing of the entire Fuel-cycle Package is proceeding. The in-core fuel management and the cyclic-mode calculations have been tested. In the immediate future, the control search options and the external cycle convergence will be tested.

## 2. Nuclear Data--Research and Development

### a. Burnup Analysis and Fission Yields for Fast Reactors (R. P. Larsen)

#### (i) Determination of the Absolute Fast Fission Yields of Burnup Monitors and Nonfission Nuclear Transformations in a Fast Reactor

Last Reported: ANL-7518, pp. 81-83 (Nov 1968).

An irradiation is being carried out in EBR-II to provide material for the determination of fast-fission yields of burnup monitors and for the study of nonfission nuclear transformations. The following materials are being irradiated: $^{233}U$, $^{235}U$, $^{238}U$, $^{239}Pu$, $^{240}Pu$, $^{241}Pu$, $^{232}Th$, and $^{237}Np$. The irradiation began in December 1966 and is estimated to be about 45% complete at the present time.

#### (ii) Development of Analytical Procedures for Fission Product Burnup Monitors

Last Reported: ANL-7518, pp. 83-84 (Nov 1968).

(a) X-ray Spectrometric Determination of Rare Earth Fission Products. Development of a method for determining rare earth fission products by X-ray spectrometry is continuing. In the procedure, an internal standard (a rare earth not produced in fission) is added to the sample; the rare earths are then separated from interferences, mounted on an aluminum plate, and assayed X-ray spectrometrically. The advantages of terbium as an internal standard and the precision attained by the use of line-intensity ratios (rare earth-to-internal standard) have been discussed previously (see Progress Report for January 1968, ANL-7419, pp. 97-98).

Present work is directed toward development of a procedure that will isolate the rare earths in a form suitable for X-ray spectrometry. Preliminary tests of a proposed separation of the rare earths by

anion exchange (see ANL-7518) showed small but significant decreases (~2-5%) in the rare earth-to-terbium ratio and rather large decreases (25-50%) in X-ray intensities. These decreases were attributed to increased solids on the aluminum X-ray plates that resulted from attack of the aluminum by residual chloride. Subsequent investigations have shown that these decreases were caused, either in part or entirely, by incomplete dissolution of the rare earths in nitric acid after evaporation of a hydrochloric acid medium to dryness (this step in the procedure immediately precedes the deposition of the rare earths on the aluminum plate). A more rigorous dissolution procedure appears to have solved the difficulties.

An electroplating technique, which was devised by Handley and Cooper* for the analysis of americium and curium by alpha spectrometry, has been investigated for the preparation of rare earth X-ray plates. The procedure involves the following steps. After the ion-exchange step and subsequent conversion of the rare earth solution to a nitric acid medium (as described above), dimethyl sulfoxide (DMSO) is added, and the rare earths are electroplated onto an aluminum plate, which serves as a cathode. With a current density of 15 $mA/cm^2$ and a potential of ~100 V, complete deposition is achieved in 15 min.

A significant improvement in the quality of the X-ray plates has been achieved by the electroplating technique. (Previously the plates were prepared by pipetting a dilute nitric acid solution and evaporating to dryness.) When the rare earths are electroplated, the deposition is more uniform, the amount of solids on the plates is decreased, and the rare earths are more adherent.

The revised procedure was tested in the following experiment. Four samples consisting of 35 $\mu$g of terbium and 100 $\mu$g of a simulated mixture of fission product rare earths were carried through the ion-exchange procedure and electroplated on aluminum. These were treated as "unknowns" and were compared with two "standards" of the same composition that were electroplated directly. The average intensity ratios (rare earth-to-terbium) for the standards and unknowns are as follows:

| | Avg Intensity Ratio | | Relative Standard Deviation |
|---|---|---|---|
| | Standards | Unknowns | |
| Nd/Tb | 0.483 | 0.482 | 0.5 |
| Pr/Tb | 0.218 | 0.217 | 1.6 |
| Ce/Tb | 0.275 | 0.273 | 2.6 |
| La/Tb | 0.161 | 0.162 | 1.7 |

The relative standard deviation is for a single unknown. Similar precision was obtained in duplicate experiments.

* Handley, H., and Cooper, J. H., A Study of Parameters Affecting Analytical Alpha Spectrometry, presented at 12th Conference on Analytical Chemistry in Nuclear Technology, Gatlinburg, Tenn., Oct. 8-10, 1968.

Although adequate precision is demonstrated by the above data, several problems related to X-ray intensities must be investigated before the accuracy of the method can be evaluated. These include (1) the effect of the secondary and tertiary ($L\beta$ and $L\alpha$) emission lines of each rare earth on the intensity of the primary ($L\alpha$) emission line that is used for the assay, and (2) the effect of the $L\beta$ and $L\alpha$ lines of cesium and barium (fission products that are not separated from the rare earths in the procedure) on the $L\alpha$ lines of the rare earths. If these effects are significant, it is expected that the problems can be overcome by establishing appropriate correction factors. This will be accomplished by plating the individual elements and determining, for each element, the relationships between the intensity of the primary emission line and the intensities of the other emission lines in the wavelength regions of interest. A small computer program will be used to handle data reduction.

b. Determination of Nuclear Constants (A. B. Smith)

Last Reported: ANL-7513, pp. 95-99 (Oct 1968).

(i) Fast Neutron Cross Sections and Other Nuclear Constants

(a) Total Neutron Cross Sections. The total neutron cross sections of lead and titanium were measured by the monoenergetic transmission method. The energy range covered for lead was from 800 to 1500 keV in 2-keV increments, with the exception of an unfinished gap between 1020 and 1120 keV. The energy range covered for the titanium measurements was from 1000 to 1500 keV in 2-keV increments. The resulting resonance structure correlated quite well with measurements made by other groups; however, the absolute energy scale differs by about 14 keV in both cases. Further investigation is underway to determine the cause of this difference.

(b) Measurements of the Ratios $\sigma_\gamma$(U-238)/$\sigma_f$(U-235 and $\sigma_\gamma$(Au-197)/$\sigma_f$(U-235). The ratio $\sigma_\gamma$(U-238)/$\sigma_f$(U-235) is one of the important quantities needed for reactor design and analysis of measured integral values. The existing measured values have been compiled. Strong discrepancies were found in the energy region from 500 to 1200 keV (max 40%), around 130 keV (17%), and a 5% difference around 20-40 keV. Measurements were performed at 30, 130, 500, and 900 keV to resolve the observed discrepancies. A sandwich fission counter was used to detect the fission counts from two circular ~250 $\mu g/cm^2$ $^{235}U$ deposits. A $^{238}U$ foil of the same size was activated for a certain time. The $^{239}Np$ activity was counted with a Ge(Li) detector. The calibration was carried out using a $^{263}Am$ sample.

The results of the measurement are given in Table III.A.1. They confirm at 30 keV the measurements by de Saussure et al.,* and at 130 keV the values obtained by Menlove and Poenitz and

*de Saussure, G., et al., ORNL-3360 (1962).

TABLE III.A.1. Values of $\sigma_\gamma(U\text{-}238)/\sigma_f(U\text{-}235)$

| $E_n$ (keV) | $R = \sigma_\gamma(U\text{-}238)/\sigma_f(U\text{-}235)$ | $\Delta R/R$ |
|---|---|---|
| 30 | 0.205 | 0.04 |
| 130 | 0.121 | 0.04 |
| 505 | 0.112 | 0.03 |
| 900 | 0.129 | 0.03 |

by Poenitz.* At 500 keV the new value is in agreement with the values reported by the latter authors and by Barry et al.,** and White.† At 900 keV the value measured by Barry et al., and by White was confirmed.

The ratio $\sigma_\gamma(Au\text{-}197)/\sigma_f(U\text{-}235)$ is of interest due to some discrepancies observed in absolute measurements of $\sigma_f(U\text{-}235)$ and $\sigma_\gamma(Au\text{-}197)$. The values given in Table III.A.2 confirm very well the values measured by Barry,†† White, Grench,‡ Diven et al.,‡‡ Poenitz et al.,§ and Poenitz, and do not indicate lower values for this ratio.

TABLE III.A.2. Values of $\sigma_\gamma(Au\text{-}197)/\sigma_f(U\text{-}235)$

| $E_n$ (keV) | $R = \sigma_\gamma(Au\text{-}197)/\sigma_f(U\text{-}235)$ | $\Delta R/R$ |
|---|---|---|
| 30 | 0.260 | 0.04 |
| 175 | 0.206 | 0.03 |
| 465 | 0.137 | 0.04 |

(c) Grey Neutron Detector. The efficiency of a grey neutron detector has been determined by two independent experimental methods in the energy range from 30 to 1400 keV. Deviations of a maximum of 3.5% from the theoretically calculated values were found. The detector was used to measure the cross section of the reaction $^7Li(p,n)^7Be$ in the energy range from 1.9 to 3 MeV. Agreement was found with measurements by Machlin and Gibbons and by Lister within 3%.

(d) Thermal-absorption Cross Section of $^6Li$. The thermal absorption cross section of $^6Li$ was measured using a pulsed-neutron source method. A cylindrical container (of 8-in. radius and 8-in. height) was pulsed every 3 ms with a burst of neutrons from the VDG, 150 $\mu$sec in duration. The time decay of the neutron flux between the bursts was determined using a small $BF_3$ detector located externally to but coaxially with the cylindrical container and feeding into an on-line computer. The decay rate for the container filled with a $^6LiCO_3$ solution was compared with the decay rate for the container filled with the same mass of $H_2O$. It is possible from this ratio to determine the thermal-absorption cross section of the $^6Li$. The final data processing has not been completed.

*Menlove, H. O., and Poenitz, W. P., Nucl. Sci. Eng. 33, 24 (1968); Poenitz, W. P., N.B.S. Special Publication 299, 1, 503 (1968).

**Barry, J. F., et al., J. Nucl. Energy 18, 481 (1964).

† White, P. H., ibid. 19, 325 (1965).

†† Barry, J. F., ibid. 18, 491 (1964).

‡ Grench, H. A., private communication.

‡‡ Diven, B. C., et al., Phys. Rev. 120, 556 (1960).

§ Poenitz, W. P., et al., J. Nucl. Energy 22, 505 (1968).

(ii) Fission Process Data

(a) Energy Dependence of the Delayed-neutron Yield from Neutron-induced Fission of $^{232}$Th, $^{235}$U, and $^{238}$U. A knowledge of the energy dependence of the delayed-neutron yield from fissile and fertile elements is important to the fields of reactor kinetics and reactor control. Although there have been extensive measurements of delayed-neutron yields and periods for thermal-neutron-induced fission and for fission induced by fast-fission-spectrum neutrons, there have been only isolated measurements reported at other energies.

Two different aspects of the delayed-neutron process were investigated. One series of measurements was made at a number of different incident neutron energies to determine if there were any change in the time dependence of the decay of the delayed-neutron activity. A second series of measurements was made to determine if there were any dependence of the total yield on the delayed-neutron activity as a function of incident neutron energy. The data for the time-dependence measurements were analyzed in terms of five exponential components.

Measurements were made for $^{235}$U at 150, 600, and 1300 keV. In no case do our data deviate more than 3 to 4% from Keepin's values over the decay-time range from 0.4 to 150 sec. Measurements were made for $^{238}$U at 1400, 1500, and 1750 keV, and for $^{232}$Th at 1450, 1500, and 1640 keV. No significant deviation from Keepin's values was observed for any of the determinations. The energies for the $^{232}$Th measurements were chosen to fall on and off resonance energies to check on the effect of the resonance structure in the $^{232}$Th fission cross section on the delayed-neutron yield.

Measurements of the total delayed-neutron yield were made for $^{235}$U at various energies from 0.25 to 1.5 MeV. For $^{232}$Th and $^{238}$U measurements were made from the vicinity of the fission threshold to 2.4 MeV. The data for all elements were normalized at 1450 keV to Keepin's determinations for fast neutrons. Within the estimated error of 5% there is no significant change in the delayed-neutron yield for $^{235}$U over the energy range from thermal energy to 1.5 MeV. Our data for $^{238}$U and $^{232}$Th are not yet completely analyzed. The much more pronounced angular distribution in the fission fragments especially near threshold and the very sharp rise at the fission threshold necessitate more detailed corrections than are required for $^{235}$U. Nevertheless at this stage it can still be stated that there is no change in excess of 10% in the delayed-neutron yield below 2.4 MeV for either $^{238}$U or $^{232}$Th.

(iii) Instrumentation and Digital Techniques. The Fast Neutron Generator has undergone successful voltage tests. The actual voltage

achieved on the terminal for several hours at a time without sparking is in excess of 5 MV, which is well above our contract requirement of 4 MV.

The building is open for beneficial occupancy, and the computer together with much of the peripheral equipment has been installed and is being tested.

## B. Reactor Fuels and Materials Development

### 1. Fuels and Claddings

#### a. Research and Development

##### (i) Behavior of Reactor Materials

###### (a) Fuel Element Behavior Modeling (P. G. Shewmon)

(1) Studies of Fuel-element Modeling (R. W. Weeks)

Not reported previously.

A new computer model is being developed to predict the in-pile behavior of cylindrical oxide-fuel elements. The new formulation will consider a different treatment of fuel swelling than that used in the ANL SWELL code. The new code will be used both to complement predictions of the SWELL code and to provide additional predictions that can be verified experimentally.

###### (b) Irradiation Behavior of Uranium-Plutonium-base Alloys (D. R. O'Boyle)

(1) Irradiation of U-Pu-Zr Alloys (H. V. Rhude)

Last Reported: ANL-7518, p. 88 (Nov 1968).

A series of irradiations is in progress to determine the influence of pressure, temperature, burnup, and alloy composition on the swelling mechanism of plutonium-containing metal fuels. Three pressure- and temperature-controlled capsules, each containing high-purity specimens of U, U-5 w/o Pu, and U-14 w/o Pu-12 w/o Zr, are presently being used for the irradiations. Capsule 1 was removed from the reactor in November 1968 following irradiation to 0.2 a/o burnup at a constant pressure of 1000 psi and a nominal temperature of 450°C. This capsule is now in the hot laboratory at BNW, and the specimens are being prepared for optical and electron metallographic examination. Capsules 2 and 3 were loaded into the reactor in early December, and will be irradiated to a burnup of 0.2 a/o

at 1000 psi. The nominal irradiation temperatures are 550°C (below the lowest four-phase reaction temperature in the ternary alloy) for Capsule 2 and 625°C (between the first and the second four-phase reaction temperatures in the ternary alloy) for Capsule 3. Because of budget limitations, alloy irradiations at other temperatures and pressures and the irradiation of other alloys in this series will not be initiated in FY 1969.

### (c) Swelling and Gas Release in Metal Fuels
(D. R. O'Boyle)

#### (1) Studies of Fuel Swelling and Gas Release
(S. R. Pati)

Last Reported: ANL-7518, pp. 88-89 (Nov 1968).

(A) In-reactor Swelling Studies. An instrumented capsule designed to study the effect of external restraints on the in-reactor swelling behavior of metallic fuels was irradiated in CP-5 for about a week prior to the rehabilitation shutdown of the reactor. Although the irradiation time was too short to gain any useful swelling data, the time was sufficient to test the capability of this capsule design to monitor the restrained as well as unrestrained swelling of fuel pellets.

The main design features of the capsule were reported in ANL-7518. The original specimen chamber was made of V-5 w/o Ti-15 w/o Cr alloy because of the high yield strength and resistance to creep during irradiation at elevated temperatures; the specimen chamber, which is filled with NaK, could safely withstand an internal pressure of 10,000 psi at 650°C. However, difficulties were encountered in making a pressure-tight seal between the Type 304 stainless steel bellows nut and the V-Ti-Cr specimen chamber, primarily because of the large differences in the thermal coefficient of expansion of the two materials. In an effort to obtain a workable capsule within the limited time available for CP-5 operation, the specimen chamber was constructed of Type 304 stainless steel so that a welded joint could be made between the chamber and the bellows nut. However, the lower yield and creep strengths of Type 304 stainless steel at high temperatures necessitated lowering the maximum allowable operating pressure and temperature of the capsule to 4000 psi and 425°C.

The capsule was placed in a water-cooled vertical thimble (VT-16) of CP-5 and irradiated for 158 hr (an intervening shutdown of $1\frac{1}{2}$ hr occurred) at an internal pressure of 3000 psi. Short-time temperature fluctuation caused by variations in reactor power was only ±2°C, whereas a long-time drift of as much as 15°C in the mean temperature of the specimen chamber was noted during the 158 hr of irradiation. The mean temperature of the specimen chamber changed from 400°C at the beginning

of the irradiation to 415°C at the end. Resistance heaters placed around the specimen chamber allow the attainment and control of temperatures up to ~70°C higher than that due to gamma heating.

Thermocouples placed radially in the specimen chamber showed a maximum temperature difference of 30°C between the hottest and coldest points along a radius of the chamber, whereas the temperature difference between two points $1\frac{1}{2}$ in. apart long the length of the chamber was ≈10°C.

The output of the linear variable differential transformer (LVDT) used to detect the volume change of the specimen was very stable throughout the irradiation period. While the reactor was coming to power, there was a change in the initial position of the LVDT core (and hence its output) because of the differential expansion of the pushrod connected to the core and the pressure tubing supporting the transformer. The position of the core remained very stable once the reactor was at full power. Throughout the irradiation, the LVDT followed reproducibly any changes in the pressure or temperature of the specimen chamber by detection of the motion of the pushrod. During the last 14 hr of irradiation the pressure in the capsule was released, and the pushrod returned to the original position that existed at the beginning of the irradiation, prior to the application of pressure. This reaction to pressure release indicated that the bellows assembly had not taken any permanent set during the irradiation. The absence of a permanent set ensured that the bellows design can be effectively used to monitor the unrestrained swelling of a fuel pellet to a desired burnup, at which point measurements of the response of the pellet to an applied hydrostatic pressure could be made. The bellows design is also suitable for changes in the level of restraint at any time during the irradiation.

Since, in this design, the volume change of the specimen is detected from displacement of NaK within the specimen chamber, fluctuations in the volume of the NaK due to temperature fluctuations in the chamber lead to uncertainties in the swelling measurements. These uncertainties increase the minimum value of swelling that can be detected unambiguously. However, estimates based on the temperature stability of the specimen chamber, during the test irradiation, and on the relative volumes of the specimen and the NaK indicated that swelling as low as 0.2% can be unambiguously detected.

## (ii) Thermodynamics of Fuel Materials

### (a) Total Vapor Pressures and Carbon Potentials in the Ternary System U-C-Pu (P. E. Blackburn and M. Tetenbaum)

Last Reported: ANL-7513, pp. 104-105 (Oct 1968).

The study of the vaporization behavior of the uranium-carbon system is continuing. Measurements of the total pressure of uranium-bearing species and carbon activity are being made as functions of temperature and $UC_x$ composition, using the transpiration method with hydrogen-methane mixtures as carrier gases. Emphasis has been placed initially on measuring carbon activities.

Measurements of carbon activity at 2255, 2355, and 2455°K have now been completed. These measurements (including those previously reported in ANL-7513) were subsequently corrected for the response of the hydrocarbon analyzer to acetylene in the exit carrier gas. The acetylene content in the carrier gas was determined by means of a chromatographic column incorporated into the transpiration complex and the application of frontal analysis. The corrected activity data are plotted in Fig. III.B.1 as a function of $UC_x$ composition.

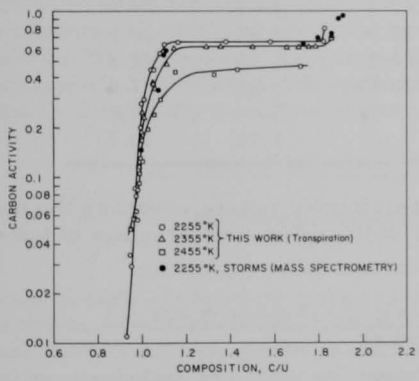


Fig. III.B.1. Activity of Carbon as a Function of Composition and Temperature

The plateaus of the 2255 and 2355°K isotherms are consistent with the miscibility gap UC + $\beta UC_2$ shown by the phase diagram proposed by Storms for the uranium-carbon system.* Our measurements indicate values of carbon-to-uranium ratios of 1.15 and 1.2 for the lower carbon boundary of the UC + $\beta UC_2$ diphasic region at 2255 and 2355°K, respectively. These are in good agreement with the compositions C/U ≃ 1.14 and 1.2 estimated from the phase diagram at these same temperatures. However, our measurements indicate values of C/U ≃ 1.78 and 1.80 for the upper carbon boundary of the UC + $\beta UC_2$ diphasic region at 2255 and 2355°K, respectively, whereas the corresponding values estimated from the phase diagram are 1.50 and 1.35. It is apparent that the compositions of the upper carbon boundary of the miscibility gap derived from our measurements are not in agreement with the phase diagram. We plan to re-examine the high-carbon region.

*Storms, E. K., The Refractory Carbides, Academic Press, New York (1967), Chap. XI, pp. 205-213.

Tentative values for the free energy of formation of $UC_x$ compositions at 2255, 2355, and 2455°K are given in Table III.B.1; these values are based on our corrected carbon activity measurements, Storms' adjusted uranium vapor pressure measurements,* and 126.5 kcal/mol as the heat of vaporization of uranium.** The calculated free energies of formation for stoichiometric uranium monocarbide are $-\Delta G_f^\circ$ = 23.3, 23.8, and 25.3 kcal/mol at 2255, 2355, and 2455°K, respectively. For comparison, the thermodynamic assessment of Holley and Storms† yields $-\Delta G_f^\circ$ = 25.2 ± 2 kcal/mol at all of these temperatures.

TABLE III.B.1. Free Energy of Formation of $UC_x$

| 2255°K | | 2355°K | | 2455°K | |
|---|---|---|---|---|---|
| C/U | $-\Delta G_f^\circ$ (kcal/mol) | C/U | $-\Delta G_f^\circ$ (kcal/mol) | C/U | $-\Delta G_f^\circ$ (kcal/mol) |
| 0.97 | 22.2 | 0.97 | 23.6 | 0.97 | 24.4 |
| 1.00 | 23.3 | 1.00 | 23.8 | 1.00 | 25.3 |
| 1.02 | 23.2 | 1.01 | 23.4 | 1.04 | 24.5 |
| 1.05 | 23.4 | 1.05 | 23.2 | 1.06 | 24.6 |
| 1.09 | 24.3 | 1.06 | 23.5 | 1.09 | 25.6 |
| 1.10 | 24.9 | 1.14 | 26.9 | 1.16 | 26.2 |
| 1.16 | 25.6 | 1.84 | 28.8 | 1.33 | 27.6 |
| 1.78 | 28.2 | | | 1.42 | 27.8 |
| 1.81 | 28.6 | | | 1.70 | 30.3 |

Future work will be directed toward extending the measurements of the vaporization behavior of $UC_x$ over a wider range of temperatures and compositions.

## 2. Radiation Damage on Structural Materials--Research and Development--In-Reactor Creep Studies

### a. In-pile Creep (J. A. Tesk)

Last Reported: ANL-7478, p. 104 (July 1968).

The creep rate of a specimen of V-15 w/o Cr-5 w/o Ti alloy was measured in a neutron flux of ~3 x $10^{13}$ n/cm$^2$-sec (E > 0.1 MeV) at 600°C and a stress of ~55,000 psi. The purpose of the experiment was to determine the effects of neutron irradiation on the creep properties of the

*Storms, E. K., The Refractory Carbides, Academic Press, New York (1967), Chap. XI, pp. 205-213.

**Ackermann, R. J., and Rauh, E. G., The Vapor Pressure of Liquid Uranium, Effects of Dissolved Tantalum, Phosphorus, Sulfur, Carbon and Oxygen, J. Phys. Chem. (in press).

†Holley, C. E., and Storms, E. K., "Actinide Carbides. A Review of Thermodynamic Properties," Thermodynamics of Nuclear Materials, 1967, IAEA, Vienna (1968), p. 397.

alloy and to check the in-reactor behavior of the encapsulated creep machine. Problems previously encountered in controlling the temperature of the capsule have tentatively been solved, and the final results of the creep measurement are being determined.

b. Void Formation and Growth (S. D. Harkness)

Last Reported: ANL-7527, pp. 104-105 (Dec 1968).

(i) Small-angle Scattering Studies of Void Formation. Studies have been started to determine void sizes and size distributions in irradiated Type 304 stainless steel by using X-ray small-angle scattering. A Kratky collimating system has been aligned for this purpose. Large amounts of scattering were obtained from voids in irradiated Type 304 stainless steel. The data are presently being analyzed.

(ii) Investigation of Irradiated Commercially Pure Vanadium. Samples for transmission electron microscopy were cut from a commercially pure vanadium liner irradiated at 430°C to a fluence of $2.5 \times 10^{22}$ n/cm$^2$. Previous tests* at ORNL had shown voids in commercially pure vanadium irradiated to about the same fluence but at a temperature of 630°C. No voids were observed in the sample irradiated at the lower temperature (430°C), which again indicates the strong temperature dependence of the void-formation phenomenon.

c. Fracture of Irradiated Metals (F. V. Nolfi, Jr.)

Not reported previously.

An investigation has been started to determine the mode of fracture of highly irradiated stainless steel, with particular emphasis on the low-ductility fracture found in creeptests in the temperature range between 400 and 650°C. Efforts will be made to determine the role of fine dispersions of voids, carbides, and other microstructures in reducing the ductility of irradiated material. Initial studies are being made with unirradiated material.

(i) Fracture in Stainless Steel. Experiments are in progress to determine if continuous intergranular carbides are sufficient to promote fracture of the grain boundaries in stainless steel upon exposure to hot flowing sodium. Thin specimens of Types 304L and 304 stainless steel were subjected to flowing sodium of low oxygen content (<3 ppm) at 650°C for ~100 hr. The specimens had been gas carburized at 1000°C prior to insertion into the sodium loop and then sensitized at 650°C. As a result, the 304L specimen contained approximately 0.5 volume fraction of carbide precipitate throughout the 0.010-in. cross section, both as a continuous

* Wiffen, F. W., private communication.

intergranular phase and as an intragranular phase. The 304 specimen, which had been carburized to a lesser degree, contained a continuous intergranular carbide precipitate to a depth of ~0.010 in. from the surfaces, and a discontinuous intergranular precipitate within the remainder of the 0.050-in. cross section.

Microscopic examination of these specimens showed no observable changes in either the surface condition or the microstructure. Efforts are underway to subject these specimens to a sensitive analysis for sodium to determine any possible sodium penetration. Future work in this area will entail similar experiments in sodium loops containing a higher concentration of oxygen, and investigations will be made of the effects of stress on sodium penetration, if any. In conjunction with the above work, a gas carburizing train was constructed. This train provides a virtually contamination-free method of carburizing.

Construction of facilities to accommodate the recently ordered scanning electron microscope (SEM) should be completed by the time the instrument arrives. In the meantime, the SEM at the Illinois Institute of Technology has been used to obtain photographs of the fractured surfaces of a number of tensile specimens of Type 304L stainless steel. Photographs were taken of specimens that had been tested at temperatures ranging from room temperature to 750°C, and at strain rates from 12 to 120%/min. The most notable feature evident in these photographs is the correlation between the density and size of presumably hard second-phase particles and the size and density of cavities of the ductile-dimple type. Changes in the fracture features due to temperature are also striking. Efforts to draw more exacting information are being deferred until the arrival of our SEM, at which time a more thorough examination of the specimens will be possible.

(ii) Fracture Sites. An analysis of the morphological stability of voids and/or bubbles under stress has been started. The purpose of this work is to determine if voids and/or bubbles growing by diffusion can change their nearly spherical morphology to one that is capable of acting as a fracture nucleus when subjected to moderately applied stresses. Two approaches to this problem are being considered. A thermodynamic approach should give some idea as to the relative driving forces for different shape changes, and, assuming success in this direction, consideration of the kinetics of shape change will follow. The latter problem is by far the most difficult, and any insight gained by first considering the thermodynamic problem will be of great value.

## 3. Techniques of Fabrication and Testing--Research and Development

### a. Nondestructive Testing--Research and Development

#### (i) Development of Nondestructive Testing Techniques (C. J. Renken)

Last Reported: ANL-7527, pp. 106-110 (Dec 1968).

##### (a) Neutron Radiography (J. P. Barton)

The usefulness of neutron radiography would be considerably expanded if, instead of reactors, convenient and inexpensive neutron sources such as small, D-T-type neutron generators and radioactive isotopes could be used.* Such sources are being studied at ANL, and we have shown that a major limitation results directly from the shortage of neutrons. High-yield neutron sources would result in prohibitive costs and, in addition, bulky shielding requirements (a particular handicap for transportable neutron-radiography facilities); thus, the maximum use of the available neutrons and the most efficient methods of neutron detection are both very important. Small-source neutron radiography will be particularly suited to applications that require only modest-quality radiography, which means that only low-ratio neutron collimators will be necessary. Consequently, a detection system of fairly large inherent unsharpness will be acceptable, if the geometric unsharpness of the system is not exceeded.

A simple neutron converter-detector system that most suits the conditions is the $^6$LiF-ZnS scintillator used in conjunction with a fast, light-sensitive film. The scintillator mixture is one part $^6$LiF (96% enriched) to four parts ZnS. $^6$Li has a cross section of 945 b for neutrons of thermal energy, and the reaction yields an alpha particle and a triton with a total energy of 4.78 MeV. The system is highly efficient (higher than competitive foil-film combinations), and about $10^5$ light photons are generated per neutron captured. The inherent unsharpness is comparatively large, but is unimportant for low-collimation applications. The discrimination against gamma radiation is excellent. The performance of this scintillator-film combination for neutron radiography is shown in Fig. III.B.2, which gives

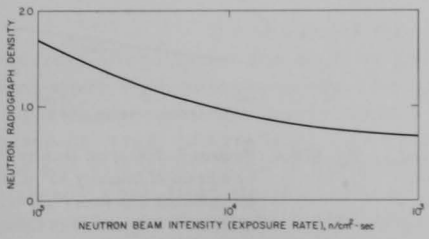


Fig. III.B.2

Neutron Radiographic Density Produced by a Constant Neutron Dose of $2 \times 10^6$ n/cm$^2$ for Different Beam Intensities ($^6$LiF-ZnS Scintillator-Type F Film Combination at 20°C)

*Barton, J. P., Neutron Radiography Using Non-Reactor Sources, Isotopes and Radiation Technology 6(2), 149-153 (Winter 1968-1969).

the film density (for $^6$LiF-ZnS scintillator plus Kodak F film) resulting from a total neutron dose of $2 \times 10^6$ n/cm$^2$ at different exposure rates. The measurements were made by using a collimated beam from the Juggernaut reactor, and neutron-beam intensities were varied by changes in the reactor power level.

A dose of $10^6$ n/cm$^2$ will produce a working radiographic film density of one when the beam intensity is $10^5$ n/cm$^2$-sec, but a much higher neutron dose would be needed to provide this same working radiographic density if the beam intensity is $10^4$ or $10^3$ n/cm$^2$-sec. At such beam intensities there is a considerable loss of efficiency because of reciprocity-law failure of the scintillator-film combination. This loss is particularly important for small-source techniques since, in these cases, the incident neutron-beam intensities will be within this range from $10^3$ to $10^4$ n/cm$^2$-sec.

Neutron radiographs have been taken with the scintillator-film combination cooled to a temperature of -20°C during the exposure period. Cooling was accomplished by means of a simple insulating jacket arranged at the exposure position and packed with solid $CO_2$. The results of measurements taken at -20°C are compared with measurements at +20°C in Figs. III.B.3 and III.B.4. These curves are for beam intensities of $10^5$ and $10^3$ n/cm$^2$-sec, respectively. The advantage of cooling the radiographic scintillator-film combination becomes significantly greater at the lower neutron-beam intensities. A plot of neutron beam intensity as a function of neutron radiographic density indicates that reciprocity-law failure is, in fact, almost entirely eliminated at -20°C. Since a plot of this type has almost zero slope, we would not expect to gain much advantage by working at even lower temperatures. Confirmation was obtained by the experimental results shown in Fig. III.B.5 for scintillator-film combinations cooled to

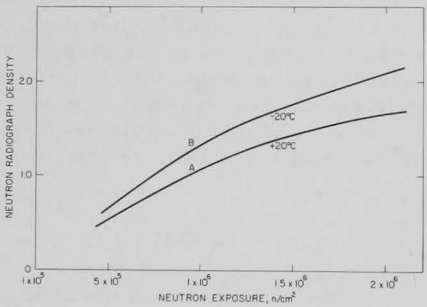


Fig. III.B.3. Neutron Radiographic Density Produced by a Beam Intensity of $10^5$ n/cm$^2$-sec for Different Exposures ($^6$LiF-ZnS Scintillator RII + Type F Film Combination at +20°C and -20°C)

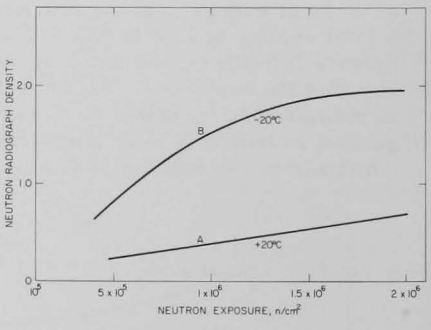


Fig. III.B.4. Neutron Radiographic Density Produced by a Beam of Intensity $10^3$ n/cm$^2$-sec for Different Exposures ($^6$LiF-ZnS Scintillator RII + Type F Film Combination at +20°C and -20°C)

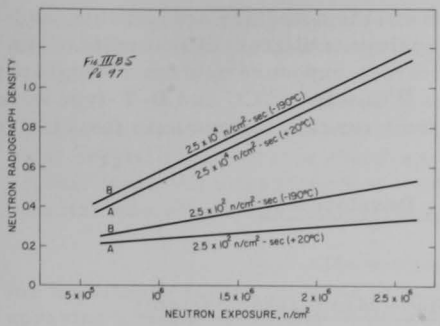


Fig. III.B.5. Neutron Radiographic Density Produced by Beams of $2.5 \times 10^4$ n/cm$^2$-sec and $2.5 \times 10^2$ n/cm$^2$-sec ($^6$LiF-ZnS Scintillator NE421 + Type F Film Combination at +20°C and -190°C)

-190°C during neutron exposure. At such temperatures the efficiency of neutron detection is only marginally better than at room temperature, and a considerable degree of reciprocity-law failure is again apparent.

A theoretical interpretation is difficult since we are concerned with the combined actions of the neutron scintillator and the film. The scintillator efficiency probably increases as the temperature is reduced below 20°C, but then peaks, and decreases again at very low temperatures. A spot check taken by exciting the $^6$LiF-ZnS scintillator with X-ray beams and then measuring the light output directly at +20°C and -20°C confirmed the presence of an increase in scintillator efficiency. For the film, mechanisms of reciprocity-law failure are complex and incompletely understood. Several such mechanisms are probably operative simultaneously, and may change with different situations.

One simple theory is to consider the latent-image formation as dependent on the collection of electrons at sensitivity centers and on the subsequent attraction of positive ions ($Ag^+$) to these sensitivity centers. In cooling from +20°C to -20°C the electron mobility is virtually unchanged, and the mobility of the $Ag^+$ ion changes very little. However, the rate of escape of the electrons from the sensitivity center is dependent on thermal excitation of the electrons; at low exposure rates, the lower (-20°C) thermal temperature leads to appreciable reduction in losses of electrons from these centers before attraction of $Ag^+$ ions. On further cooling to -190°C, the electron mobility and electron thermal excitation at the sensitivity center remain effectively unchanged; however, there is a considerable decrease in the mobility of the positive ion ($Ag^+$), which leads to loss of latent image for low exposure rates.

These simple theories must, however, be less than completely adequate for the neutron-radiographic scintillator-film combination, since each neutron produces a single large light pulse with over $10^5$ light photons emitted instantaneously. The film exposure is therefore a series of large, intermittent light pulses that make local dots on the image one at a time. This is quite different from photographic exposure to a steady weak-light source, such as the sky at night, and, in the case of the neutron-radiography combination, we would not have expected reciprocity-law failure because of changes in the rate of these individual large pulses (i.e., due to changes in neutron-beam intensity).

Nevertheless, the effects noted are appreciable, and controlled cooling of neutron-radiographic scintillator-film combinations during exposure should be of value in direct-exposure neutron radiography with sources such as $^{241}$Am-Be, $^{241}$Am-$^{242}$Cm-Be, $^{252}$Cf, and D-T-type accelerators. There may be some applications for this technique in fast-neutron radiography.

## C. Engineering Development

### 1. Research and Development

#### a. Development of Master-Slave Manipulator Systems (R. C. Goertz)

Last Reported: ANL-7513, pp. 112-113 (Oct 1968).

(i) Mark-E4A Test and Modification. The detailed drawings of the Mark-E4A electric master-slave manipulator have been updated to show the manipulator as it has been fabricated. The new drawings have yet to be checked. Some of the new drawings show improvements; further testing might show the need for more.

The slave gearbox with the Vespel (polyamide plastic) gear, which was irradiated to $10^9$ R gamma, has been cycled 17,000 times under full-load conditions and about 500,000 times under 50%-load conditions. The gear has worn some and has a backlash of about 0.002 in. at the pitch line (it had nearly zero backlash at the beginning of the test). The manipulator would still operate reasonably well with the 0.002-in. backlash; we are preparing to cycle it another 500,000 times.

We are preparing the manipulator for overall cyclic testing. All the gearboxes on both the master and slave have been dismantled, checked (in some instances, modified), and reassembled. The remaining parts of the slave arm are being checked down to the individual parts. Changes will be made on items seriously needing it. One example is a coupling on the Z-motion drive that is too springy and has worked loose several times.

#### b. Instrumentation and Control

(i) Boiling Detector (T. T. Anderson)

(a) Acoustic Method

(1) High-temperature Detector Development (T. T. Anderson and R. H. Selner)

Last Reported: ANL-7527, pp. 114-115 (Dec 1968).

The surfaces of two Z-cut lithium niobate crystals have been coated with an organic-vehicle metallizer and fired in an oxygen

furnace. The resulting electrodes had a more metallic sheen than previous electrodes, which had been fired in an air furnace.

One of these electroded lithium niobate crystals has been brazed with gold-nickel alloy to the container diaphragm on the front crystal face and to a stainless steel acoustic backing on the rear crystal face. An ultrasonic test signal applied to the partially assembled detector was electrically detectable.

Alternative bonding methods are being investigated for high-temperature acoustic detectors. A trial test was made of plasma spraying a nickel film onto lithium niobate. Adherence of the film was minimal, and the high-temperature gradient involved with this process cracked the 2-mm-thick crystal of lithium niobate. To minimize mechanical stresses between lithium niobate and the sensor body, diaphragms have been hydroformed from fully annealed stainless steel. A circular groove around the crystal-contact area is expected to prevent distortions and to compensate for temperature gradients between diaphragm and the cylindrical container. These diaphragms and lithium niobate crystals are being prepared for tests involving rf-sputtering of electrodes.

(2) Irradiation Tests of Piezoelectric Materials (T. T. Anderson)

Not reported previously.

Electronic measurement techniques are being evaluated for determining the dynamic properties of piezoelectric materials during irradiation. From trial tests, an immittance-measuring instrument was found to be applicable to measuring piezoelectric-device properties, which might be expected to vary during irradiation.

(3) Sound Measurements in EBR-II (T. T. Anderson)

Last Reported: ANL-7527, p. 115 (Dec 1968).

From acoustic measurements of the EBR-II reactor, parameters such as flow noise and electrical interference can be determined for an acoustic boiling detector. A sodium-immersible detector is not yet available, so measurements of sound and vibration now have to be made in a moderate-temperature environment outside the reactor primary tank.

Components of the EBR-II reactor that provide an acoustic path to the primary sodium system have been instrumented with accelerometers, which have been fastened onto the components near the operating floor level. Vibration measurements consisted of earphone

monitoring, oscilloscope display, audiospectrum recording (0-10 kHz), and ultrasonic-spectrum recording (0-100 kHz). Preliminary results indicate that most of the acoustic noise depends on the rotational speed of the primary-pump motors. Additional tests are planned to locate sources of sound associated with the primary sodium system, to determine the relative contributions by motors, pumps, and flowing sodium.

The same instrumentation was used to monitor sounds from the remote-handling operations during refueling, sound associated with rod drops, and low-frequency vibrations of the reactor components.

(4) Heater Tests for Sodium-boiling Detection
(B. B. Spillane)

Not reported previously.

For developing the technology of sodium-boiling detection, it is desirable to simulate boiling of sodium in a blocked-flow dummy subassembly. The test subassembly, containing a high-flux heater, is being fabricated for insertion into a sodium facility. In design of the heater fixture, an anticipated problem of heater burnout at the lead wires has been reduced by operating the single-ended heater inverted with the leads coming down into the sodium, and with the sodium functioning as an electrical-return lead.

c. Heat Transfer and Fluid Flow

(i) Heat Transfer in Liquid Metal Cooled Reactor Channels
(R. P. Stein and J. V. Tokar)

Last Reported: ANL-7518, pp. 97-99 (Nov 1968).

(a) LMFBR High-flux Operation and Its Consequences. Procurement bids have been sought for all major loop components, such as the preheater, top plenum, hot traps, dump tank, and vacuum chamber.

Tests of liquid-metal helical induction pumps indicate that it is feasible to construct such a pump as needed for the stainless steel heat-transfer loop, in which sodium in the pump would be as hot as 1000°F and the flow characteristics would be 400 psi at 10 gpm and 200 psi at 40 gpm. Such a pump is being constructed.

The vacuum-chamber ion and sublimation pumps for the electron-bombardment heater have been ordered.

(ii) Electron Bombardment Heater Test Facility (R. D. Carlson and R. E. Holtz)

Last Reported: ANL-7518, p. 99 (Nov 1968).

The operation of the 7-pin electron-bombardment heater (EBH) has been hindered by mechanical problems, mostly involving attachment of the thoriated-tungsten filaments to the electrodes. Modifications are being made to eliminate this problem; additional efforts are augmenting the development of the 7-pin EBH cluster.

Figure III.C.1 shows the EBH that is being tested. This 7-pin bundle has 3/8-in.-OD x 24-in.-long simulated fuel pins with double filaments. A second type of heater arrangement is being designed to provide a 7-pin bundle of 1/4-in.-dia pins and a 36-in. heated length. These pins have a single filament and power is supplied from both ends of the pin.

d. Engineering Mechanics

(i) Structural Dynamics Studies--Parallel-flow-induced Vibrations (M. W. Wambsganss, Jr.)

Last Reported: ANL-7527, pp. 115-117 (Dec 1968).

(a) Transducer Development. The installation of seven miniature pressure transducers (0.0004 in.$^2$ area) has been completed. The transducers are flush-mounted on a stainless steel test rod. Five transducers are mounted in a longitudinal direction at spacings of 0.036, 0.157, 0.348, and 0.740 in.; three are mounted in a circumferential direction at spacings of 0.069 and 0.157 in., with one transducer common to the two directions.

With the associated charge amplifiers set on the "medium time-constant" setting, the frequency response of the transducers is essentially flat over the range of frequencies tested (5 to 100 Hz). However, in operation, this time-constant setting gives rise to a dc drift, making it necessary to operate on the "short time-constant" setting. On this setting, the lower frequencies are slightly attenuated.

A series of flowtests are being performed using the instrumented test rod to measure the pressure field. The transducers are effectively insensitive to the strain levels encountered during the flowtests; strain sensitivity was a problem plaguing early attempts at constructing workable transducers.

(b) Structural Dynamics Test Loop. Final design of the small structural dynamics test loop and the preparation of fabrication

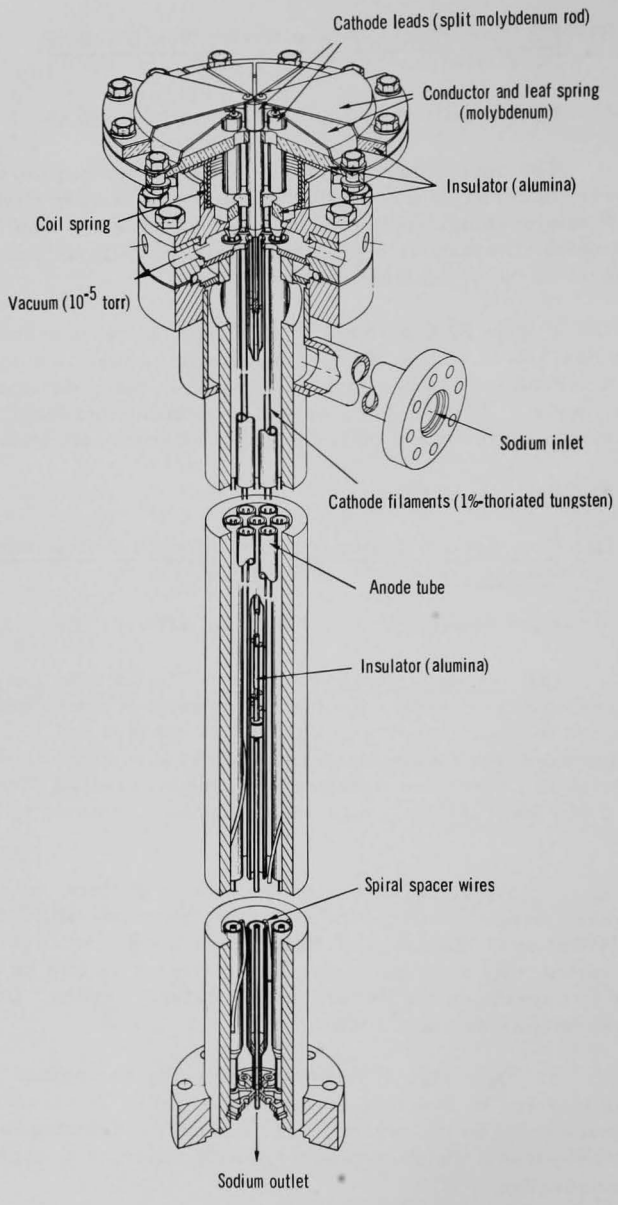


Fig. III.C.1. Electron-bombardment-heated Simulated Fuel Test Section

drawings have been completed. The majority of the components such as piping, isolation sections, accumulator, and valves have been procured. Delivery of the pump has been delayed 90 days because of a strike at the manufacturing plant.

(c) Flowtest Single Cylinders. A series of flowtests are being performed using as the test element the stainless steel rod instrumented with miniature pressure transducers discussed above. In addition to recording the pressure-time histories from the surface of the test element, we are recording pressures from three locations (inlet, midpoint, and exit) on the wall of the test section, test-element displacements at the midpoint, and accelerations at locations on the pump and on a flange of the test section.

These data will be processed using a spectrum analyzer and time-delay correlator to obtain the mean-square-value spectral densities and space-time correlation representations. Analysis and interpretation of these results will permit evaluation of the miniature pressure transducers and will give insight into the space-time behavior of the convecting pressure field.

(d) Damping Analysis. An experiment is being designed to study the influence of water flow velocity on the damping characteristics of a cylindrical rod. With the rod mounted within a test section and vibrated on a shaker while water is pumped through the test section at various flow velocities, modal magnification factors will be measured; with the mode shape known, the modal damping factors can be computed.

(ii) Structural Dynamics Studies--Crossflow-induced Vibrations (M. W. Wambsganss, Jr. and S. S. Chen)

Last Reported: ANL-7527, pp. 117-119 (Dec 1968).

The motion of cylindrical rods and banks of rods as influenced by a crossflowing fluid is being studied to develop new methods for analyzing, testing, and evaluating the reliability and structural life of heat exchangers. Because reactor heat exchangers have relatively complex geometries, boundary conditions, and flow patterns, the initial investigation is of a fundamental nature. Forcing functions are being characterized and various damping mechanisms are being studied.

(a) Analysis of Interaction and Tube-spacing Effects. The steady-state response of a tube vibrating between stops has been analyzed using a one-mode approximation (see ANL-7527). Because the flexural stress and shearing force contain second and third derivatives of the displacement, several modes should be included to obtain accurate results. This is accomplished in the following manner. From a one-mode approximation, the velocity and the phase angle between the exciting force and the

motion of the tube as it passes the equilibrium position (q = 0) are known. The conditions at that instant are taken as the initial ones for the refined analysis. Then the dynamic stresses are obtained by the classical normal-mode method. Responses of a simply supported tube are given in Figs. III.C.2 and III.C.3, where the shearing force s is $C_s(EI/\ell^2)\epsilon$, the bending stress $\sigma$ is $C_\sigma(Er/\ell)\epsilon$, r is the radius of the tube, x is the distance from the support, and the other notations are as given in ANL-7527.

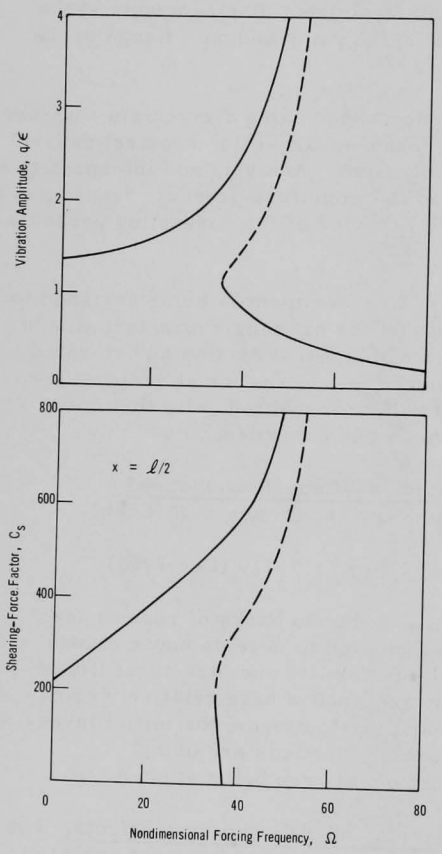


Fig. III.C.2. Amplitude Response and Shearing Force of a Simply Supported Tube for R/ε = 1000 and a Damping Ratio of 0.01

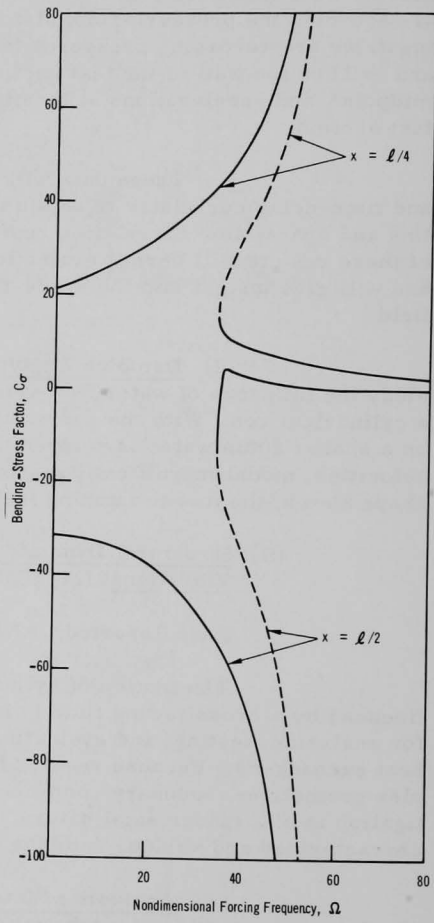


Fig. III.C.3. Flexural Stresses of a Simply Supported Tube for R/ε = 1000 and a Damping Ratio of 0.01

The analysis is based on the assumption that there is no relative motion between the tube and the stops at the contact point. In reality, local deformation exists at the contact area. For the elastic indentation, the Hertz law is widely used in the dynamic case, i.e.,

$$\alpha = kP^{2/3},$$

where $\alpha$ is the relative approach of the two bodies, P is the contact force, and k is the Hertz constant. If the stop is a cylindrical hole whose axis is parallel to that of the tube, such as the baffle plate in a heat exchanger, and if we assume that the stress is uniformly distributed across the width of the hole, then the Hertz law is reduced to the linear form $\alpha = kP$.

To investigate the effect of the local deformation at the contact point, the impact developed by the instantaneous arrest of a moving beam is analyzed. A simply supported beam having initial velocity u is brought to rest at two ends instantaneously. At the midpoint it strikes a spring of stiffness $k_s$. The impact developed at the spring is a function of the relative stiffness $k_s/k_b$, as shown in Fig. III.C.4, where $k_b$ is the stiffness of the beam. It is clear that, if the relative stiffness is larger than $10^4$, it is reasonable to assume that we have a rigid stop. Because such is the case when a heat-exchanger tube impacts with a baffle plate, the assumption of negligible local deformation is justified in this analysis.

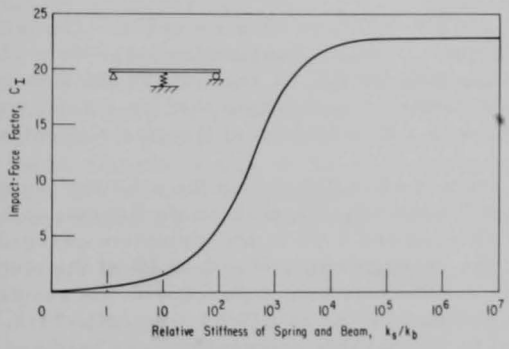


Fig. III.C.4

Impact on a Spring at Midpoint Developed by the Instantaneous Arrest of a Simply Supported Beam. Impact = $(C_I/\ell)(EIM)^{1/2}u$.

## D. Chemistry and Chemical Separations

### 1. Aqueous and Volatility Processes--Research and Development--Fluoride Volatility Process

#### a. Fluorination Chemistry and Procedures (M. J. Steindler)

Last Reported: ANL-7518, pp. 103-105 (Nov 1968).

A second statistically designed series of five experiments simulating the fluoride-volatility processing of fast reactor fuels is

underway, using the 2-in.-dia fluid-bed reactor. In each run the charge is 650 g of particulate (solid solution) 20 w/o $PuO_2$-$UO_2$, 1100 g $Al_2O_3$ (-40 +170 mesh), 0.75 g $NpO_2$ (the proportion expected at a burnup of 100,000 MWd/ton), and 69 g of a mixture of fission product oxides (simulating the same burnup). The reaction steps consist of oxidation (in some runs) with 20 v/o oxygen, fluorination with 8-20 v/o fluorine-nitrogen for 3 hr at 350°C to remove uranium, and a subsequent recycle-fluorination with concentrated fluorine to remove plutonium.

In these experiments, the objective is to determine the effects of each of three variables on uranium and plutonium retention in the final bed:

1. the inclusion or omission of an oxidation step;

2. two temperature sequences in the recycle-fluorination with concentrated fluorine (one beginning at 400°C, the other at 500°C, both ending at 550°C);

3. two fluorine-concentration sequences in the recycle-fluorination with concentrated fluorine (a fast buildup in which fluorine concentration increases from 20 to 90 v/o in ~35 min and a slow buildup in which fluorine concentration increases to 90 v/o in 1 hr.

Two runs (FF-B1 and FF-B2) have been completed. Oxidation of the fuel was omitted in each run. Uranium fluorination steps were identical. The plutonium fluorination step for FF-B1 was 4 hr at 500°C and 4 hr at 550°C with a fast buildup of fluorine concentration; that for FF-B2 was 4 hr at 400°C and 4 hr at 550°C with a slow buildup of fluorine concentration.

The hexafluoride product collected during the uranium fluorination step (3-hr reaction of unoxidized $PuO_2$-$UO_2$ with dilute fluorine at 350°C) contained 66% of the uranium charged and 5.9% of the plutonium charged in Run FF-B1 and about 100% of the uranium charged and 10.1% of the plutonium charged in Run FF-B2. These results may be compared with the results of the uranium-fluorination step in Runs FF-A1 to FF-A5 (see ANL-7518, p. 105) in which simulated fuel of comparable composition was oxidized, then fluorinated with 10-15 v/o $F_2$ to give a product containing 69.7 to 96.5% of the uranium charged and 0.6 to 27.7% of the plutonium charged. During the first hour of uranium fluorination in Runs FF-B1 and FF-B2, the U/Pu ratio in the product was $3 \times 10^3$ and higher. These results suggest that a quantitative separation of uranium from plutonium may be possible by continuous fluorination with fluorine under carefully controlled conditions.

The peak rate of production for $PuF_6$, as calculated from plutonium concentrations in bed samples, averaged 6.4 lb/(hr)(ft$^2$) at 500°C in Run FF-B1 and 4.5 lb $PuF_6$/(hr)(ft$^2$) at 400°C in Run FF-B2. Both peak rates

occurred during the second half-hour of the initial recycle-fluorination period. The average rate of production at 500°C was 2.3 lb $PuF_6/(hr)(ft^2)$ while the reactor operated at a reaction efficiency of 23.1% [based on the reaction $PuF_4(s) + F_2(g) \rightleftharpoons PuF_6(g)$ and the fluorine flowrate]. At 400°C, the average production rate was 2.0 lb $PuF_6/(hr)(ft^2)$, and the reaction efficiency was 46.5%.

The results also showed that 2.2% of the plutonium charged remained in the final bed after Run FF-B1, while 1.6% of the plutonium charged remained in the final bed after Run FF-B2. These plutonium retentions are higher than those of some previous runs made under slightly different operating conditions.

b. Purification Procedures and Fission Product Chemistry (M. J. Steindler)

Last Reported: ANL-7518, pp. 105-106 (Nov 1968).

(i) Fission Product Chemistry. A conceptual fluoride-volatility process for irradiated $UO_2$-$PuO_2$ fast reactor fuel includes a step in which uranium is volatilized as $UF_6$ by the reaction of powdered fuel oxide with an oxygen-fluorine mixture at 350°C. An exploratory investigation was performed (see ANL-7518) in which selected fission products (as the element or oxide) were reacted with 10% $F_2$-$O_2$ at 350°C to determine the products formed.

Additional exploratory experiments have been performed in which Nb, $Nb_2O_5$, Mo, $MoO_3$, and Te were oxyfluorinated in the presence and absence of $U_3O_8$. Results showed that (1) there is no noticeable interaction of $UF_6$ and the products of oxyfluorination of the selected fission products, (2) the oxyfluorination products of fission product elements and of their oxides are not necessarily identical, and (3) the reaction rates of the elements are substantially greater than the reaction rates of their oxides.

c. Engineering Design, Analysis, and Evaluation (N. M. Levitz)

Last Reported: ANL-7527, p. 120 (Dec 1968).

The report on a conceptual fluoride volatility process for recovering uranium and plutonium from FBR fuels is nearly complete.

2. Closed Cycle Processes--Research and Development--Compact Pyrochemical Processes

a. Laboratory Process Development (I. Johnson)

Last Reported: ANL-7513, pp. 120-121 (Oct 1968).

A liquid Cu-Mg-Ca alloy is used in the reduction step of the salt-transport process for the recovery and purification of fast breeder

reactor fuels. The phase relations of this alloy are being investigated to provide more complete information on the factors influencing the reduction reaction. Preliminary results indicate that there are no ternary compounds in the system with melting points above the temperature (850°C) to be used for the reduction reaction. An alloy of the composition Cu-37 a/o Mg-34 a/o Ca was found to be completely liquid over the temperature range from 517 to 854°C. At 850°C, no upper limit is set by the phase relations for the calcium content of the Cu-Mg-Ca alloy that may be used for the reduction reaction. Thus, the initial calcium concentration in the reduction alloy may be chosen to optimize the reduction reaction.

Concurrent studies of the phase relations in Cu-Mg-U alloys have shown that U-Cu intermetallics are formed in the copper-rich region of the system, but that their rates of formation are extremely low in the more magnesium-rich regions of the system, even at temperatures above 1000°C. These preliminary results indicate that uranium-copper intermetallic compounds are unlikely to form in the reduction step of the process. Such compounds are undesirable, since their formation could lead to some coprecipitation of plutonium.

b. Process Engineering Studies (R. D. Pierce)

Last Reported: ANL-7527, pp. 120-121 (Dec 1968).

A graphite crucible coated with vapor-deposited tungsten (see Progress Report for June 1968, ANL-7460, p. 115) is being tested to determine if this material can be used in pyrochemical processing equipment. In the most recent test, the crucible was charged with a Mg-44 a/o Cu alloy and an 80 m/o $CaCl_2$-20 m/o $CaF_2$ salt mixture, and heated at 800°C for 98 hr with agitation. Examination of the crucible after pouring out the melt and cooling to room temperature revealed no signs of cracking or leakage.

c. Experimental Flowsheet Investigations (R. D. Pierce)

Last Reported: ANL-7527, pp. 121-122 (Dec 1968).

Construction and design work on the Plutonium Salt Transport Facility (see Progress Report for September 1968, ANL-7500, p. 115) is continuing. Piping of the helium-purification systems for gloveboxes 2 and 3 has been completed, except for liquid-nitrogen fill piping. Electrical work on these systems has begun. The construction of the equipment-storage towers above the gloveboxes has been completed, and electrical work on the hoists inside these towers is underway. The enclosure that houses three vacuum pumps and a vacuum-supply tank has been completed. The piping between equipment in this enclosure and gloveboxes 2 and 3 and transfer lock 7 is about 80% complete. The refrigeration compressor, cooling coils, and atmosphere-recirculation duct for glovebox 3 have been installed.

Fabrication of the top flanges for the three main processing vessels in box 3 is nearly complete. Work is continuing on the agitator-shaft-bearing assemblies and heat shields. The top flanges for the four receiver vessels in box 3 are complete except for the heat shields. Two 200-gal helium-storage tanks have been installed, one above box 2 and one above box 3. Installation of piping between the tanks and associated process equipment and glovebox-atmosphere controls has commenced.

With the exception of designs for the equipment for glovebox 2 (retorting and extraction equipment), which has a later completion date, design work on all items for the facility installation has been completed.

d. Liquid Metal-Molten Salt Contactors (R. D. Pierce)

Last Reported: ANL-7527, p. 122 (Dec 1968).

A multistage mixer-settler apparatus is being designed for use with the liquid metal-molten salt systems in the salt-transport process for the recovery of fast breeder reactor fuels. This equipment will be constructed for process demonstrations in the Plutonium Salt Transport Facility (see Progress Report for September 1968, ANL-7500, p. 115).

Various mixer-settler and agitator-pump designs are being tested in mockups constructed of plastic and metal. A modification of the agitator-pump design described in the Progress Report for November 1968, ANL-7518, pp. 112-113, is now being tested. In this latest design, the upper section of the pump has a larger diameter than the lower section, and the mixing blades are larger than those used in the earlier design. The larger upper section produces a higher pumping capacity, and the larger blades provide a high degree of agitation.

An existing plastic mixer-settler model is being used to study flow patterns through a mixer-settler stage. The test model is being operated with both the light and heavy phases circulating, with either phase recycling or transient. The tests have demonstrated that complete control of both phases can be achieved by means of weirs located in the settling chamber.

Two runs have been completed in a facility for testing metal-salt contactors for pyrochemical processing (see Progress Report for August 1967, ANL-7371, pp. 98-99). Partial results of the first run (MSL4) were reported in the Progress Report for November 1968, ANL-7518, pp. 112-113.

In Run MSL4, mixer-settler #1 was charged with 18.2 kg of Cd-2.2 a/o Mg and 3.055 kg of uranium, and mixer-settler #2 was charged

with 12.34 kg of Cd-45 a/o Mg. The equipment was heated to 600°C, and a $MgCl_2$-30 m/o NaCl-20 m/o KCl salt phase was circulated between the mixer-settlers for 312 min. About 2.81 kg or 93.4% of the uranium charged to mixer-settler #1 was transported to mixer-settler #2 by means of 1150 kg of salt that was circulated between the two mixer-settlers. The calculated overall mass-transfer coefficient ($k_sA$) of uranium in mixer-settler #2 was fairly constant at 50 to 60 kg U/(min)(wt fraction U in salt phase) when the agitation rate was 460 rpm. This value is lower than the maximum value calculated for mixer-settler #1, which had an agitation rate of 640 rpm. The mass-transfer coefficient observed in mixer-settler #1 ranged from 16 to more than 200 kg U/(min)(wt fraction U in salt phase). The lower values are attributed to an initial low rate of dissolution of solid uranium pieces in the Cd-Mg alloy.

In Run MSL5, a 4-g piece of irradiated copper was dissolved in the Cd-Mg alloy in mixer-settler #1 to provide a metal-phase tracer to measure the entrainment of metal in the salt phase transferring from mixer-settler #1 to #2. The run lasted for 520 min, and three different rates of salt flow and agitator speeds were used in mixer-settler #1. The results of Run MSL5 indicate excellent phase separation and minimal metal entrainment in the salt phase. Less than 5 g of the Cd-Mg alloy was entrained in more than 1100 kg of salt that circulated through the mixer-settlers.

e. Decladding and Fuel Resynthesis (R. D. Pierce)

Last Reported: ANL-7527, pp. 122-123 (Dec 1968).

In the salt-transport process for fast breeder reactor fuels, stainless steel cladding is removed from the spent fuel by dissolution in molten zinc. An experiment was conducted to determine the effect of irradiation on the rate of dissolution of stainless steel in zinc. In this experiment, six 0.14-in.-dia by 2.6-in.-long rods of Type 304 stainless steel were dissolved in 10 kg of molten zinc in an alumina crucible at 800°C. One of the rods had been irradiated in EBR-II to a level corresponding to a burnup of ~2.2 a/o for LMFBR core fuel. The zinc solution was sampled eleven times over a 260-min period, and the samples were analyzed for both total iron concentration and radioactivity. The analyses showed that the irradiated rod dissolved more than twice as fast as the unirradiated rods. Since unirradiated Type 304 stainless steel has been shown to dissolve at a practical rate for fuel decladding by zinc dissolution, the conclusion is that irradiated fuel (equivalent to ~2% burnup) can be declad readily by the zinc dissolution technique.

## 3. General Chemistry and Chemical Engineering--Research and Development

### a. Characterization of Carbon-bearing Species in Sodium (F. A. Cafasso)

Last Reported: ANL-7513, p. 124 (Oct 1968).

Transport of carbon in liquid sodium-steel systems by a mechanism involving the formation of disodium acetylide, $Na_2C_2$, has been postulated.* To support this mechanism, experiments to determine the stability and solubility of $Na_2C_2$ in sodium, and the heat and free energy of formation of $Na_2C_2$, will be carried out. An apparatus suitable for both the stability and solubility measurements has been fabricated and is currently being assembled; equipment for determining $\Delta Hf(Na_2C_2)$ and $\Delta Gf(Na_2C_2)$ is available. A quantity of $Na_2C_2$ has been prepared for the measurements by the disproportionation of $NaHC_2$ at ~110°C. The measurements are expected to begin shortly.

### b. Identification of Mechanism(s) of Carbon Transport in Sodium Systems (F. A. Cafasso)

Last Reported: ANL-7513, p. 125 (Oct 1968).

The study of carbon behavior in systems containing liquid sodium would be greatly facilitated if it were certain that the container material did not interact with the system. The inertness of various materials in this regard is being tested. Materials selected for study are those that are available in high purity, are fabricable, do not form compounds with sodium, and have very low solubility in sodium. The first materials tested were copper (which does not form stable carbides), nickel (which forms an unstable carbide), and tantalum (which forms stable carbides, but may still be useful in sodium systems because of favorable kinetics).

Capsules made of these metals were loaded with reactor-grade sodium containing 10 ± 2 ppm carbon, then sealed and heated at 650°C for 120 hr. After cooling to ambient temperature, the capsules were opened and the sodium was analyzed for carbon.

Carbon contents of 9, 6, and 15 (all ±2) ppm were found in the sodium from the copper, tantalum, and nickel capsules, respectively. Thus, the carbon content of the sodium was not significantly altered when heated in copper. In contrast, the tantalum appeared to getter about half the carbon, and the nickel, which contained a trace of carbon, underwent decarburization and added carbon to the sodium. These findings indicate that copper may be a suitable container material. Further tests of its inertness will be made by examining its reactivity to various carbon compounds in liquid sodium.

---

*Luner, C., Feder, H. M., and Cafasso, F., Carbon Transport in Sodium Systems, presented at the International Conference on Sodium Technology and Large Fast Reactor Design, Argonne, Illinois (November 7-9, 1968).

c. Determination of the Solubility of Helium in Sodium (F. A. Cafasso)

Last Reported: ANL-7527, pp. 123-124 (Dec 1968).

Since helium is a potential cover gas for sodium in fast breeder reactors, its solubility in sodium is being measured as a function of temperature (400-600°C) and pressure (3-10 atm). The technique involves saturating sodium with a $^4$He-$^3$He mixture,* stripping the dissolved helium from sodium with an argon sparge, separating the bulk of the argon on a liquid-nitrogen-cooled molecular sieve trap, collecting the untrapped gas, and assaying it for helium with a mass spectrometer. How well the helium can be recovered from the argon sparge was recently tested.

Argon containing about 1 ppm $^3$He, which simulates the helium-in-argon concentration expected in solubility measurements, was introduced into the stripping section of the apparatus, and the analytical sequence outlined above was carried out. The results of several such experiments indicated a wide range of helium recoveries. After experimenting with some of the conditions, e.g., varying the temperature of the molecular sieve trap and changing stripping gases, conditions were found that gave consistent recoveries of helium, and the solubility measurements were begun.

d. Kinetics of Solution and Precipitation of Sodium Oxide (F. A. Cafasso)

Last Reported: ANL-7513, p. 126 (Oct 1968).

A study of the morphological features of sodium oxide crystals that precipitate from sodium solution is underway. Various techniques are being evaluated for application to this study. The technique of scanning-electron microscopy appears promising for initial studies on the morphology and particle-size distribution of sodium oxide crystals embedded in a sodium matrix. A closer examination of this approach is now being made.

e. Surface Phenomena in Liquid Sodium (F. A. Cafasso)

Last Reported: ANL-7513, p. 127 (Oct 1968).

(i) Surface Diffusivity Studies. The role of surface diffusion in the corrosion of structural materials in liquid sodium has not yet been elucidated. A study of this effect is now underway. The experimental technique involves comparison of the rate of decay of surface scratches annealed in liquid sodium with the rate of decay in a helium (or hydrogen) atmosphere.

---

* The $^3$He functions as a tracer: if the $^3$He/$^4$He ratio of the recovered soluble helium differs from that of the saturating gas, contamination is indicated, for which corrections can be made.

In preparation for this study, annealing furnaces and auxiliary equipment have been assembled. Procedures for polishing specimens to suitable flatness, producing closely spaced scratches on the surface of a specimen, and examining the surface topography by interference microscopy have been developed. The initial materials being examined are iron and Type 304 stainless steel. Preliminary scratch-annealing experiments with these metals have been carried out to determine the temperature and time required for significant diffusion to occur.

## PUBLICATIONS

Argonne Code Center: Directory of Cooperating Installations
M. K. Butler, Marianne Legan, Ethelyn Lindsay, and L. Ranzini
ANL-7497 (Oct 1968)

Steam-Water Condensing-injector Performance Analysis with Supersonic Inlet Vapor and Convergent Condensing Section
Michael A. Grolmes
ANL-7443 (May 1968)

Engineering-Scale Studies of the Fluorination of Uranium Oxide with Bromine Pentafluoride
J. T. Holmes, L. B. Koppel, J. D. Gabor, D. Ramaswami, and A. A. Jonke
Ind. Eng. Chem. Process. Res. Develop. 8(1), 43 (1969)

Rule of Thumb for Fast Flux Irradiations
C. N. Kelber
Nucl. Appl. 6, 6-9 (Jan 1969) Letter

Heat Capacity and Thermodynamic Properties of Plutonium Dioxide
O. L. Kruger and H. Savage
J. Chem. Phys. 49, 4540-4544 (Nov. 15, 1969)

Preparation of First Mark IA Fuel Alloy for EBR-II
W. E. Miller, G. J. Bernstein, J. F. Lenc, and R. C. Paul
ANL-7474 (Aug 1968)

Uranium Nitride-Sodium Paste Fuel for Fast-reactor Blankets
P. A. Nelson and M. G. Chasanov
ANL-7475 (Aug 1968)

Addendum to the Report on High Conversion Critical Experiments
K. E. Plumlee
ANL-7203 Addendum (Aug 1968)

Multilevel Effects on Infinite Dilution Resonance Integrals
E. M. Pennington and D. A. Sargis
Nucl. Sci. Eng. 35, 297-298 (Feb 1969) Note

Neutron Single Particle Levels in a Wood-Saxon Potential
K. Takeuchi and P. A. Moldauer
Phys. Letters 28B(6), 384-386 (1969)

R-Matrix Methods in Shell-Model Reaction Calculations
K. Takeuchi and P. A. Moldauer
Bull. Am. Phys. Soc. 14, 52 (Jan 1969) Abstract

High Temperature Thermodynamic Properties of Oxygen-Deficient Urania
M. Tetenbaum and P. D. Hunt
J. Chem. Phys. 49(11), 4739-4744 (Dec 1968)

Reaction of $PUO_2$ with Molten $MgCl_2$
D. A. Wenz and I. Johnson
Inorg. Nucl. Chem. Letters 4, 735-738 (Dec 1968)

# IV. NUCLEAR SAFETY

## A. Reactor Kinetics--Other Reactor Kinetics--Research and Development

### 1. Accident Analysis and Safety Evaluation (G. J. Fischer)

#### a. Accident Mechanics

Last Reported: ANL-7445, pp. 129-130 (April 1968).

The fast reactor accident-analysis code SAS1A has been thoroughly reorganized. Such features as input and output have been made attractive in anticipation of making the code publicly available in the near future. Documentation, which may be the limiting factor for availability, is being assembled.

While SAS1A will be a fast-running and exceptionally useful tool for fast reactor safety-evaluation studies, it is obvious that such limitations as the use of point kinetics and single-channel analysis in SAS1A represent undesirable restrictions. A new code, SAS1B, has been planned as a means of relieving many of these problems.

One of the partial restrictions in SAS1A is that a modified version of the two-dimensional Bethe-Tait-type weak explosion code by APDA,* called MARS/SAS (see ANL-7445), is employed as a module for computing the consequences of major disassembly accidents. A two-dimensional hydrodynamics module has been created. This will allow explicit calculation of physical displacements of the core and blanket during disassembly and provide an excellent basis for more accurate estimation of reactivity. This can be particularly useful for careful calculation of implosive behavior near low-power regions, as for loops in fuel test reactors.

For purposes of early testing of this two-dimensional hydrodynamics module for realistic accident conditions, the module was linked to the Doppler effect and other feedback portions of MARS/SAS. The product is a fast reactor explosion code with a distinct advantage over MARS/SAS. This code is being documented and will be quickly available through the Argonne Code Center under the name of VENUS.**

The VENUS code is a "spin-off" of the SAS1B development program which was achieved with a minimum of time and man power cost. Figures IV.A.1 and IV.A.2 briefly indicate the consequence of applying

*Hirakawa, N., MARS--A Two-dimensional Excursion Code, APDA-198 (1967).

**Sha, W. T., and Hughes, T. J., VENUS--A Two-dimensional Weak Explosion Code Using LaGrangian Hydrodynamics, to be published as an ANL document.

VENUS to a 1000-MWe oxide-fueled pancake reactor having a core height of 50 cm and two zones of enrichment.

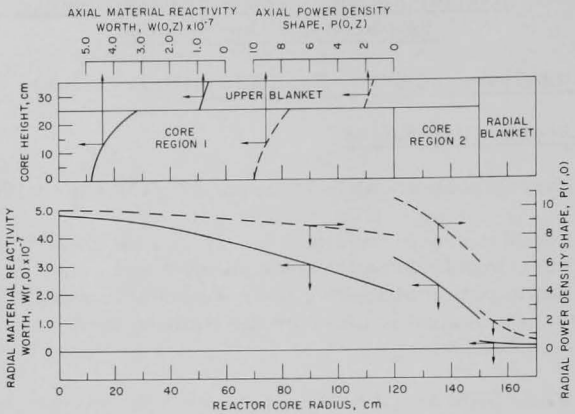


Fig. IV.A.1. Axial and Radial Power and Material-worth Distributions for 1000-MWe Oxide-fueled Pancake Reactor of Conservative Design

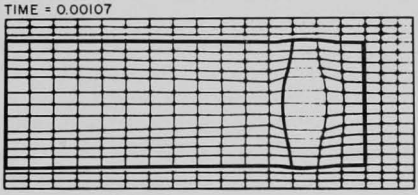


Fig. IV.A.2

Computer-generated Display of Physical Displacements of Core at One Time Step in the Disassembly Accident. Note the implosive motion of the boundary between the outer enriched zone and the central core zone.

## 2. Reactor Control and Stability

### a. Transfer Function Techniques to Measure Large Fast Reactor Stability (L. Habegger)

Last Reported: ANL-7527, pp. 127-128 (Dec 1968).

(i) Spatial Effect. The MACH-I diffusion-theory code* has been used to obtain representative temperature-dependent values of the few-group cross sections appearing in the space-time reactor-kinetics model. The values were computed by collapsing the 26-group ANL-233 cross-section set. The reactor system used in the computation was a

*Meneley, D. A., Kvitek, L. C., and O'Shea, D. M., MACH I, A One-dimensional Diffusion-Theory Package, ANL-7223 (June 1966).

1000-MWe oxide-fueled cylindrical LMFBR with a height-to-diameter ratio of 0.8 and 400-kW/liter power density. Additional physical parameters were the same as had been used in a previous parametric study.

These computed parameters will be used for computing space-dependent transfer functions. Effects on the transfer functions of variations in these parameters will also be studied.

## 3. Coolant Dynamics

### a. Critical Flow (H. K. Fauske, M. A. Grolmes)

Last Reported: ANL-7518, p. 120 (Nov 1968).

(i) Sodium Tests. Two-phase liquid-fraction data for sodium have been obtained in the sodium-flashing facility using an electromagnetic flowmeter to measure the average liquid velocity in the two-phase region. In the study of sodium liquid-vapor pressure drops, the average liquid volume fraction at a conduit cross section is an important variable. Figure IV.A.3 shows the measured liquid volume fraction as a function of the Lockhart-Martinelli flow modulus.* The measurements, which cover a large range of the modulus, demonstrate good agreement with the Lockhart-Martinelli correlation, which is based on low-pressure air-water and steam-water data. The values of the vapor quality (weight fraction x) used in calculating the flow modulus were obtained from measured temperature profiles. For the range of variables investigated, these values differ only slightly from calculated thermodynamic-equilibrium values when these are based on measured axial pressure profiles. The agreement shown by Fig. IV.A.3 verifies earlier data (see Progress Report for October 1968, ANL-7513, p. 131), which suggest that the hydrodynamic behavior of one-component two-phase flows of metallic and nonmetallic fluids are quite similar. These liquid-fraction data agree fairly

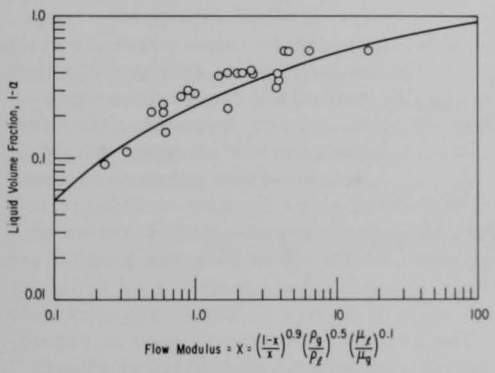


Fig. IV.A.3. Comparison between Measured Sodium Liquid Volume Fraction (data points) and the Lockhart-Martinelli Correlation (solid line). Symbol x is vapor quality, ρ is density, μ is viscosity, ℓ is liquid, and g is vapor.

*Lockhart, R. W., and Martinelli, R. C., Chem. Eng. Progress 45, 39 (1949).

well with the recent potassium data of Baroczy,* but differ greatly from earlier one-component metallic data** that indicate much higher liquid-volume fractions for a given flow modulus.

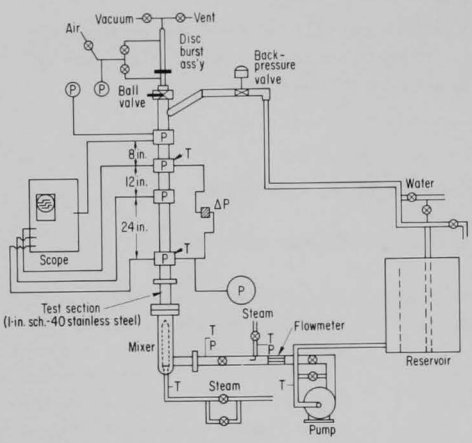


Fig. IV.A.4. Sonic-velocity Test Apparatus. The pressures at the four points above the test section are measured by quartz transducers.

(ii) Sonic Velocity and Pressure-wave Progapation. Additional measurements of the propagation velocities of compression and rarefaction pressure pulses in steam-water mixtures have been obtained in the test apparatus shown in Fig. IV.A.4. The results agree with previous data (see Progress Report for July 1968, ANL-7478, p. 125), but more information has been obtained about the characteristics of the total wave. Pressure pulses large enough to cause pressure spikes and complete collapse of vapor behind the front of the wave have been observed. Thus far, the collapse of vapor behind the wavefront appears to have no influence on the wavefront velocity, which gives further confidence in the ability to describe the wavefront velocity in liquid-metal systems on the basis of steam-water and air-water results. The data are being analyzed in more detail.

(iii) Voiding Models. The results of the first phase of experimental studies of transient flow regimes in support of analytical efforts to develop coolant-channel voiding models have been assembled into a filmstrip. The filmstrip, consisting of high-speed motion pictures, shows several events in the expulsion of Freon-11 initially saturated at 80°F and subjected to rapid depressurization in the apparatus shown in Fig. IV.A.5. Two principal modes of expulsion have been observed. One occurs only when there is a suitable artificial nucleation site (such as a scratch on the inside surface of the glass channel), in which case a single bubble grows, occupies the entire cross section of the channel, and causes a slug-type expulsion of the upper column of liquid; this type of expulsion lends support to analytical models that are being developed. The other expulsion mode, consisting of a well-defined two-phase interface that propagates downward

*Baroczy, C. J., Chem. Eng. Progress Symposium Series 64 (1968).

**Lurie, H., ANL-7100, Proceedings of the Conference on Application of High Temperature Instrumentation to Liquid-Metal Experiments--September 28-29, 1965 (September 1965); Smith, L. R., Rasin Tek, M., and Balzhiser, R. E., Am. Inst. Chem. Eng. Journal 12, No. 1, 50 (1966).

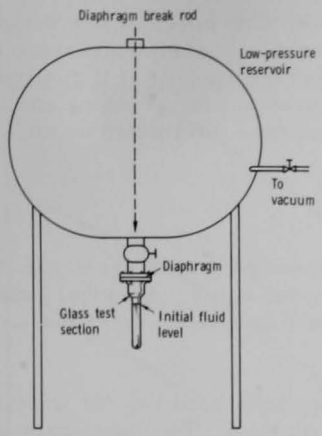


Fig. IV.A.5. Apparatus for Studying the Transient Flow Regime

into the liquid column, occurs either (a) after a slug-type expulsion from a channel that has a bubble-nucleation site or (b) independently, in a glass test section that is clean and scratch-free so that it does not have a nucleation site.

Future test sections are being planned with simulated multipin arrangements. With control over the location of nucleation sites, the radial as well as axial growth of bubbles will be observed.

b. Coolant Dynamics (R. M. Singer and R. E. Holtz)

Last Reported: ANL-7527, pp. 128-129 (Dec 1968).

(i) Sodium Superheat Experiments. The theoretical study of inert-gas effects in the incipient boiling of liquid metals is continuing. The analysis of pool boiling has been completed. It was shown that inert-gas diffusion can play an important role in the determination of incipient-boiling superheats and might explain much of the existing confusion in this field. The analysis is being extended to forced-convection systems.

(ii) Coolant-expulsion Experiments. The piezoelectric pressure transducer mounted in the expulsion apparatus operated erratically and was replaced by a strain-gauge-type transducer. A leak developed at a fitting in the inert-gas manifold system and was repaired. Data are being acquired.

(iii) Experiments with Transients. Several difficulties have arisen in the calibration of the calorimetric flow-measurement device; it has been decided to calibrate the device in sodium instead of water.

c. Convective Instability (R. M. Singer)

Last Reported: ANL-7527, p. 129 (Dec 1968).

(i) Flow-coastdown Experiment. Fabrication and delivery of components for the experimental loop continues. The thermocouples are being installed in the test section.

4. Core Structural Safety (C. K. Youngdahl and K. Y. Narasimhan)

Last Reported: ANL-7513, pp. 133-136 (Oct 1968).

a. Dynamic Plasticity Analysis of Circular Shells. A number of problems involving extensive Phase-2 deformations have been run for

impulsive ring loads with arbitrary pulse shapes. The previous conclusions that the impulse I and mean time $\tau_m$ are the most important characteristics of a pulse shape in determining the final shell deformation is still confirmed by the latest results. It appears to be more convenient for graphing and intuitive reasoning purposes to replace the mean time parameter by an effective load parameter $\psi_e$ defined as

$$\psi_e = I/2\tau_m. \tag{1}$$

For rectangular pulse shapes the effective load and peak load are equal; for other shapes the effective load is less than the peak value. A topical report on the equivalence of dynamic ring loads for the final plastic deformation of a circular cylindrical shell is being prepared.

Some Phase-1 deformation examples have been run for impulsive loads that vary with axial position as well as with time. The time shape of the impulse was rectangular for each of these problems while the axial shape (see Progress Report for January 1968, ANL-7419, pp. 154-157) was taken as

$$\phi_\gamma(\xi) = \left(\frac{\gamma+1}{a\gamma}\right)\left[1 - \left(\frac{\xi}{a}\right)^\gamma\right], \quad 0 \le \xi < a$$

$$= 0, \quad \xi \ge a, \tag{2}$$

for $\gamma = 1/4$, 1, 4, and $\infty$. The results obtained thus far are insufficient to draw any general conclusions, but it appears likely that the important parameters in determining the final shell deformation are the impulse I and the effective load $\psi_e$, as for the concentrated ring load, plus the static yield load $\psi_s$, which is a function of the axial shape of the load.

b. Hexagonal-shell Analysis. To gain an understanding of the influence of the membrane force (due to internal pressure) in the hexagonal shell on the displacements, the shell has been analyzed considering large elastic deformations. For high internal pressures the membrane force becomes increasingly important. Eventually, as the pressure is increased, the hexagonal shape becomes circular and the membrane force predominates almost entirely over the bending moment. To simplify the analysis, variations in the axial direction are neglected. However, the fact that the internal pressure always acts normal to the deformed shape is taken into account. Lower and upper bounds for stresses and displacements are determined by considering hexagonal shells with hinged and fixed corners, respectively. The variation of the membrane force along the length of a bay due to the change in curvature is also considered for the case with hinged corners. This variation is found to be less than 1% and so can be neglected even for large deformations.

Figure IV.A.6 shows the ratio of maximum total stress ($\sigma_t$) to the maximum bending stress ($\sigma_m$) in an equivalent fixed beam of the length

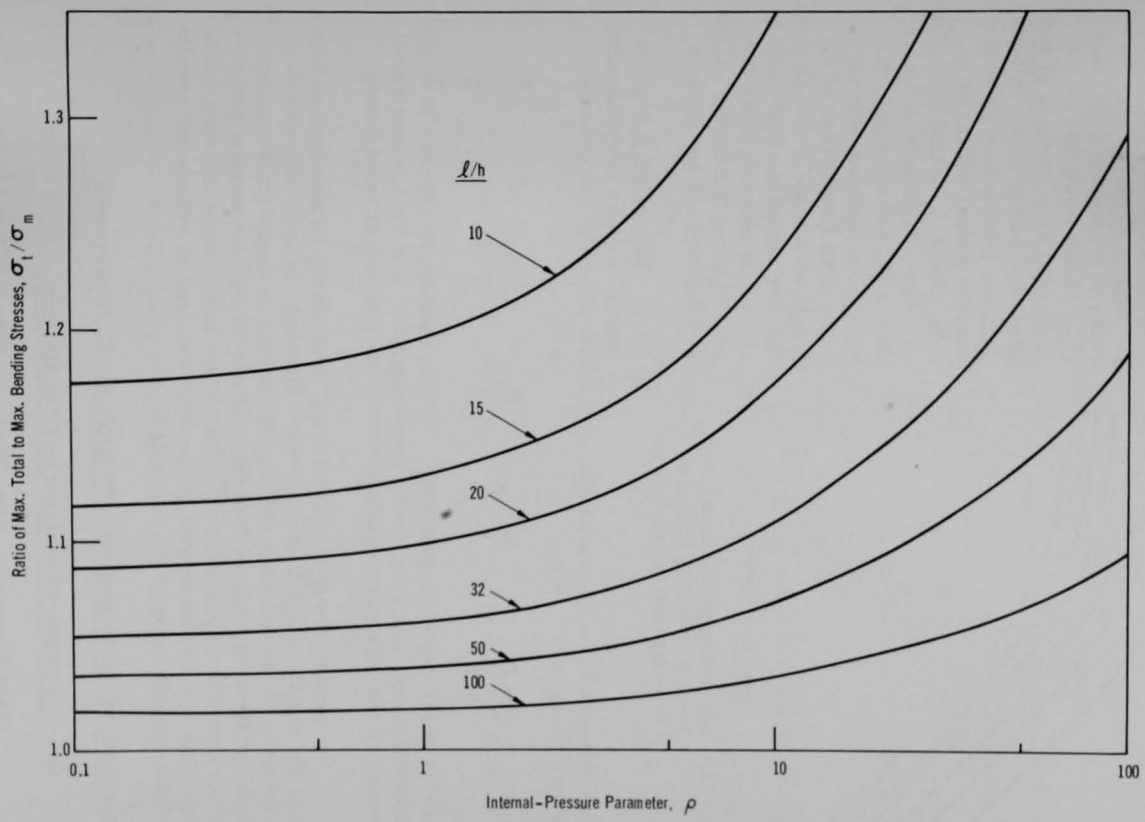


Fig. IV.A.6. The Ratio of Total Stress to Bending Stress as a Function of the Pressure Parameter for Various Values of $\ell/h$

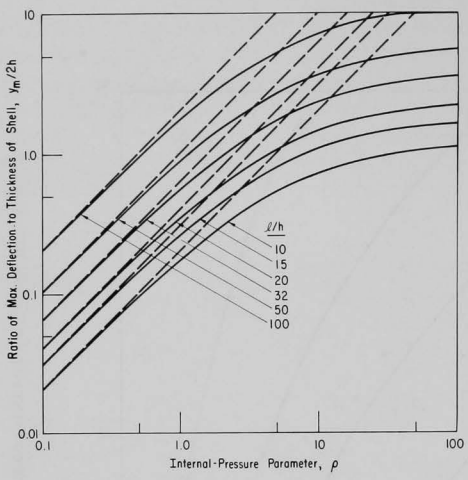


Fig. IV.A.7. Ratio of Maximum Deflection to Total Thickness of Shell as a Function of Pressure Parameter for Various Values of $\ell/h$

of a bay but with no axial restraint as a function of the internal-pressure parameter $\rho$. Figure IV.A.7 shows the ratio of maximum deflection ($y_m$) to the thickness of the shell (2h) as a function of the pressure parameter. In both figures, curves are given for various values of the ratio $\ell/h$, where $\ell$ is half the length of a bay. Figure IV.A.7 also shows (by broken lines) the maximum deflection in an equivalent fixed beam of the length of a bay. It can be seen that the actual displacements deviate noticeably from the broken lines for higher values of the pressure parameter.

Figure IV.A.8 gives master curves for maximum stress and maximum displacement over a wide range of the internal-pressure parameter. Here,

$$\beta = \frac{\sigma_m}{\sigma_n}\frac{2h}{\ell}; \qquad n = \frac{N\ell^2}{D}; \qquad \delta = \frac{y_m}{\ell}; \qquad \rho = \frac{P\ell^3}{D},$$

where P is the internal pressure, $\sigma_n$ is the membrane stress, N is the membrane force, and D is the flexural rigidity. The broken line corresponds to the maximum displacement in an equivalent fixed beam.

Analysis was also conducted considering extensional deformation of the middle surface of the shell. Although the influence of this deformation on the stresses and displacements is small for the range considered here, it reveals that calculations based on linearization, wherein extensional and bending deformation are considered separately to calculate the displacements of the corners, lead to erroneous results beyond a certain value of the $\ell/h$ ratio.

## 5. Fuel Meltdown Studies with TREAT (C. E. Dickerman)

### a. Development of Experimental Methods

Last Reported: ANL-7527, pp. 129-132 (Dec 1968).

(i) Studies of Fast-neutron Converter for TREAT. Reactor physics calculations using transport theory in one-dimensional cylindrical

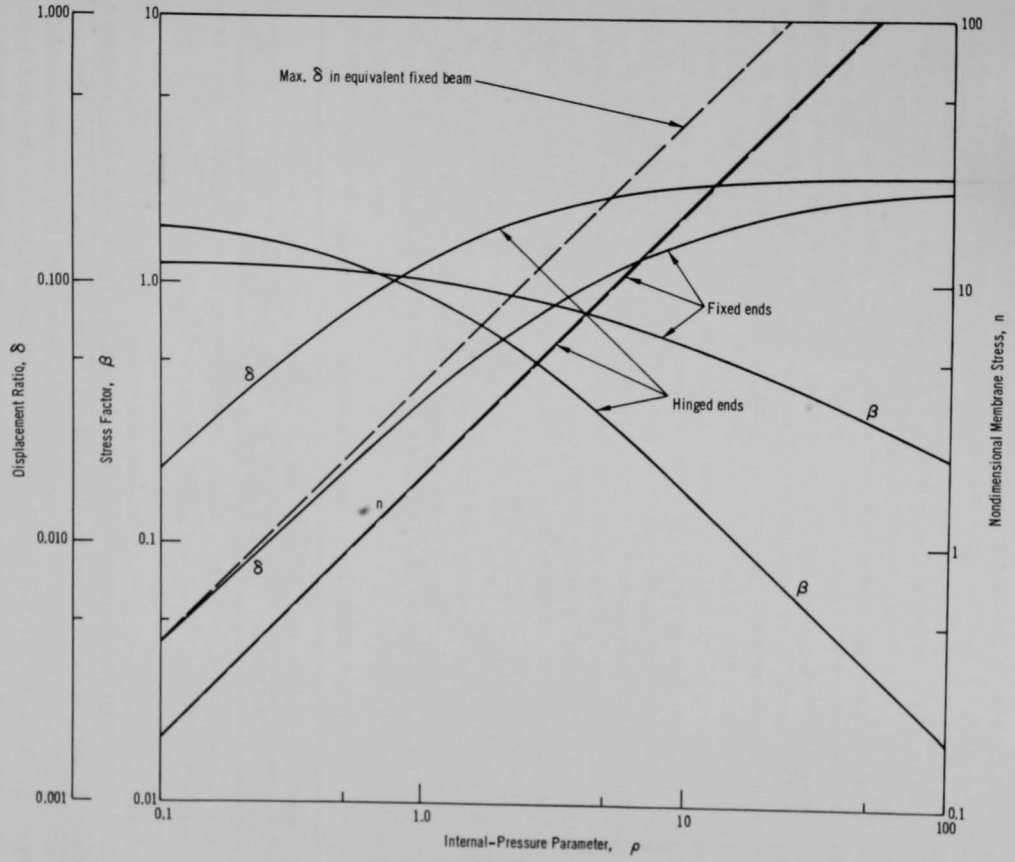


Fig. IV.A.8. Master Curves for Maximum Stress and Maximum Displacement

geometry were performed on the fast-flux converter model for TREAT to examine the feasibility of testing fuel-pin clusters larger than 7 pins. Samples considered were clusters of 7 (reference case), 17, and 37 pins. In all cases each test pin was assumed to consist of fully enriched $(U+Pu)O_2$ pellets of 0.625-cm diameter and cladding of 0.051-cm-thick stainless steel. A conservative set of converter enrichments was used, corresponding to maximum converter temperatures of ~1200-1400°C for a maximum core temperature of 600°C. The current design specification is a converter maximum temperature of 1800°C for core maximum of 600°C, which may make possible increased energy input to the sample over that for the converter enrichments used in these calculations. The wall thickness of the test loop for the 7-pin case was that of the Mark-II integral sodium loop; wall thickness for the other two clusters were increased to preserve the same wall thickness-to-diameter ratio. The input for the 37-pin cluster is not as favorable as for the 7- and 17-pin cases, since it used a somewhat less efficient, one enrichment outer converter region rather than the two-enrichment outer-converter region of the other two cases.* Results are summarized in Table IV.A.1. The symbol $\Delta T_c$ (max) is the maximum temperature rise in the converter; $R_E$ is the ratio of central sample energy input, corresponding to $\Delta T_c$ (max), to the energy required to raise oxide adiabatically to its melting point and supply the heat of fusion. The quantity $\bar{E}_{fiss}$ is the median energy of neutrons undergoing fission in the center of the cluster; the spectrum at the center of the 37-pin cluster is quite hard. From the calculations it appears that clusters of 37 pins can be adequately accommodated neutronically in this type of converter, and that radial maximum to minimum power ratios of about 1.2 will be encountered (this is higher than the reference value of 1.1, but should be tolerable).

TABLE IV.A.1. Results for 37-pin-cluster Survey

| Size of Test Cluster (Pins) | Radial Power Density Ratios: Max Cluster / Min Cluster | Max Converter Power / Cluster Centerline | Cluster Centerline / Max Core | $\Delta T_c$ (max) (°C) | $R_E$ | $\bar{E}_{fiss}$ |
|---|---|---|---|---|---|---|
| 7 | 1.16 | 0.12 | 40 | 1200 | 2.36 | 0.47 |
| 17 | 1.17 | 0.13 | 37 | 1200 | 2.16 | 0.70 |
| 37 | 1.17 | 0.16 | 37 | 1340 | 2.16 | 1.05 |

(ii) Preliminary Tests of the Mark-II Integral Sodium TREAT Loop. The prototype version of the Mark-II Integral Sodium Loop has been completely outfitted and subjected to preliminary out-of-pile operational testing. This loop is the first of the Mark-IIB loops, and as the prototype contains known deviations from the loop specifications, which were considered acceptable in a loop to be used for preliminary tests and development of operational techniques. These include deficiencies that would be

*Iskenderian, H. P., Study of Conversion of TREAT Facility for Testing of Fast Reactor Subassemblies, Trans. Amer. Nucl. Soc. 11, No. 2, 643 (1968).

most likely to occur during fabrication and result in some compromise of the specifications; detailed testing of the prototype thus can serve to confirm the design and specifications with a measure of conservatism. Deviations include one weld with an inclusion consisting of extraneous electrode metal, internal undercutting of two welds from incomplete penetration, two welds with filler material of unverified chemistry, and alignment of loop-pump flanges that was outside the specification for degree of parallelism. Despite the deviations from the stringent specifications demanded for the Mark-II loops, it was recognized from the outset that the final judgement as to the quality and/or usability of any given loop would rest upon the outcome of the final prooftest of the particular unit, at pressure and temperature. Hence, successful prooftest of the prototype would qualify the loop for experimental use in the meltdown program, while in no way justifying the relaxation of the quality-control specifications previously enumerated as a means of assuring a conservative design.

During the tests of heater, power, and instrumentation circuitry, unexpected mishaps resulted in minor changes in the design of some components and operational sequences, and supplied considerable information concerning the durability of the loop and its behavior under conditions that had been considered to offer severe potential hazards. Such incidents constitute the essential reason for the construction of a prototype facility, and the behavior of the loop during potentially hazardous occurrences in progressive testing, with the after-effects of the mishaps, become a valid test of the loop design. The incidents with the prototype resulted in the acquisition of data which made unnecessary the performance of further, independent tests to determine the answers to questions on the loop durability, the consequences of potential hazards, and of the malfunction of loop components.

One of the queries made concerned the danger to the containment integrity of the loop resulting from a severe electrical malfunction or failure of the electromagnetic sodium pump. Extensive pump-design tests with a "bench-assembled" pump had demonstrated ruggedness in the event of internal electrical breakdown. This pump was used for the prototype loop, although one phase of the 3-phase Annular Linear Induction Pump (ALIP) developed a short to ground. However, the electrical fault only impaired the efficiency of the pump and had no effect whatsoever on the integrity of the pump's Inconel flow tube, or of the loop proper. During the approach to temperature during the first prototype loop test, the ALIP was operated at about half-maximum current to supplement the heat input by the external resistance heaters. After the loop had reached 800°F, the ALIP silicone coolant flow was reduced to near zero. Relatively high temperatures in the ALIP and its coolant circuit resulted. The ALIP stator temperature reached about 550°C, well above the temperature limits of the epoxy potting compound of the pump coils;* despite the extensive destruction

*Primary insulation of the aluminum coils is an aluminum oxide surface layer on the aluminum wire.

of this material insulation, as evidenced by the considerable charred epoxy observed in the inspections made afterwards, the prototype ALIP has continued to function well.

The question had been raised concerning the use of the temperature-resistant silicone oil as the coolant for the ALIP, and the consequences of a coolant spill from line breakage, or seal failure, in direct contact with the loop while at maximum temperature within its enclosure. The Dow-200 low-viscosity silicone fluid was selected for its very high temperature stability, but it was recognized that the liquid would burn under the proper conditions of temperature and oxygen availability.

This relatively extreme temperature to which the ALIP was subjected resulted in the failure of one of the power through-connectors of the pump, which had been mechanically damaged during the outfitting and repaired with an epoxy cement. This provided a leak in the silicone coolant system, at the top of the pump, while the loop was at 950°F. Approximately a half-gallon* of the silicone sprayed out into the can, flowed down over the lower half of the loop, and collected in the bottom of the container. Although the silicone saturated the insulation and heaters of the hottest portion of the loop, the only result was the appearance of a large quantity of smoke; there was no ignition of the silicone, nor any perceptible damage to insulation, heaters, or any component of the loop.

In any sodium- or NaK-filled system, the hazards presented by the accidental spillage of the molten liquid metal through vessel rupture or seal leakage are always in question. The proposed use of the Mark-II loop in the TREAT reactor enhanced the seriousness of the question as directed to this facility, with its 1.5-liter contents of sodium at high temperatures. This concern was coupled with concern that differential thermal expansion between the two legs of the loop could be a potential hazard. Preliminary verification of the design was obtained by a stress analysis, but because of the complicated geometry, a prooftest was required. In the next test, with the ALIP flow-tube temperature at 150°F, and the test section temperature at 750°F (i.e., with a temperature differential of approximately 600°F between the test section and pump legs of the loop), the lower O-ring seal of the ALIP unit developed a small leak, and about 500 cc of molten sodium, at 700°F, was dropped down within the secondary can upon the thermal insulation which was still saturated with silicone coolant after the first incident. Again, while some smoke was visible, there was no fire, nor was there detectable damage following the necessary steam-cleaning of the loop.

---

*This is approximately 75% of the coolant inventory.

The use of Inconel X-750 for the ALIP flow tube requires a 25-in. length of a material having a linear thermal expansion coefficient of $8.0 \times 10^{-6}$ in./in.-°F to be clamped tightly into one leg of a closed, elongated loop composed of Type 316 stainless steel, with a coefficient of $9.6 \times 10^{-6}$ in./in.-°F. The differential thermal expansion of the opposing legs of the loop, as the device is brought from ambient to 1000°F, could impose severe thermal stresses upon the upper and lower bends. Since there has been some difference of opinion as to the model to use in calculating the resultant stresses in the loop members, the question as to the device's capability to endure such stresses was raised.

Following the sodium-leak incident, the ALIP unit was removed from the loop for examination of the flanges and O-rings. While the pump was out of the loop, the pump interflange distance was found to be unchanged (within 0.002 in.), despite the extreme abuse resulting from the very high temperature differential between the Type 316 stainless steel test-section side and the ALIP flow tube of Inconel X-750. This provides a conclusive indication that the compound-curved offset bends of the loop, above and below the ALIP, react to the expected axial load of differential thermal expansion as massive, but efficient, springs, and are self-relieving. Further, the great strength of the Inconel pump flow tube is not affected by the tensile load applied by the upper and lower loop bends when at temperature, and the massive Inconel pump clamps are too strong to exhibit the slightest yield or shift under the maximum loads to be applied within the loop's rated temperature and internal pressure.

The seal leak at the pump flange was found to be the result of using a design in which flange clamps were deliberately slightly sprung open, to protect the contact side of the flange. With this type of clamp, the O-ring seal capacity was discovered to be a function of the clamp-spring constant as the bolts were tightened; the seal leaked at 4200 psi, whether the fluid was gas, water, or sodium, and with the clamped flange at room or at elevated temperatures. Replacement of the sprung clamps with straight clamps, at half the previous bolt torque, provided a seal which was found to easily contain 10,000 psig in tests outside the loop.

The tests of the loop have indicated a remarkable stability of output signal from the dc-electromagnetic flowmeters. With an excitation current of 1 A, the signal level is only about 1.2 mV; however, the signal-to-noise ratio is so high that no perceptible noise in the output can be observed on the loop instrumentation.

The remaining, final test to be performed on the Prototype Mark-II loop will be of the prooftest of the device's containment capability, to 5550 psig, at 800°F.

## 6. Materials Behavior and Energy Transfer

### a. Segregation in Ceramic Fuels (M. G. Chasanov)

Last Reported: ANL-7513, p. 141 (Oct 1968).

Work is continuing to determine the extent of migration and segregation in mixed uranium-plutonium fuels under a thermal gradient. Two $(U_{0.8}Pu_{0.2})O_{1.97}$ pellets were annealed in a thermal gradient of about 1000°C/cm for approximately 100 hr each. The top surface temperature of the pellets was ~2350°C. These experiments were performed to investigate possible stoichiometric effects on plutonium migration in mixed-oxide fuels. Microprobe scans of these pellets have been carried out; the data are currently being analyzed.

Experimental investigation of the effects of thermal gradients on plutonium distribution in mixed-carbide fuel pellets is also underway. These pellets contain 4.61 w/o carbon, 81.0 w/o uranium, and 14.4 w/o plutonium. Cylindrical specimens were pressed (at 19,000 psi), using carbides produced in a fluidized bed, and then sintered for 90 min at 2100°C. Experiments of 100- and 500-hr duration, similar to those for the mixed oxides, have commenced.

### b. Interactions of Fuel, Cladding, and Coolant (D. R. Armstrong)

Last Reported: ANL-7513, p. 140 (Oct 1968).

(i) Fragmentation Study in Water. Studies of the fragmentation of molten materials while being quenched in a liquid medium are continuing. The fragmentation process is an important step in providing the necessary surface area for energy exchange in a vapor explosion. [Previous work (see Progress Report for July 1968, ANL-7478, pp. 128-130) showed that fragmentation will occur if the Weber number ($\rho Dv^2/\mu$, the ratio of dynamic to surface forces) is greater than 20, and that fragmentation is enhanced if the temperature of the molten metal is at or near the critical temperature of the liquid.] Fragmentation behavior when molten tin contacts liquid water is being investigated; 0.3-g quantities of molten tin at 330°C (the critical temperature of water is 373°C) are dropped into water at 22°C, and the fragmentation is observed by photographing the event using stroboscopic illumination.

As shown in Fig. IV.A.9, which illustrate the fragmentation behavior of molten tin upon contact with water under identical conditions, it has been discovered that the extent of metal fragmentation can vary markedly even when the method and conditions of contact are identical. Slight fragmentation, principally at the air-water interface, is shown in the left photo,

but extensive fragmentation followed by vigorous dispersion of the fragments is shown in the right photo. In the latter case, two fragmentation events are discerned: an initial breakup near the interface, and a second, more violent event at a depth of 2 cm. From these experiments, we conclude that it would be difficult to predict the extent of fragmentation for a single-particle system, but that particle-size distributions can be predicted statistically for multiparticle systems, as shown in ANL-7478.

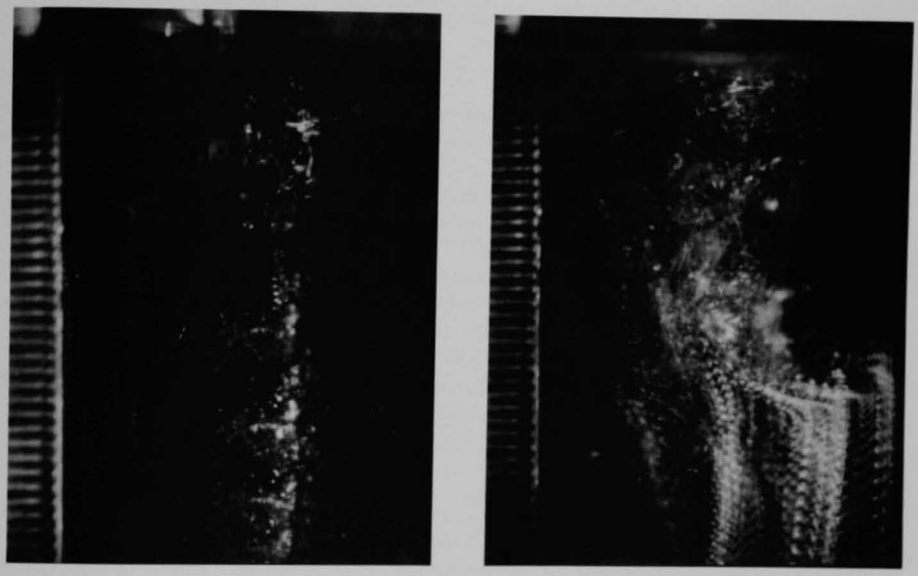

Fig. IV.A.9. Two Modes of Fragmentation (slight, at left, and extensive, at right) Observed when Molten Tin Samples Were Dropped into Water under Identical Conditions: 0.3-g Tin Samples at 330°C Entering 22°C Water at 345 cm/sec. Strobe-light frequency was 120 Hz.

Experiments to characterize further the fragmentation phenomena are being made by high-speed motion-picture photography. It is expected that analyses of these films will help explain the differences in fragmentation behavior.

(ii) Fragmentation Study in Sodium. The development of a method to contact molten $UO_2$ with liquid sodium continues. Recent attempts to melt $UO_2$ in a tungsten crucible were thwarted by failure of the crucible during the $UO_2$-loading procedure, which involved a sequence of two melting steps. The phenomena attendant to the crucible failure were peculiar in that fused $UO_2$ had coated the entire internal and external surfaces of the crucible, which suggests that molten $UO_2$ is a highly mobile fluid of low viscosity and interfacial tension.

c. Violently Sprayed Sodium-Air Reaction (R. O. Ivins)

Last Reported: ANL-7513, pp. 140-141 (Oct 1968).

Both the experimental and analytical studies in this effort have been terminated. A topical report describing the work has been prepared.

7. Fast Reactor Safety Test Facility Study (C. N. Kelber)

Last Reported: ANL-7527, p. 132 (Dec 1968).

a. Program Definition and Justification. The preliminary draft of the report is scheduled to contain ten chapters and a number of appendixes. The review procedure is: after a detailed outline has been proposed and reviewed by all project personnel and consultants from the whole LMFBR safety program at the Laboratory, a rough draft of a chapter is written. This is reviewed by the project manager and by those members of the project with which there is the greatest interface. This constitutes the first level of review. Following revision, the next draft is reviewed by consultants familiar with the work area in question and the LMFBR safety program. This is the second level of review. The third level of review includes the entire proposed preliminary draft (except for possible specific omissions whose content will be outlined) by Laboratory staff involved in technical direction and coordination of the LMFBR safety program, and program office representatives.

All chapters except the summary and conclusions and Chapter IX, Instrumentation, have passed the level-one review. Chapter VII on super-prompt-critical accidents is in the process of revision before level-two review. All other chapters are being revised preparatory to level-three review.

Appendixes on the fast-neutron hodoscope; the program for fuel-element-failure propagation program, and problems in making loss-of-flow tests have received level-two review. An appendix on molten fuel-coolant interaction and one on the equation of state are being prepared for level-one review.

## B. TREAT Operations

1. Reactor Operations (J. F. Boland)

Last Reported: ANL-7527, p. 133 (Dec 1968).

Two temperature-limited transients were run with a dummy experimental capsule in the reactor to obtain additional data on the operating characteristics of the slotted reactor with fuel temperatures above 400°C

(see Progress Report for August 1968, ANL-7487, p. 109, and ANL-7527). A maximum fuel temperature of 575°C was recorded following the second transient. Since this temperature was close enough to the 600°C operating limit that the present data can be extrapolated to 600°C conditions with confidence, further testing of the reactor without experiments is considered unnecessary at this time. The reactor power and energy characteristics for a transient that produced a maximum fuel temperature of 575°C are compared in Fig. IV.B.1 to the maximum transient permitted under previous operating limits.

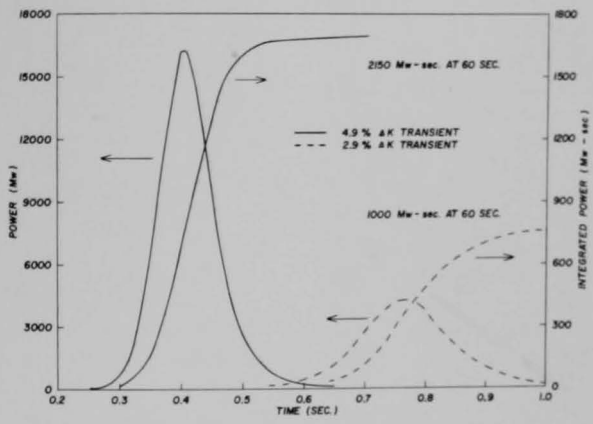


Fig. IV.B.1. Power and Energy Characteristics of TREAT Transients under New and Old Operating Limits

Neutron radiographs were made of 15 experimental capsules from EBR-II Irradiation Subassembly XO39, and one group of EBR-II driver-fuel elements.

The electronics for the 340-channel fast-neutron hodoscope were installed at the reactor, and checkout of the system is in progress (see Progress Report for June 1968, ANL-7460, p. 126).

2. Development of Automatic Power Level Control System (J. F. Boland)

Last Reported: ANL-7527, p. 133 (Dec 1968).

Processing of the purchase order for the hydraulic control-rod-drive system continued during this reporting period (see Progress Report for July 1968, ANL-7478, p. 133).

## PUBLICATIONS

Force-reflecting Servomechanisms with Signal-transmission Time Delay
William M. Thompson
ANL-7488 (Sept 1968)

Laboratory Investigations in Support of Fluid-bed Fluoride Volatility Processes. Part XX. Fission-product Tellurium Off-gas Disposal in the Fluid-bed Fluoride Volatility Process
D. R. Vissers and M. J. Steindler
ANL-7464 (Aug 1968)

ARGONNE NATIONAL LAB WEST
3 4444 00007940 0